

INFORMATION TO USERS

This manuscript has been reproduced from the microfilm master. UMI films the text directly from the original or copy submitted. Thus, some thesis and dissertation copies are in typewriter face, while others may be from any type of computer printer.

The quality of this reproduction is dependent upon the quality of the copy submitted. Broken or indistinct print, colored or poor quality illustrations and photographs, print bleedthrough, substandard margins, and improper alignment can adversely affect reproduction.

In the unlikely event that the author did not send UMI a complete manuscript and there are missing pages, these will be noted. Also, if unauthorized copyright material had to be removed, a note will indicate the deletion.

Oversize materials (e.g., maps, drawings, charts) are reproduced by sectioning the original, beginning at the upper left-hand corner and continuing from left to right in equal sections with small overlaps. Each original is also photographed in one exposure and is included in reduced form at the back of the book.

Photographs included in the original manuscript have been reproduced xerographically in this copy. Higher quality 6" x 9" black and white photographic prints are available for any photographs or illustrations appearing in this copy for an additional charge. Contact UMI directly to order.


UMI[®]

Bell & Howell Information and Learning
300 North Zeeb Road, Ann Arbor, MI 48106-1346 USA
800-521-0600

FREQUENCY-DIVERSE ULTRASONIC TARGET DETECTION
USING BAYES, FUZZY DISCRIMINANT, AND NEURAL NETWORK
CLASSIFIERS

BY
HAN CHIEH SUN

Submitted in partial fulfillment of the
requirements for the degree of
Doctor of Philosophy in Electrical Engineering
in the Graduate College of the
Illinois Institute of Technology

Approved 
Advisor

Chicago, Illinois
May 1999

ORIGINAL ARCHIVAL COPY

ACKNOWLEDGMENT

The author wishes to express his sincere gratitude to his major professor, Dr. Jafar Saniie, for his skillful guidance and assistance through all phases of this research. Dr. Saniie contributed a substantial amount of his time and effort to this research, and his help and encouragement are greatly appreciated.

The author is very grateful to his defense committee members, Dr. T. Wong, Dr. G. Atkin, and Dr. P. Greene for their comments, suggestions, and time in reviewing this thesis. A sincere gratitude is extended to Dr. M. A. Malik for his friendship and stimulating discussions.

The author wishes to dedicate this thesis to his parents, Mrs. Fu Chiang Chen, and Mr. Te Lung Sun, for their love, guidance, and countless efforts in supporting and encouragement. A special appreciation is to author's sisters, Lin Lin and Wei, for their understanding and continuous help during his graduate studies. The author would like to express his love and appreciation for his fiancée, Yi Chien Liu, for her patience, understanding, and love.

H.C.S.

TABLE OF CONTENTS

	Page
ACKNOWLEDGMENT	iii
LIST OF TABLES	vi
LIST OF FIGURES	vii
ABSTRACT	x
 CHAPTER	
I. INTRODUCTION.....	1
1.1 Introduction of Ultrasonic Non-Destructive Evaluation.....	1
1.2 Propagation of Ultrasonic Wave in Solids.....	3
1.3 Ultrasonic Pulse-Echo Measurement.....	5
1.4 Brief Introduction to the Research.....	7
1.5 Thesis Outline.....	9
II. SPLIT SPECTRUM PROCESSING.....	12
2.1 Introduction.....	12
2.2 The Fundamentals of SSP.....	14
2.3 NDE Applications of SSP Filters.....	26
III. STATISTICAL DISCRIMINANT FUNCTIONS.....	29
3.1 Introduction.....	29
3.2 Bayes Classifier.....	30
3.3 Maximum A Posteriori (MAP) Estimation Classifier.....	33
3.4 Simulated Results.....	36
3.5 Experimental Results.....	45
3.6 Conclusion.....	47
IV. FUZZY DISCRIMINANT FUNCTIONS.....	50
4.1 Introduction.....	50
4.2 Fuzzy Sets and Membership Function for Ultrasonic Signals..	51
4.3 Fuzzy Entropy.....	56
4.4 Simulated and Experimental Results.....	59

CHAPTER	Page
V. NEURAL NETWORKS.....	68
5.1 Introduction.....	69
5.2 Elementary Model of Neural Networks.....	70
5.3 Neural Network Detector.....	74
5.4 The Backpropagation Learning Process.....	75
5.5 The Design of the Neural Networks.....	77
5.6 Simulated and Experimental Results.....	81
5.7 Comparison of Neural Network with Bayes, MAP, and Fuzzy Classifiers.....	90
VI. THE COMPARISON OF NEURAL NETWORKS WITH OTHER DETECTION TECHNIQUES.....	97
6.1 Introduction.....	97
6.2 Recently Proposed Techniques.....	98
6.3 Simulated and Experimental Results.....	99
6.4 Conclusion.....	112
VII. SUMMARY AND CONCLUSION.....	113
BIBLIOGRAPHY.....	117

LIST OF TABLES

Table	Page
3.1 Flaw/Clutter Ratio Enhancement of Bayes Classifier and MAP Classifier using Simulated Signals.....	46
3.2 Flaw/Clutter Ratio Enhancement of Bayes Classifier and MAP Classifier using Experimental Signals.....	49
4.1 Flaw/Clutter Ratio Enhancement of SSP Algorithm Combined with Fuzzy Discriminant using Simulated Data.....	63
4.2 Flaw/Clutter Ratio Enhancement of SSP Algorithm Combined with Fuzzy Discriminant using Experimental Data.....	66
5.1 Flaw/Clutter Ratio Enhancement of SSP Algorithm Combined with Neural Network using Simulated Signals.....	88
5.2 Flaw/Clutter Ratio Enhancement of SSP Algorithm Combined with Neural Network using Experimental Signals.....	92
5.3 Flaw/Clutter Ratio Enhancement by using Bayes, MAP, Fuzzy and Neural Network Classifiers.....	93
6.1 Flaw/Clutter Ratio Enhancement of Various Processing Techniques using Experimental Signals.....	106
6.2 Flaw/Clutter Ratio Enhancement of Various Processing Techniques using Simulated Signals.....	107

LIST OF FIGURES

Figure	Page
1.1 The Attenuation Behavior as a Function of Frequency and Position.....	4
1.2 The Overall Scattering Behavior as a Function of Normalized Grain Diameter.....	6
1.3 Pulse Echo Measurement and Data Acquisition Equipment.....	8
2.1 Block Diagram of Split-Spectrum Processor.....	16
2.2 Split Spectrum Schemes using Gaussian Filters.....	17
2.3 An Experimental Ultrasonic Signal.....	21
2.4 SSP Output and Amplitude Histogram of Grain Signals.....	22
2.5 The Normalization Effect of SSP on Ultrasonic Signal Spectrum.....	24
2.6 The Covariance Matrix.....	27
3.1 The Block Diagram of Bayes Discriminant System.....	32
3.2 The Block Diagram of MAP Classifier.....	34
3.3 The Typical Processed Results by using Statistical Classifiers.....	38
3.4 The Processed Results by using 4 SSP Channels (BW=1MHz).....	39
3.5 The Processed Results by using 8 SSP Channels (BW=1MHz).....	40
3.6 The Processed Results by using 16 SSP Channels (BW=1MHz, Signal 1)..	41
3.7 The Processed Results by using 16 SSP Channels (BW=1MHz, Signal 2)..	42
3.8 The Processed Results by using 16 SSP Channels (BW=1.5MHz).....	43
3.9 The Processed Results by using 16 SSP Channels (BW=2MHz).....	44
3.10 The Typical Processed Results by using Experimental Data.....	48
4.1 Fuzzy Discriminant System.....	52

Figure	Page
4.2 The Normalized Membership Functions of Clutter and Target Signals.....	55
4.3 Graphic Display of the Function $\mu * \exp(1 - \mu)$ in Discrimination of Target and Clutter.....	58
4.4 The Typical Processed Results by using Simulated Signal.....	60
4.5 The Membership Function Obtained by using Simulated Data.....	61
4.6 The Typical Processed Results by using Experimental Signal.....	64
4.7 The Membership Function Obtained by using Experimental Data.....	65
5.1 A General Three Layer Neural Network.....	71
5.2 Nonlinear Model of a Neural Node.....	72
5.3 Three Different Neural Activation Functions.....	73
5.4 The Block Diagram of SSP Combined with a Three Layer Neural Network	78
5.5 The Simulated Training Data and Desired Response.....	80
5.6 A Typical Processed Results by using a Simulated Signal.....	82
5.7 The Processed Results of using Different Numbers of Neural Nodes in the Hidden Layer.....	84
5.8 The Flaw/Clutter Ratio vs the Number of Neural Nodes in the Hidden Layer.....	85
5.9 The Mean-Squared Error vs. Epoch.....	86
5.10 The Network Error vs the Number of Neural Nodes in the Hidden Layer...	87
5.11 The Experimental Training Data and Desired Response.....	89
5.12 A Typical Processed Result by using an Experimental Signal.....	91
5.13 The Training Data for Separating Two Adjacent Flaw Echoes.....	94
5.14 The Processed Results of Separating Two Adjacent Flaw Echoes.....	96

Figure		Page
6.1	The Decomposed Signal on Time-Frequency Plane (The flaw and grain echoes have different frequency components).....	101
6.2	The Processed Output by using Experimental Data.....	103
6.3	The Decomposed Signal on Time-Frequency Plane (The flaw and grain echoes have same frequency components).....	108
6.4	The Processed Output by using Simulated Data.....	109

ABSTRACT

The utilization of ultrasonic testing has been extended to many applications including the testing of complex materials and high-resolution medical imaging systems. These applications demand a system that will detect and classify target echoes efficiently and accurately. The scope of this thesis is to utilize split-spectrum processing (SSP) combined with nonlinear classifiers to detect ultrasonic target echoes in the presence of microstructure scattering noise.

In ultrasonic nondestructive evaluation (NDE), a broadband acoustic pulse is transmitted into a specimen, and then targets (i.e., crack, flaw, delamination...) as well as microstructure (i.e., grains) will reflect this pulse. The reflected signal is highly complex due to the interference of multiple echoes with random amplitude and phase. Furthermore, the frequency-dependent absorption and scattering property of the specimen will also cause the energy attenuation of the signal. Therefore, the success of ultrasonic target detection depends on the effectiveness of the signal processing algorithm and the development of a robust classification technique. In this study, SSP is used to display the diversity of ultrasonic signals on the time-frequency plane. Then, the nonlinear classifiers are applied to detect targets according to the signal features obtained on that plane. The SSP is implemented by using Gaussian bandpass filters. The parameters of the Gaussian filters include the number of filters, the bandwidth, and their center frequencies. These parameters and signal characteristics govern the signal correlation among the SSP channels. The nonlinear classifiers studied in this thesis include statistical classifiers, fuzzy classifiers, and neural networks (NN). The statistical

classifiers, including the Bayes classifier and the maximum a posteriori (MAP) estimation classifier, are developed based on the estimation of the target and clutter probability density function (PDF). The fuzzy classifier, a novel development, is obtained by modifying the fuzzy entropy. To implement the fuzzy classifier, it is necessary to build the membership functions based on the statistical properties of the ultrasonic signals.

Neural networks (NN), due to their trainability and adaptability, are powerful tools for signal classification. Without solution methodology or mathematical models of the target signals, NN can recognize the target patterns after a training process. In NDE applications the important issue in the design of the NN is the selection of the training strategy and training data such that a target echo embedded in a scattering noise can be recognized.

In this thesis, we present the mathematical derivation for these techniques and use both simulation and experimental results to demonstrate their applications in ultrasonic nondestructive testing. Results obtained in this investigation demonstrate that target detection using these techniques is a viable approach when the flaw-to-clutter ratio is about 0 dB. A comparative result is presented in this thesis, which shows that SSP-NN exhibits the best performance when compared to other model-based detection techniques presented in this thesis.

CHAPTER I

INTRODUCTION

The objective of this thesis is to apply various signal processing techniques to analyze backscattered ultrasonic signals. The specified goal is the development of a signal detection system, that utilizes the inherent properties of grain and flaw signals exhibited on the time-frequency plane, to separate flaw echoes from grain echoes. In this thesis, split-spectrum processing (SSP) is used to perform a signal pre-processing in which many signal features that cannot be observed in the time or frequency domain can be displayed on the joint time-frequency plane, and in addition the signal-to-noise ratio can be enhanced. Once the signal features are obtained by using split-spectrum processing, several classifiers including statistical classifiers, fuzzy classifiers, and neural networks (NN) can be used to detect flaw signals. This thesis presents the development and analysis for the processing of ultrasonic signals based on the previous highlight.

1.1 Introduction of Ultrasonic Non-Destructive Evaluation

Ultrasound has been utilized by the industry for nondestructive testing since the early 40's. Nowadays, ultrasonic testing is widely used in medical diagnosis too. The objective of the ultrasonic non-destructive evaluation (NDE) of materials is to learn their characteristics through the analysis of the backscattered ultrasonic signals. Research in the area of ultrasonic images has been emphasized, because an ultrasonic wave can propagate through materials to considerable depths, without damaging the testing object.

This allows extracting information from deep within the testing object by examining the backscattered ultrasonic signal. However, this information is highly complex due to the interference of multiple backscattered echoes with random amplitude and phase. Therefore, in order to examine the backscattered ultrasonic signal, an effective signal processing is necessary. It is the objective of this investigation to develop a technique in order to extract and display the features of ultrasonic signals for material testing.

Most NDE techniques are obtained by using the statistical and spectral processing techniques [1-9]*. Basically, these techniques were developed based on the probabilistic nature of ultrasonic signals. An important result determined by the previous methodologies is that the ultrasonic scattering signal is random and nonstationary, and its frequency characteristic is governed by the scattering absorption and dispersion of echoes. This makes the ultrasonic nondestructive testing a challenging problem. In recent years, many researchers successfully applied the time-frequency analysis [10-20] to display the energy of ultrasonic signals on the joint time-frequency plane and thereby enhance the signal-to-noise ratio (i.e., SNR) of target signals. The time-frequency analysis is desirable to investigate the nonstationary characteristics of ultrasonic signals. Therefore, split-spectrum processing is used to study the nonstationary characteristics of ultrasonic signals. It is also important to develop a signal detection algorithm to detect the target of interest. Since most NDE applications deal with the signals embedded in highly noisy environments, a simple linear filtering technique is unable to obtain a

* Numbers in brackets refer to numbered references in the bibliography

satisfactory performance. In order to improve the performance, we use nonlinear methods including fuzzy theory, and neural network theory in our design. In this thesis we present the application of the split-spectrum processing coupled with a nonlinear signal classifier for ultrasonic flaw detection.

1.2 Propagation of Ultrasonic Wave in Solids

Most ultrasonic nondestructive evaluations are applied on solid materials such as steel and composites. An ultrasonic wave propagated in solid materials, in general, is affected by three factors: beam spreading, absorption, and scattering. Beam spreading is primarily decided by transducers and is a geometric function. Absorption results from the energy transformation by which the energy of ultrasonic wave is converted to the heat energy of specimen. This transformation losses energy permanently and cannot be used in material inspection. Scattering is caused by the reflection at grain boundaries, small cracks, and other material nonhomogeneities. This reflection changes the intensity of an ultrasonic wave depending on the microstructure of testing materials, therefore this phenomena, on the contrary, can be used to investigate the grain size or the size and orientation of the defect (i.e., flaw) of testing materials.

Both absorption and scattering cause the attenuation of ultrasonic waves by diminishing its intensity or its energy. The general attenuation behavior of ultrasonic signals in solid materials is shown in Figure 1.1. However, they limit the ultrasonic testing differently. Absorption is a direct conversion of ultrasonic wave energy to heat energy. This effect can be reduced by using lower frequencies with lesser absorption or

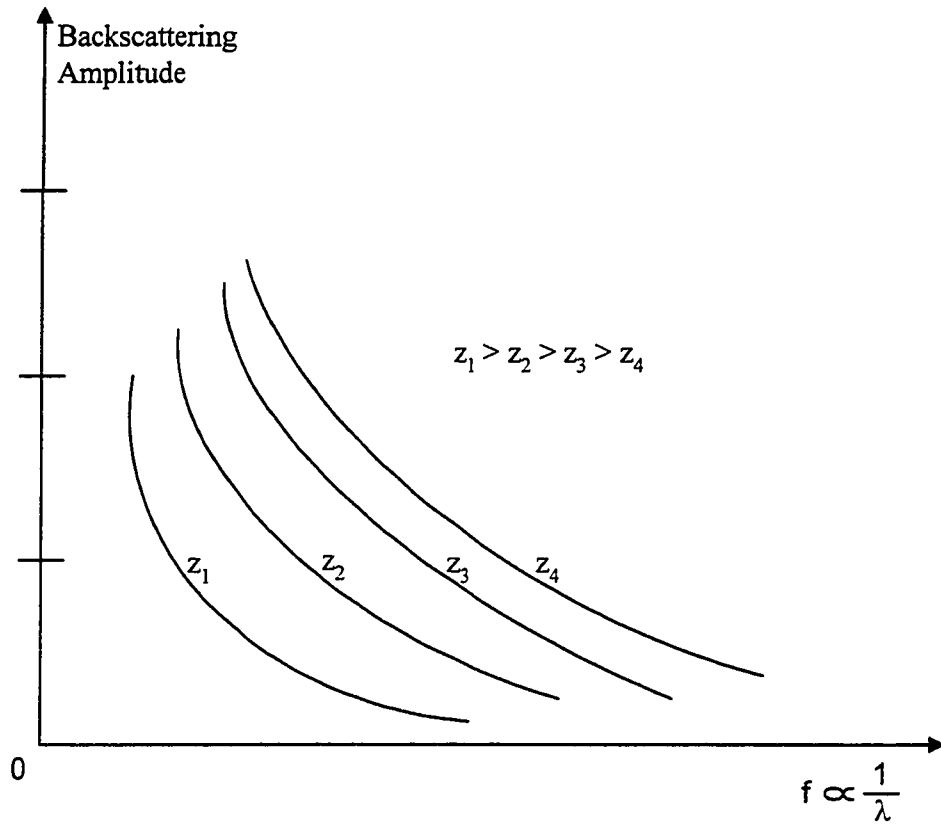


Figure 1.1 The Attenuation Behavior as a Function of Frequency and Position

increasing the intensity of ultrasonic waves. The scattering loss is determined by the grain diameter relative to ultrasonic wavelength. According to the ratio of the ultrasonic wave to the mean grain diameter (λ/\bar{D}), the effect [16] of scattering can be classified to three distinct regions: Rayleigh, Stochastic, and Diffusion regions as shown in Figure 1.2. In the Rayleigh region (i.e., $\lambda/\bar{D} > 1$, the wavelength is relatively large compared to grain diameter), the scattering coefficient is proportional to the fourth power of the frequency. In the regions of Stochastic (i.e., $\lambda/\bar{D} \cong 1$) and Diffusion (i.e., $\lambda/\bar{D} < 1$), the ultrasonic wave is scattered between grains and the scattering coefficient is proportional to the frequency squared. Our analysis deals with the Rayleigh scattering region. If a broad-band echo is used, the attenuation results in a downward shift of the spectrum in the frequency domain. More specifically, higher frequencies are attenuated more than lower frequencies; therefore, lower frequencies present higher amplitude than higher frequencies. In addition, in the Rayleigh region, due to the scattering phenomena, an upward shift of the spectrum in the frequency domain is also expected. The overall result is that the echo reflected from flaws has a lower frequency compared to that of the echo backscattered from internal microstructure of testing materials.

1.3 Ultrasonic Pulse-Echo Measurement

Ultrasonic inspection is typically performed using the pulse-echo method. In this method the same transducer is used as a transmitter and a receiver. A packet of broadband ultrasonic pulse would be fired by the transducer and travels through testing material.

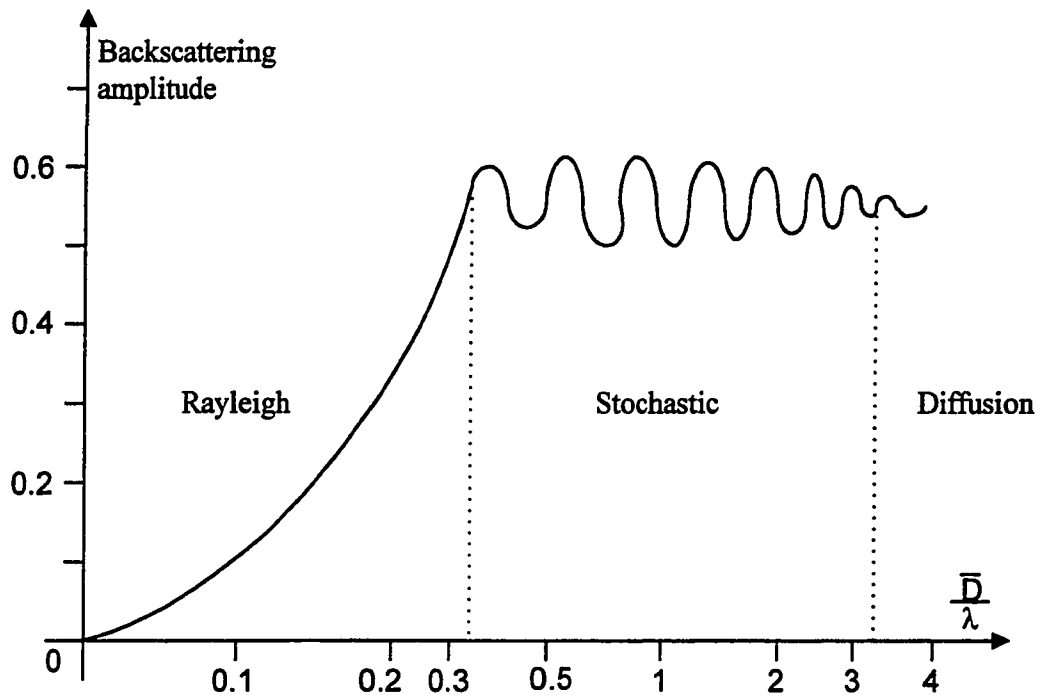


Figure 1.2 The Overall Scattering Behavior as a Function of Normalized Grain Diameter

When the ultrasonic pulse strikes cracks or grain boundaries it will be reflected running in the opposite direction in the testing material. Then the transducer receives the backscattered ultrasonic signal that contains the structure information of the testing material. Figure 1.3 illustrates a typical arrangement of laboratory equipment used in the pulse-echo method for the acquisition of ultrasonic backscattered signals. The major components of the system include an ultrasonic pulser, a transmitting/receiving piezoelectric transducer, a high-speed digitizer and a processing computer with IEEE-488 interfacing. The pulser and transducer are used to generate a burst of ultrasonic pulses and transmit them into the specimen of interest. The transducer also receives the backscattered ultrasonic signal and passes the signal to the digitizer. The high-speed digitizer converts the analog ultrasonic signal to digital signal such that the technology of modern digital signal processing can be used to process the ultrasonic signal. The function of the processing computer is to conduct the whole experimental procedure and process the acquired signal according to the methodologies developed in this thesis.

1.4 Brief Introduction to the Research

Our objective in this research is to develop an ultrasonic flaw detection system. The solution provided by this thesis includes two processes: signal feature extraction and signal classification. The signal feature extraction is to extract and enhance target signals from grain signals and is performed by using split-spectrum processing. The split-spectrum processing basically chops the ultrasonic signal using a class of bandpass filters. Signal classification has been studied for many years, and several methods have been

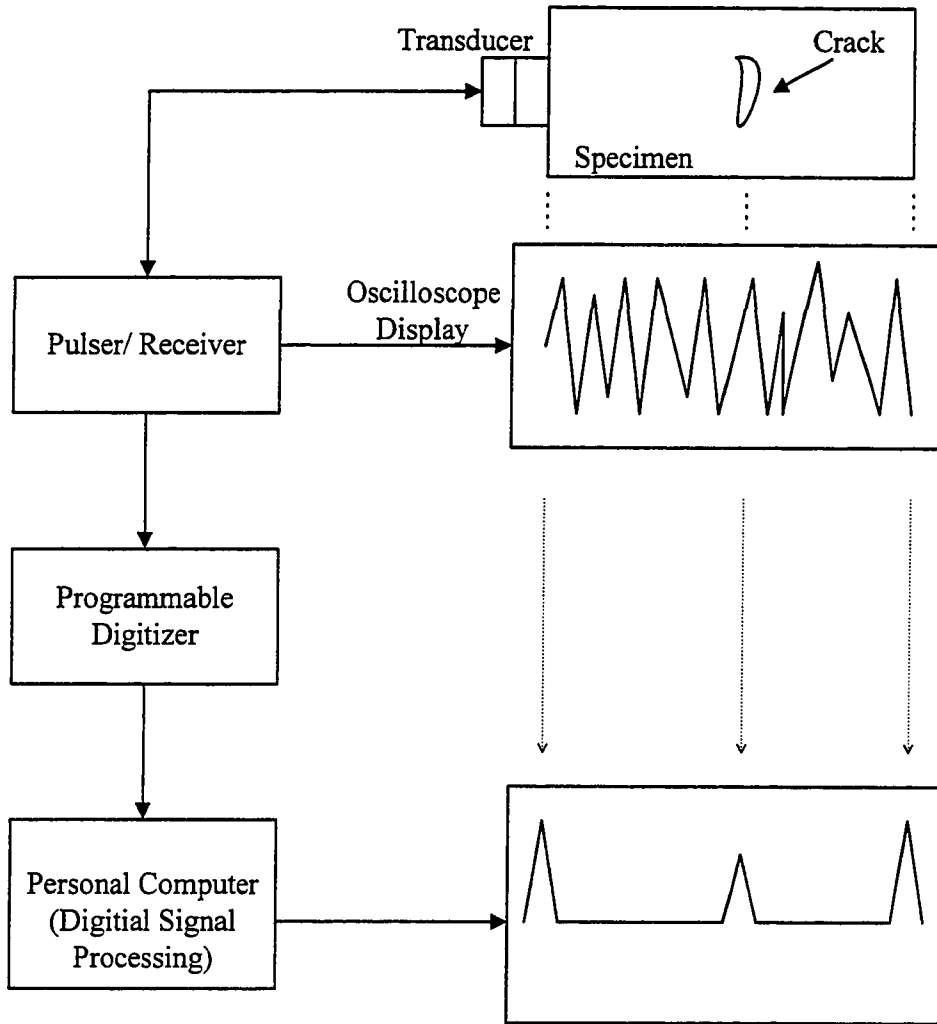


Figure 1.3 Pulse-Echo Measurement and Data Acquisition Equipment

successfully reported [21]. In this thesis, the statistical methods including the Bayes classifier and the MAP classifier are used in the ultrasonic detection problems. In general, the statistical methods estimate the probability of the presence of ultrasonic signals of interest. Therefore, the key issue is in the estimation of the signal probability density function (PDF). Besides, in this thesis, newly developed methodologies including a fuzzy classifier and a neural network classifier are also applied to the ultrasonic flaw detection problems. Fuzzy theory estimates the existing possibility of ultrasonic signal of interest, and the key issue is on the building of the fuzzy membership functions that are used to indicate the existing possibility of signals of interest. Neural networks are non-linear parallel mapping processing. Without any mathematical model of the interested signal, neural networks can learn the signal patterns by a training process. The training process iteratively uses some sample-input signals and their desired responses to adjust the connecting weights between neural nodes until the mapping error can be minimized. After a proper training, the neural network can work like a human brain to recognize target signals embedded in a noisy environment.

1.5 Thesis Outline

The organization of this thesis is as follows. A literature survey of split-spectrum processing in ultrasonic applications is presented in Chapter II. This chapter includes the fundamentals of the split-spectrum processing, the signal models after the SSP, and the selection considerations of the SSP filters in the application of NDE. Chapter III introduces the statistical discriminant functions. The fundamentals of the statistical

estimation are presented, and specifically the Bayes classifier and the MAP classifier are discussed in this chapter. Both methods use the estimation theory to estimate the parameters of the probability density function of interested signals.

In Chapter IV, we review the theory of fuzzy set, and introduce a novel fuzzy discriminant classifier used to detect the flaw echoes from background noise. The fuzzy discriminant classifier includes membership functions and a discriminant function. The fuzzy membership functions are created by incorporating the PDF (probability density function) of signals and background noise. The inclusion of the PDF can guarantee and enhance signal detection. The discriminant function is obtained by modifying the fuzzy entropy, and can utilize the output of fuzzy membership functions (i.e., a fuzzy set) to detect the target signals.

In Chapter V, a three-layer feedforward neural network is developed. This three-layer neural network is trained by using a backpropagation learning process. After properly training the neural network, the neural network can perform a highly complex non-linear mapping process. This non-linear processing can separate target signals from background noise by mapping them to different places in the signal space. In addition, the neural network designed for the detection is highly desirable, since the VLSI implementation for the real-time application is feasible. In Chapter VI, we compare the performances of the neural network and Bayes classifier to the performances of recently proposed techniques including the order statistical filters and the polarity thresholding in the application of ultrasonic flaw detection.

Both the simulated and experimental data are applied to all previous theories. The data is introduced in Chapter III, and used to test the SSP algorithm as well as all

classifiers. The test results are compared to find the best classifier. The last chapter, Chapter VII, presents the summary of this thesis work and future recommendations.

CHAPTER II

SPLIT SPECTRUM PROCESSING

In this chapter, we review the literature of the split spectrum processing (SSP) and present how to apply the SSP algorithm to the application of ultrasonic flaw detection. Section 2.1 briefly introduces some important discoveries concerning the SSP algorithm in ultrasonic applications in the last two decades. Section 2.2 shows the fundamentals of the SSP by studying its structure. The signal properties and the signal models after processed by SSP algorithm are discussed too. In addition, the significant differences of using orthogonal and non-orthogonal Gaussian filters in the SSP algorithm are presented in this section. Section 2.3 presents the considerations of selecting the parameters of the SSP filters. These parameters include the number of filters, the bandwidth of filters, and the center frequencies of filters. Besides, we explain why we select the Gaussian filters as the SSP channels for the application of ultrasonic flaw detection.

2.1 Introduction

In the application of ultrasonic non-destructive evaluation (NDE), the ultrasonic signal is composed by multiple backscattered grain and flaw echoes with random amplitude and phase. This causes the signal energy of both the flaw and the grain echoes spreading over the same frequency band; therefore, a single filter is unable to separate flaw echoes from grain echoes.

A suitable solution for this situation is to employ split-spectrum processing (SSP). The SSP divides the signal frequency band into several smaller frequency bands, and these frequency bands can be implemented by using FIR or IIR filters. Each filter extracts signal energy according to its frequency range. This property is very useful for the analysis of ultrasonic signals because the ultrasonic signal backscattered from grains is randomly distributed within the frequency bands, and the ultrasonic signal backscattered from flaws usually has a big amplitude and is concentrated on the frequency bands. Therefore the output from the SSP algorithm can be used to enhance the SNR of flaw signals and thereby to present their signal features.

In the last two decades, some research [22–29] shows that the SSP algorithm is capable to improve signal detection results especially in the presence of interference noise. Newhouse, Bilgutay, Saniie, and Furganson [22] found that clutter echoes are uncorrelated when the echo is simultaneously transmitting with two or more channels centered at different frequency bands. Therefore by using the SSP coupling with a minimization algorithm, they successfully improve the flaw-to-clutter (F/C) ratio. Bilgutay and Saniie [23] investigated the material grain size by using the SSP algorithm, and found that the SSP algorithm is useful in the applications of the industrial examination of large-grained materials.

In recent years, the ultrasonic flaw detection problem has been greatly improved by combining the SSP algorithm with a non-linear operation. Nihat, Bilgutay, Uthai, and Saniie [24] show that by using the SSP algorithm, at any time instant, clutter echoes have wide variation compared to flaw echoes. Therefore followed by a polarity thresholding operation, the SSP algorithm is able to detect the flaw echoes. In addition to the polarity

thresholding, several nonlinear operations such as the order statistic filter [7-8], the morphology filter [30] were presented in the last few years. All these papers present strong evidences to support that the SSP is a useful tool to enhance the SNR ratio in the NDE applications

However, due to the nature of ultrasonic signals (frequency agility and diversity caused by the backscattering of specimen), the tuning of the SSP frequency bands is very sensitive. Besides, filter parameters such as the number of filters, the bandwidth of filters, and the center frequencies of filters affect the results of the SSP algorithm. Lacking knowledge of how the phase and amplitude information is affected by the SSP algorithm, formulating the SSP algorithm becomes difficult. Therefore, for a particular application, to obtain these parameters we need to carefully examine signal properties. In the following section, we present the fundamentals of the SSP algorithm and then apply it to the NDE applications.

2.2 The Fundamentals of SSP

The purpose of the SSP is to enhance the signal SNR ratio by splitting signal spectrum into smaller frequency bands or channels. This method is very helpful if the spectrum of background noise is randomly distributed in the frequency domain and the spectrum of target signals is concentrated in the frequency domain. This is because that since the target signals appeared concentrically in the frequency domain, the correlation among the SSP channels could be used to enhance the SNR ratio. On the contrary, if the noise is randomly distributed on the SSP channels then the correlation will be small. Due

to this reason, in the design of the SSP, the selection of the SSP filter should be based on extracting the target signal by using their correlation on the SSP channels, which is decided by the parameters of the SSP filters, and the signal spectrum property [27].

The implementation of the SSP algorithm is shown in Figure 2.1. The received signal is denoted by $r(n)$, and the output of the i th filter is written as $z_i(n)=h_i(n)*r(n)$, where $h_i(n)$ is the impulse response of the i th filter and $*$ denotes the convolution operator. At any time instant, the filtered signals can be represented as $z(n)=[z_1(n), z_2(n), \dots, z_k(n)]^T$, where k is the total number of bandpass filters and T denotes the transpose. The vector $z(n)$ is defined as a signal feature which carries the signal characteristics and is dependent on the number of filters and filter parameters. Following the bandpass filters is a scaling factor. The scaling factor is employed to obtain the equally powered output signal on the SSP channels, because the power spectrum of received ultrasonic echoes is not uniformly distributed. This modification can equalize the contribution of all channels. The selection of scaling factor is discussed in the next subsection.

2.2.1 Signal Models of SSP. In order to detect flaw echoes, the SSP channels should cover the spectrum of target signals. But since the center frequency of target signals is unknown, the SSP channels should cover the overall frequency bands. In this case, the spectrum of target signals can be assumed to appear on all channels or only on some channels. Due to this assumption, partitioning frequency band as shown in Figure 2.2 is a suitable selection in which the bandpass filters are chosen with a partially overlapped Gaussian windows such that some correlation between the neighboring bands

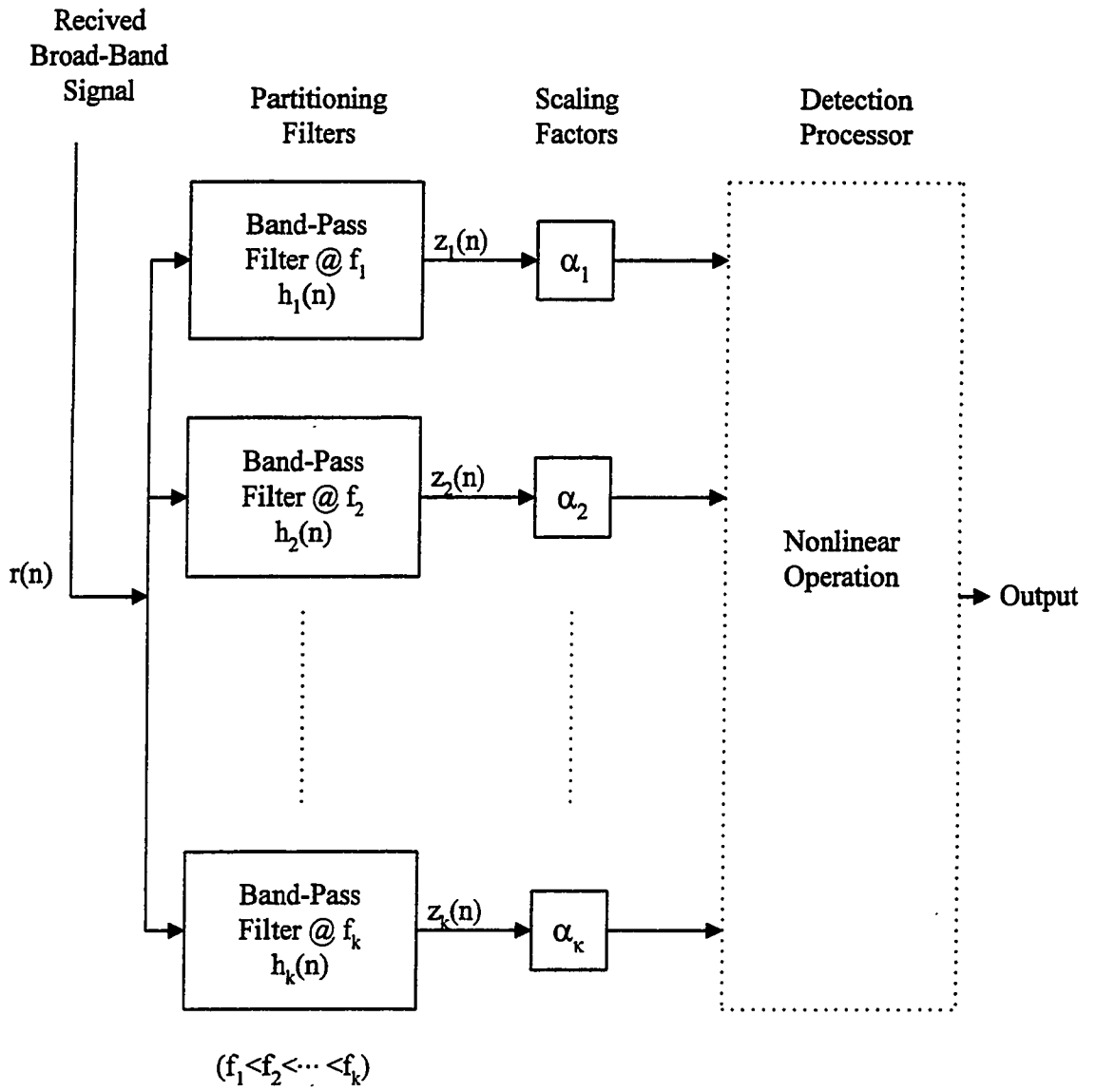


Figure 2.1 Block Diagram of Split-Spectrum Processor

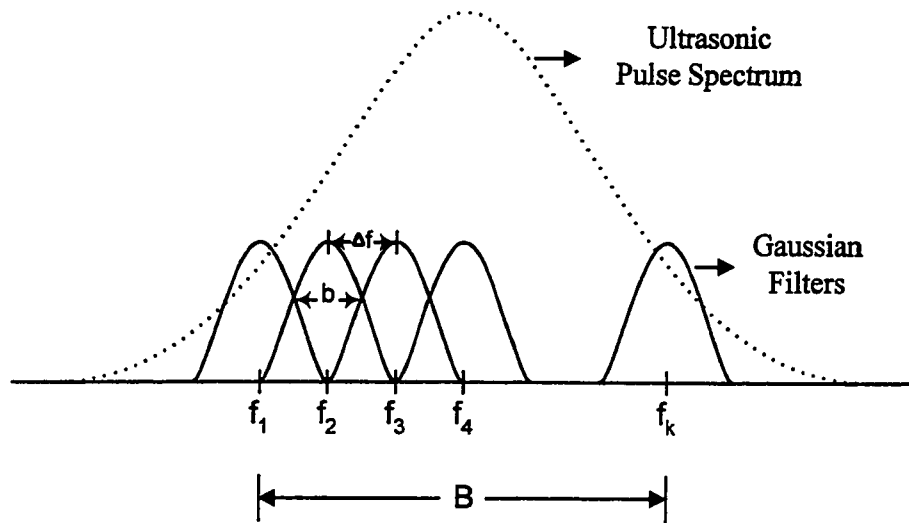


Figure 2.2 Split Spectrum Scheme using Gaussian Filters

is expected. In this figure, f_i is the center frequency of i th channel, and is decided by the number of the bandpass filters when each channel is designed to have the same bandwidth b . If the value of b is very small, then the output signal of the bandpass filters can be modeled as a narrowband signal and can be approximated [31] as

$$z_i(n) = \sum_l a_l \cos[(\omega_i + l\Delta\omega)nT + \theta_l(n)] \quad (2.1)$$

where $\Delta f \ll b$, z_i is assumed to be a Gaussian random variable. This assumption is obtained by investigating the histogram of the output signal of the bandpass filters. The a_l is random variable and is expected to be large in the vicinity of f_i . The random phase, θ_l , is governed by the random arrival time of echoes and is considered to be uniformly distributed from $-\pi$ to π . Therefore, the mean of the random variable z_i can be written as

$$E[z_i] = \sum_l E[a_l] E[\cos[(\omega_i + l\Delta\omega)nT + \theta_l(n)]] \quad (2.2)$$

The term $E[\cos[(\omega_i + l\Delta\omega)nT + \theta_l(n)]]$ is zero, so $E[z_i] = 0$. The variance can be obtained by

$$\sigma_{z_i}^2 = E[z_i^2] = \sum_l \frac{E[a_l^2]}{2} \quad (2.3)$$

From the Equation (2.1), we can obtain the following equation:

$$z_i(n) = \left[\sum_l a_l \cos(l\Delta\omega nT + \theta_l) \right] \cos(\omega_i nT) - \left[\sum_l a_l \sin(l\Delta\omega nT + \theta_l) \right] \sin(\omega_i nT) \quad (2.4)$$

This equation can be resolved to X and Y components:

$$z_i(n) = x(n) \cos(\omega_i nT) - y(n) \sin(\omega_i nT) \quad (2.5)$$

According to the central limit theory [41], for a large value of l , X and Y are normally distributed, and can be written as

$$f_x(x) = \frac{1}{\sigma\sqrt{2\pi}} \exp\left(-\frac{x^2}{2\sigma^2}\right) \quad (2.6)$$

$$f_y(y) = \frac{1}{\sigma\sqrt{2\pi}} \exp\left(-\frac{y^2}{2\sigma^2}\right) \quad (2.7)$$

Since the random variables a_i and θ_i are independent, the mean of variable X and Y are:

$$E[x] = \sum_i E[a_i] E[\cos(l\Delta\omega nT + \theta_i)] \quad (2.8)$$

$$E[y] = \sum_i E[a_i] E[\sin(l\Delta\omega nT + \theta_i)] \quad (2.9)$$

It is apparent that $E[x]=E[y]=0$. Therefore, the variance can be found by the following equations

$$\sigma_x^2 = E[x^2] = \sum_i \frac{E[a_i^2]}{2} = \sigma^2 \quad (2.10)$$

$$\sigma_y^2 = E[y^2] = \sum_i \frac{E[a_i^2]}{2} = \sigma^2 \quad (2.11)$$

From the Equation (2.4)-(2.11), the probability density function of x and y can be rewritten as

$$f_x(x) = \frac{1}{\sqrt{2\pi\sigma^2}} \exp\left(-\frac{x^2}{2\sigma^2}\right) \quad (2.12)$$

$$f_y(y) = \frac{1}{\sqrt{2\pi\sigma^2}} \exp\left(-\frac{y^2}{2\sigma^2}\right) \quad (2.13)$$

It can be proved that x and y are uncorrelated [32] such that $E[xy]=E[x]E[y]=0$. Then the joint probability of x and y can be presented as

$$f_{xy}(x, y) = \frac{1}{2\pi\sigma^2} \exp\left(-\frac{x^2 + y^2}{2\sigma^2}\right) \quad (2.14)$$

By using the polar coordinates, the joint probability of x and y can be rewritten as

$$f_{R\theta}(r, \theta) = \frac{r}{2\pi\sigma^2} \exp\left(-\frac{r^2}{2\sigma^2}\right) \quad (2.15)$$

Finally the distribution of R can be found by

$$f_R(r) = \int_{-\pi}^{\pi} f_{R\theta}(r, \theta) d\theta \quad (2.16)$$

which is

$$f_R(r) = \frac{r}{\sigma^2} \exp\left(-\frac{r^2}{2\sigma^2}\right) \quad (2.17)$$

Equation (2.17) is referred to as the Rayleigh probability function. The mean, the second moment, and the variance can be found in term of

$$E[r] = \sqrt{\frac{\pi}{2}} \sigma \quad ; \quad E[r^2] = 2\sigma^2 \quad ; \quad \sigma_r^2 = \left[2 - \frac{\pi}{2}\right] \sigma^2 \quad (2.18)$$

To confirm the theoretical derivation, an experimental ultrasonic data, as show in Figure 2.3, is processed by an eight-channel SSP algorithm, and then filtered by an envelope detector. Figure 2.4 shows the output of the SSP channels as well as the histogram of the envelope filtered signals. As shown in this figure, the histograms (bar lines) are very close to the Rayleigh probability function (dash line).

Since the spectrum of grain signals has a Gaussian shape as shown in Figure 2.5(a), the energy will be unevenly distributed on each channel when we apply it to the SSP algorithm. This is undesirable because other channels with large amplitude may suppress some channels with smaller amplitude in the detection processing. To solve this problem, power equalization is necessary on each channel and this is the reason we involve the scaling factor in the previous section. Since we are dealing with the statistical properties of the SSP and each channel should be treated equally, scaling by the standard

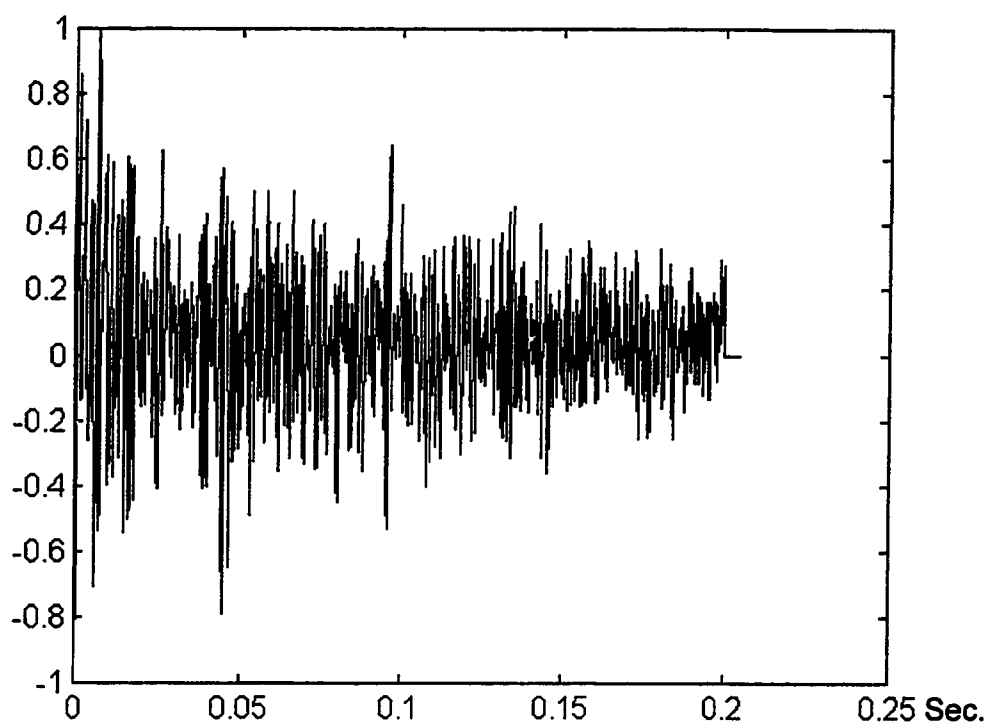


Figure 2.3 An Experimental Ultrasonic Signal (Transducer Center Frequency = 5 MHz, Sampling Rate = 100 MHz, Spicement : No 5 steel)

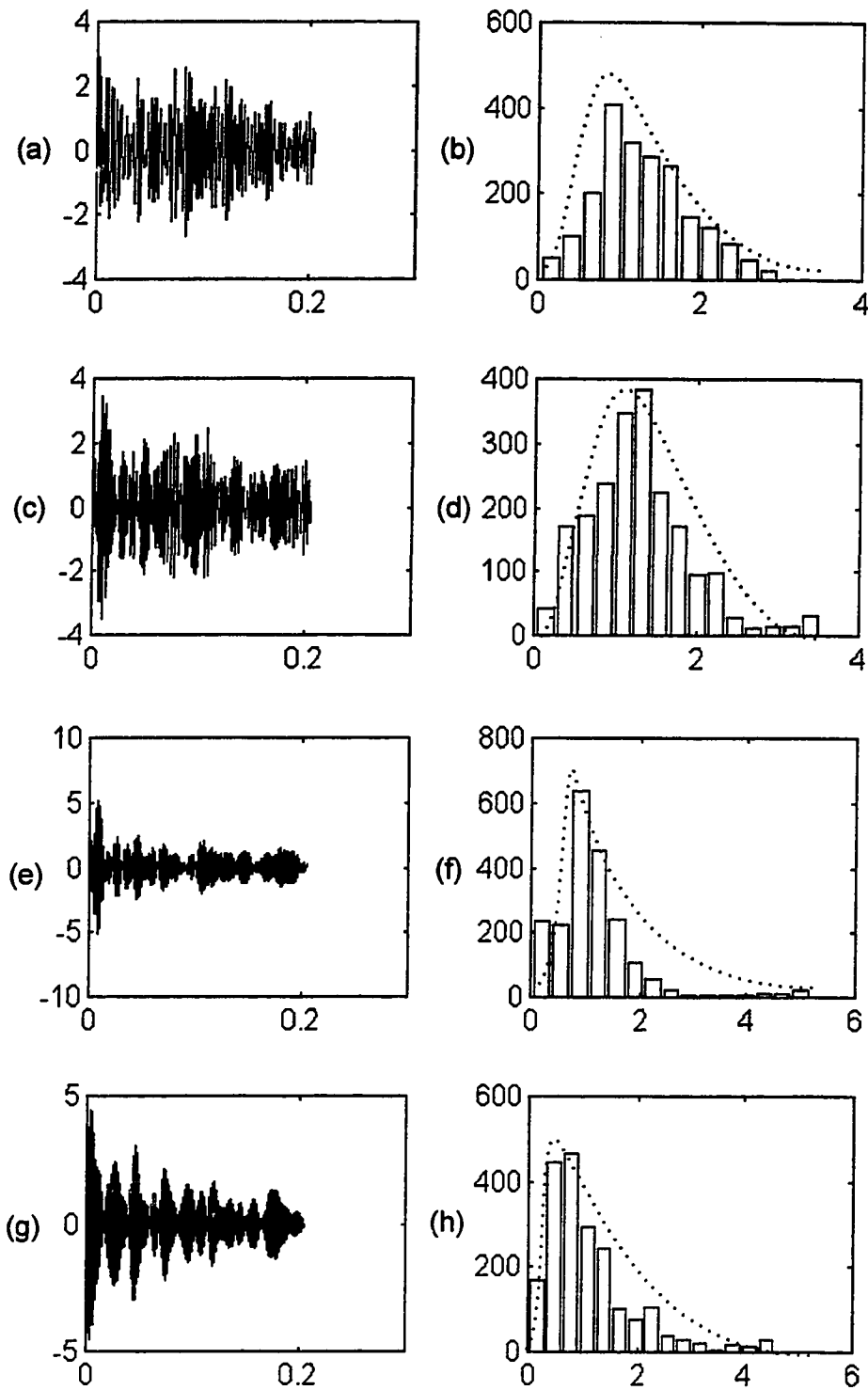


Figure 2.4 SSP Output and Amplitude Histogram of Grain Signals (Page 1 of 2)

- | | |
|----------------------|-----------------------------------|
| (a) Channel 1 Output | (b) Channel 1 Amplitude Histogram |
| (c) Channel 2 Output | (d) Channel 2 Amplitude Histogram |
| (e) Channel 3 Output | (f) Channel 3 Amplitude Histogram |
| (g) Channel 4 Output | (h) Channel 4 Amplitude Histogram |

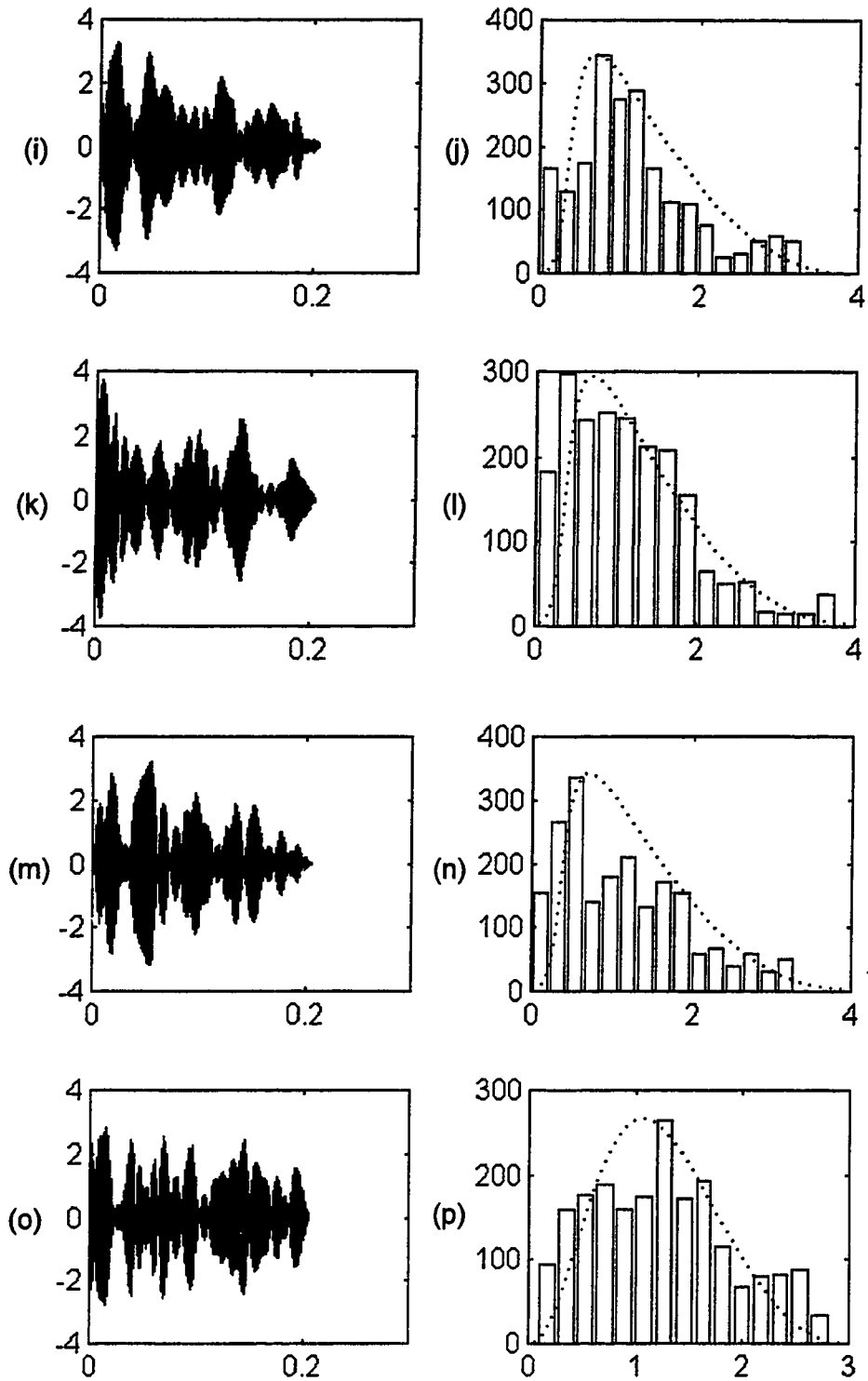


Figure 2.4 Continued (Page 2 of 2)

- | | |
|----------------------|-----------------------------------|
| (i) Channel 5 Output | (j) Channel 5 Amplitude Histogram |
| (k) Channel 6 Output | (l) Channel 6 Amplitude Histogram |
| (m) Channel 7 Output | (n) Channel 7 Amplitude Histogram |
| (o) Channel 8 Output | (p) Channel 8 Amplitude Histogram |

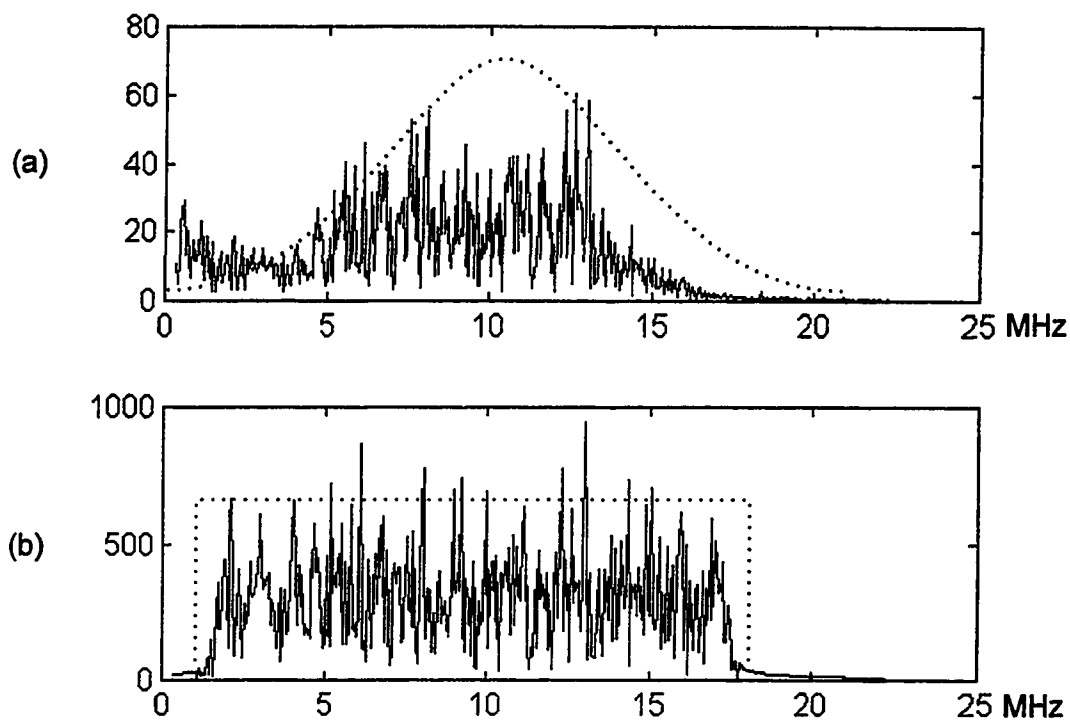


Figure 2.5 The Normalization Effect of SSP on Ultrasonic Signal Spectrum
 (a) The Spectrum of an Experimental Ultrasonic Signal
 (b) The Normalized Spectrum (Using 16 Gaussian Bandpass Filters, $B=1\text{MHz}$
 $f_1=2\text{MHz}$, $f_2=3\text{MHz}$,....., $f_{16}=17\text{MHz}$, the Center Frequency of Transducer= 10MHz)

deviation becomes a good choice. In this case, the output signal on each channel is normalized to have the same variance. Besides, the mean on each channel should also be normalized to zero (dc value does not carry the flow information). After normalization, the spectrum of grain signal can be represented as the band limited white noise signal as shown in Figure 2.5(b). This normalization also help to improve the signal model of the output signal of bandpass filters in Equation (2.1). Since the variance and the mean on each channel are normalized to be the same, the random variables, a_i and θ , could be assumed to be the same on all channels. The center frequency ω_i becomes the only difference variable in this signal model.

2.2.2 Statistical Properties of SSP. From a statistical point of view, the properties of SSP can be obtained by examining the correlation among the SSP channels. The fundamental estimation of the correlation is the second order cross correlation function, $E[z_i z_j]$, where z_i and z_j are the output from the channel i th and j th respectively (assuming the means are zero on all channels).

Basically, $E[z_i z_j]$ finds the expected value of the product $z_i z_j$, which is used to find the angle between two vectors in the linear algebra. Therefore, if the channels are orthogonal, the $E[z_i z_j]$ will equal to zero meaning that no correlation is existing. If the channels are non-orthogonal, then $E[z_i z_j]$ can give us the value of correlation. Therefore, it is reasonable to use the covariance matrix to represent the correlation among channels for further use. The covariance matrix is represented as

$$\Sigma = \begin{bmatrix} \sigma_{11}^2 & \sigma_{12}^2 & \cdots & \sigma_{1k}^2 \\ \sigma_{21}^2 & \sigma_{22}^2 & \cdots & \vdots \\ \vdots & \vdots & \cdots & \vdots \\ \sigma_{k1}^2 & \vdots & \cdots & \sigma_{kk}^2 \end{bmatrix} \quad k \text{ is the number of channels.} \quad (2.19)$$

where

$$m_i = \frac{1}{N} \sum_{n=1}^N z_i(n) \quad m_i \text{ is the mean on channel } i. \quad (2.20)$$

$$\sigma_{ij}^2 = \frac{1}{N} \sum_{n=1}^N z_i(n)z_j(n) - m_i m_j \quad \sigma_{ij} \text{ is the covariance of channel } i \text{ and } j. \quad (2.21)$$

The correlation is affected by the frequency bands of the SSP filters. If the bandwidth of the SSP channels is non-orthogonal and highly overlapped, then higher correlation will appear among the SSP channels; otherwise, the correlation will be small. In Figure 2.6, we present two SSP covariance matrices. Figure 2.6(a) is the covariance matrix obtained by eight non-orthogonal Gaussian channels and Figure 2.6(b) is the covariance matrix obtained by eight orthogonal Gaussian channels. Both of the non-orthogonal and the orthogonal Gaussian filters use same filter parameters (i.e., center frequencies, and bandwidth). In Figure 2.6(a), since the filters are overlapped we can find the correlation appeared between adjacent filters. However, the orthogonal filters provide a diagonal matrix as shown in Figure 2.6(b).

2.3 NDE Applications of SSP Filters

In the ultrasonic flaw detection problems, it has been found that the spectrum of grain signals is random but basically keeps in a Gaussian shape, and the spectrum of flaw

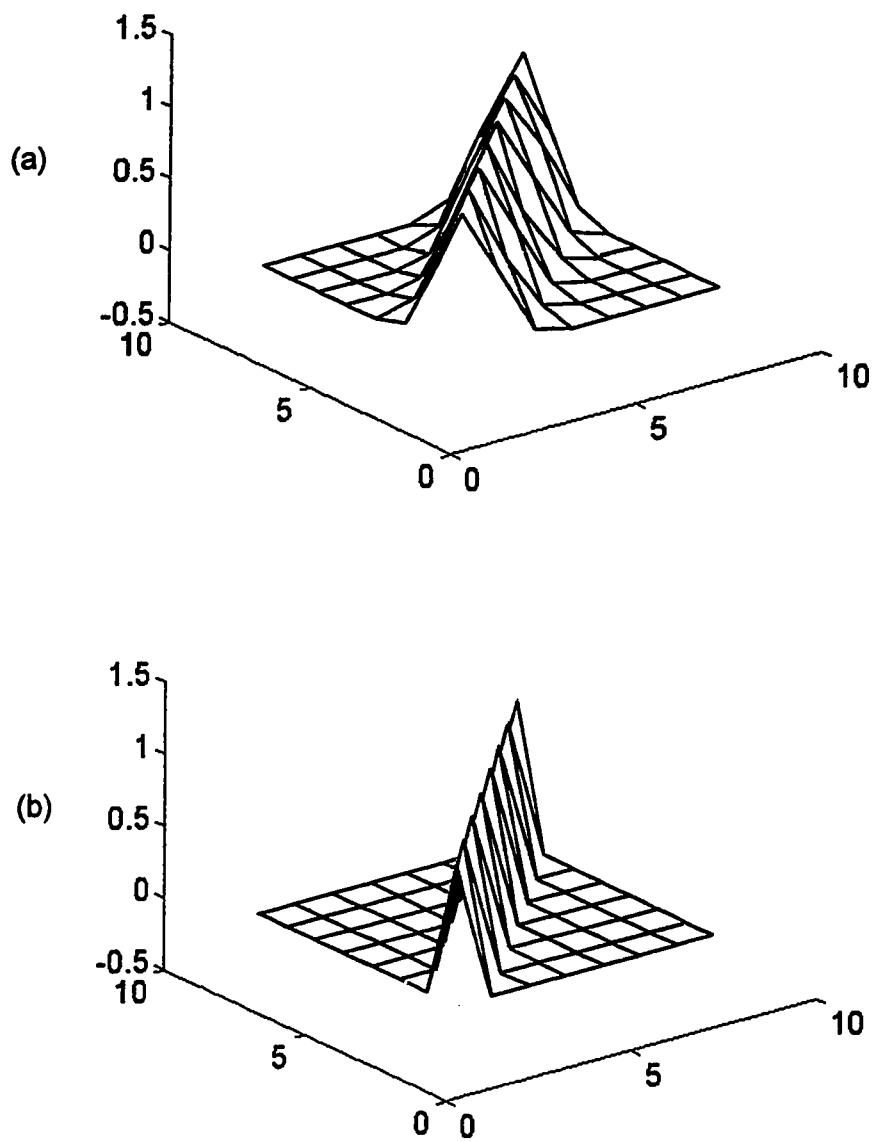


Figure 2.6 The Covariance Matrix
(a) Non-Orthogonal Channels
(b) Orthogonal Channels

signals is also in a Gaussian shape with an unknown center frequency. Besides, non-orthogonal signal space can present the signal correlation that is an useful factor to detect the similarity of the interested signals. This reason could contribute significant advantages in the NDE applications. Therefore, we select Gaussian filters to implement the SSP channel as shown in Figure 2.2. The parameters of selecting the filters include the number of the filters, the bandwidth of the filters, and the center frequencies of filters. In general, increasing the number of the bandpass filters will increase the correlation among SSP channels if the total frequency range covered by the filter banks remains unchanged. However, increasing the number of filters demands higher computational time. If the number of filters is too small then some information related to clutter or flaw echoes might be lost, because the filters cannot effectively cover the entire signal band. On the other hand, increasing the bandwidth while the number of filters is fixed will introduce large overlap, which as a result reduces the sensitivity of clutter noise to different frequency bands. In addition, since the SSP is trying to extract the signal features by using a class of bandpass filters, the bandwidth of the filters should be smaller than the bandwidth of the interested signals. A good discussion of the effects of the number of the SSP channels and the bandwidth of the SSP channels can be found in Saniie's research [27].

In the following chapters, several signal detection classifiers including statistical, Fuzzy, and neural network classifiers are developed to couple with the SSP algorithm and apply to the application of ultrasonic flaw detection. In order to compare their performance, a parameter set will be selected in the next chapter and used in the rest of the chapters such that the comparison can be reasonable.

CHAPTER III

STATISTICAL DISCRIMINANT FUNCTIONS

3.1 Introduction

In the previous chapter, we introduced the SSP algorithm that, according to the signal frequency diversity, creates the signal feature vectors containing the information related to the microstructure of testing materials. In this chapter, we apply statistical discriminant functions to the signal feature vectors for detecting the flaw echoes embedded in a noisy environment. In recent years, statistical methods have been successfully used in ultrasonic flaw detection and improved ultrasonic medical imaging [23], [33-39]. In particular, minimum detection and polarity thresholding [23],[33] have been studied extensively and shown to be effective for flaw detection. These results present evidence that the statistical classifiers are capable of separating flaw echoes from clutter echoes as long as they are able to classify the statistical differences of clutter and flaw echoes.

This chapter introduces two statistical methods and applies them to the application of ultrasonic flaw detection. In Section 3.2, we present the Bayes classifier [40]. The Bayes classifier utilizes the statistical differences of clutter and flaw echoes over the frequency bands to separate them. Specifically, the probabilities of the appearances of both the clutter and flaw echoes will be estimated, and the likelihood ratio is utilized to produce a discriminant function. In Section 3.3, we develop the maximum a posteriori (MAP) estimation to detect ultrasonic flaw echoes. The objective of the maximum a posteriori

estimation is to enhance the signal feature vectors obtained by using the SSP algorithm, and we then calculate the variance of the enhanced feature vectors to determine the signal pattern (i.e., either clutter or flaw echoes). In this chapter, the performances of Bayes classifier and MAP classifier are examined by using both the simulated and experimental data. The results are presented in Section 3.4.

3.2 Bayes Classifier

In the development of Bayes classifier [40], two hypotheses, H_0 and H_1 , are assumed to exist in the signal space. The hypothesis, H_0 , represents a flaw echo embedded in clutter echoes, and the hypothesis, H_1 , represents clutter echoes. By this assumption, the criterion for decision making can be written as

$$\phi(z) = \frac{p(z/H_0)}{p(z/H_1)} > \frac{p(H_1)}{p(H_0)} \rightarrow H_0 \quad (3.1)$$

$$\phi(z) = \frac{p(z/H_0)}{p(z/H_1)} < \frac{p(H_1)}{p(H_0)} \rightarrow H_1 \quad (3.2)$$

where $\phi(z)$ is the likelihood ratio serving as the discriminant function and z is the output of the SSP channels after normalized by the scaling factors (discussed in Chapter II). In Equations 3.1 and 3.2, $p(H_0)$ is the probability of the presence of flaws, $p(H_1)$ is the probability of the presence of clutter, and $p(H_1)/p(H_0)$ is the detection threshold. $p(z/H_0)$ is the probability density function of flaw-plus-clutter, and $p(z/H_1)$ is the probability density of clutter echoes.

In the design of the Bayes classifier, the major barrier is to estimate a priori probability density functions for both flaw and clutter classes. To solve this problem, we

inspected the histogram of the ultrasonic signals at the output of the SSP channels and found they were in a Gaussian shape. According to this observation, we assumed that the elements of the feature vectors (i.e., the output of SSP channels) are Gaussian-distributed, and then the joint probability density function of the elements of feature vectors can be represented as the following

$$f(z) = \frac{1}{(2\pi)^{k/2} (|\Sigma|)^{1/2}} \exp[-\frac{1}{2}(z - M)^T \Sigma^{-1}(z - M)] \quad (3.3)$$

where $|\Sigma|$ is the determinant of the covariance matrix Σ defined in Equation 2.19, the matrix Σ^{-1} is the inverse of Σ , and k is the dimension of the feature vectors. Since it is a normal distributed feature vector, it is more convenient to write the likelihood ratio (i.e., discriminant function) in a log form:

$$\ln \phi(z) = -\frac{1}{2}[(z - M_0)^T \Sigma_0^{-1}(z - M_0)] + \frac{1}{2}[(z - M_1)^T \Sigma_1^{-1}(z - M_1)] \quad (3.4)$$

To obtain the threshold value, we assumed that the probability of $p(H_0)$ and the probability of $p(H_1)$ are equal. This assumption is made according to the fact that only two classes exist within the signal space. By using this assumption, the decision rule of Bayes classifier can be expressed as

$$\ln \phi(z) > 0 \rightarrow H_0 \quad (3.5)$$

$$\ln \phi(z) < 0 \rightarrow H_1 \quad (3.6)$$

Since the probabilities for the hypotheses H_0 and H_1 are not necessary to be equal, the threshold value may not be zero. In practice, the threshold value can be found by carefully examining the discriminant function. Finally, the overall system diagram is drawn in Figure 3.1.

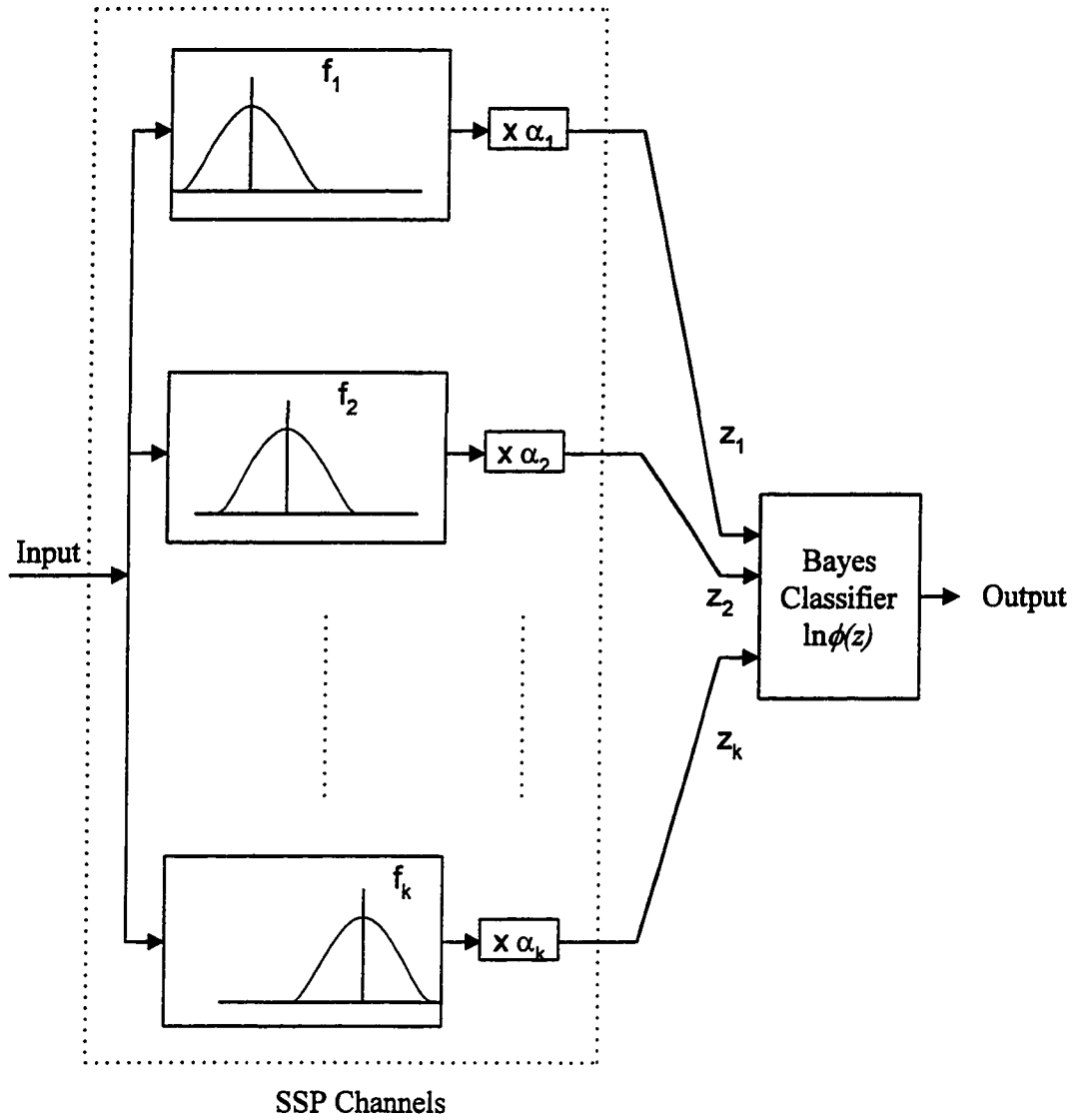


Figure 3.1 The Block Diagram of Bayes Discriminant System

In practice, we applied the SSP algorithm to grain signal and grain plus a target signal to find the parameters, Σ_0 , Σ_I , M_0 , and M_I . In this study, the backscattered echo from the back surface of the test material was used to simulate the target signal. This is due to the fact that the backscattered echo from the back surface of testing materials has the similar physical characteristics as the flaw echoes.

In the next section, we present another statistical method, MAP, which estimates the flaw echoes with the statistical information of clutter and without any prior knowledge of flaw echoes.

3.3 Maximum A Posteriori (MAP) Estimation Classifier

By using the Bayes classifier, the major barrier is to estimate a priori probability density for both clutter and flaw echoes. In the following section, we develop another statistical methodology that without estimating the prior knowledge of flaw echoes can still detect the flaw echoes when the flaw-to-clutter ratio is about 0dB. This methodology involves three processes, as shown in Figure 3.2. The first process is the SSP algorithm that, as discussed in Chapter II, creates the signal features according to the signal frequency diversity resulting in the improvement of SNR ratio. The second process is called the Maximum A Posteriori (MAP) estimation. This estimation can enhance the feature vectors by maximizing a posteriori conditional density that is useful in finding different types of estimates of random vectors. Since the enhancement is performed according to the statistical properties of clutter echoes, the processed feature vectors will present similar statistical parameters such as the mean or variance for clutter echoes but

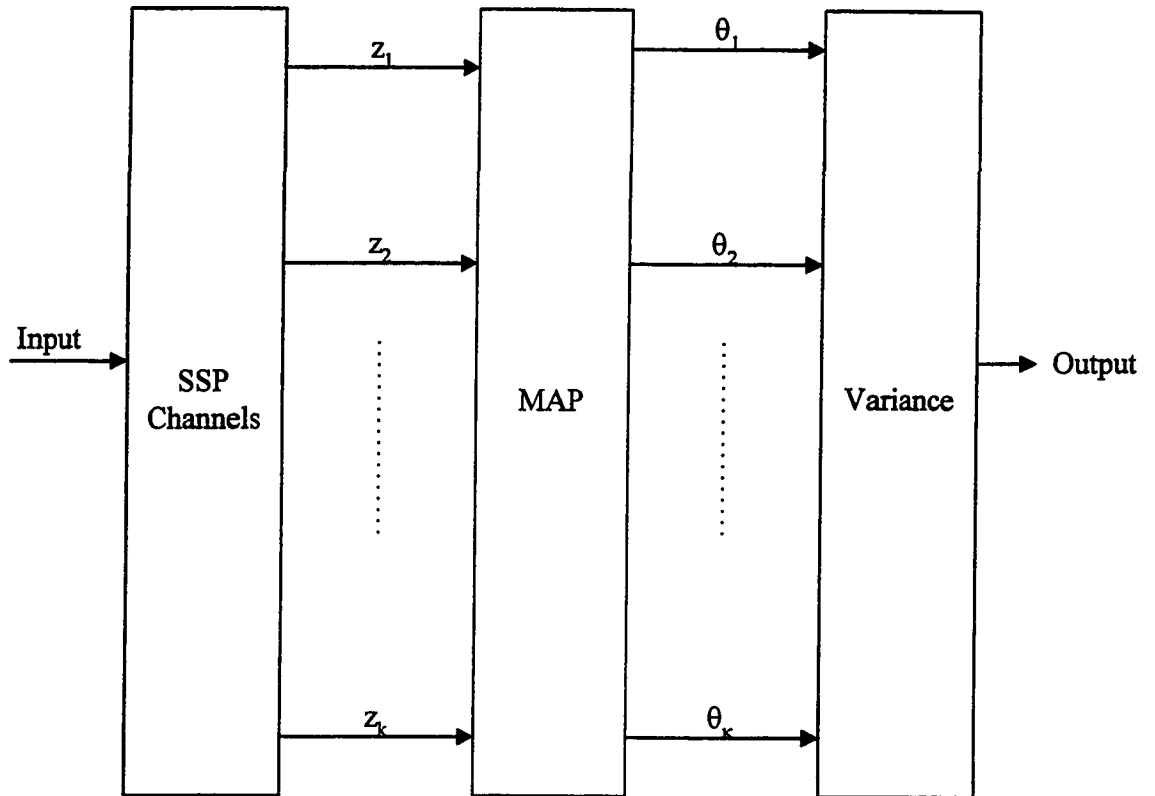


Figure 3.2 The Block Diagram of MAP Classifier

not for flaw echoes. Therefore, by calculating the simple variance of the feature vectors we are able to filter out flaw echoes.

3.3.1 Mathematical Derivation. To derive the mathematical representation, we assume that the observed signal can be written as

$$z = \omega + \theta \quad (3.7)$$

where z is the output of the SSP channels, ω represents clutter echoes and θ represents flaw echoes. Then due to the fact that the joint probability density function of the elements of the clutter feature vectors is assumed to be Gaussian distribution, the following conditional density function can be held.

$$f(\omega) = \frac{1}{\sqrt{(2\pi)^k |\Sigma|}} \exp\left(-\frac{1}{2} \omega^T \Sigma^{-1} \omega\right) \quad (3.8)$$

with a corresponding assumption in Equation (3.7), Equation (3.8) becomes

$$f(\theta | \omega) = \frac{1}{\sqrt{(2\pi)^k |\Sigma|}} \exp\left[-\frac{1}{2} (z - \theta)^T \Sigma^{-1} (z - \theta)\right] \quad (3.9)$$

It is more convenient to write the conditional density function in a log form.

$$\ln f(\theta | \omega) = -\frac{1}{2} \ln[(2\pi)^k |\Sigma|] - \frac{1}{2} (z - \theta)^T \Sigma^{-1} (z - \theta) \quad (3.10)$$

In order to estimate θ , we maximize $f(\theta | \omega)$ by the following equation.

$$\frac{\partial \ln f(\theta | \omega)}{\partial \theta} = \frac{\partial}{\partial \theta} \left[-\frac{1}{2} (z - \theta)^T \Sigma^{-1} (z - \theta)\right] = 0 \quad (3.11)$$

$$\Rightarrow \frac{\partial}{\partial \theta} [z^T \Sigma^{-1} z - \theta^T \Sigma^{-1} z - z^T \Sigma^{-1} \theta + \theta^T \Sigma^{-1} \theta] = 0 \quad (3.12)$$

$$\Rightarrow (-z^T \Sigma^{-1})^T - \Sigma^{-1} z + [\Sigma^{-1} + (\Sigma^{-1})^T] \cdot \theta = 0 \quad (3.13)$$

Therefore the estimation of θ can be obtained as

$$\theta = [\Sigma^{-1} + (\Sigma^{-1})^T]^{-1} \cdot [(z^T \Sigma^{-1})^T + \Sigma^{-1} z] \quad (3.14)$$

Since the vector z represents either clutter signal or clutter plus a flaw echo, the vector θ is expected close to a zero vector when a clutter signal appears, and a non-zero vector when clutter plus a flaw echo appears. In order to classify the estimated feature vectors for either clutter or a flaw echo, we calculate the variance of the estimated feature vectors as the threshold value.

3.4 Simulated Results

To verify the effectiveness of the previous statistical methods, we perform a computer simulation. According to the research of Saniie [1], the spectrum of the backscattered ultrasonic signal is expected an upward shift due to scattering, and a downward shift due to attenuation. Therefore, in order to generate the grain-scattering signal, 512 Gaussian shape echoes with a normal distributed amplitude are superimposed on uniformly distributed positions. These Gaussian echoes have a 7 MHz center frequency and a bandwidth of 2.5 MHz. The sampling rate is 100 MHz, and due to random interference of multiple echoes, the spectrum is random spreading from 1MHz to 13MHz. The flaw echo was simulated by a single Gaussian echo ($f_c=5\text{MHz}$ and $\text{BW}=2.5\text{MHz}$) with a desirable amplitude such that the ratio of the flaw echo to the largest possible clutter echo has a ratio less than or equal to unity (i.e., 0 dB). Then the superposition of the grain-scattering signal and the simulated flaw echo at a known position results in the simulated

signal. Once the simulated signal is obtained, the statistical classifiers are tested with different clutter signal patterns. A typical processed result is shown in Figure 3.3.

In the design of the SSP channels, three parameters, the number of filter, the bandwidth of filters, and the center frequencies of filters are critical. These parameters decide the correlation among the SSP channels and thereby play the key roles in the investigation of the frequency diversity. Since the transmitted echoes only cover a finite band of frequency, a finite number of filters can be used for splitting the spectrum. We have examined the processed results by using 4, 8, and 16 SSP channels, as shown in Figure 3.4 –3.6. In these figures, the frequency range covered by the filter bank is from 1 MHz to 12 MHz, and each filter has a 1 MHz 3-dB bandwidth. The results show that as long as the filter bank can cover the entire signal band, an increasing of the SSP filters did not show much improvement in the processed output. For a given number of filters on the SSP algorithm, increasing the bandwidth of the filters introduces large overlap in each frequency band and results in too much correlation. This effect will reduce the sensitivity of clutter noise to the different frequency bands, and consequently, the ability of detection will be reduced as shown in Figure 3.7 – 3.9. In these figures, the filter bank covers from 1 MHz to 12 MHz and the number of filters is 16. The bandwidth of filter is increased from 1 MHz to 2 MHz. The results show that the performance of the Bayes classifier is significantly decreased, and this is caused by the disability of extracting the target information from the signal. However, since the MAP classifier does not use target information; therefore, on the contrary, the sensitivity of flaw echoes, compared with clutter echoes, is improved and results in the improvement of the MAP performance.

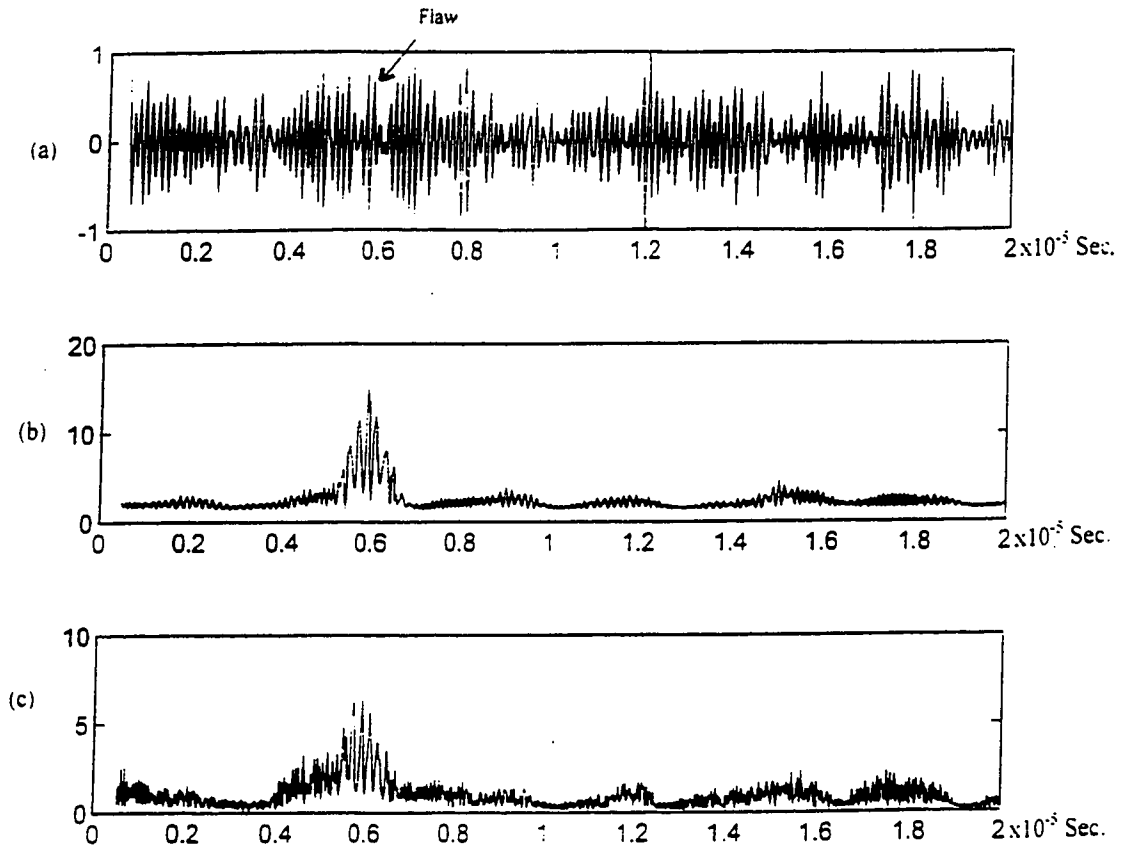


Figure 3.3 The Typical Processed Results by using Statistical Classifiers

- (a) The Simulated Ultrasonic Signal,
- (b) The Processed Result by using Bayes Classifier,
- (c) The Processed Result by using MAP Classifier.

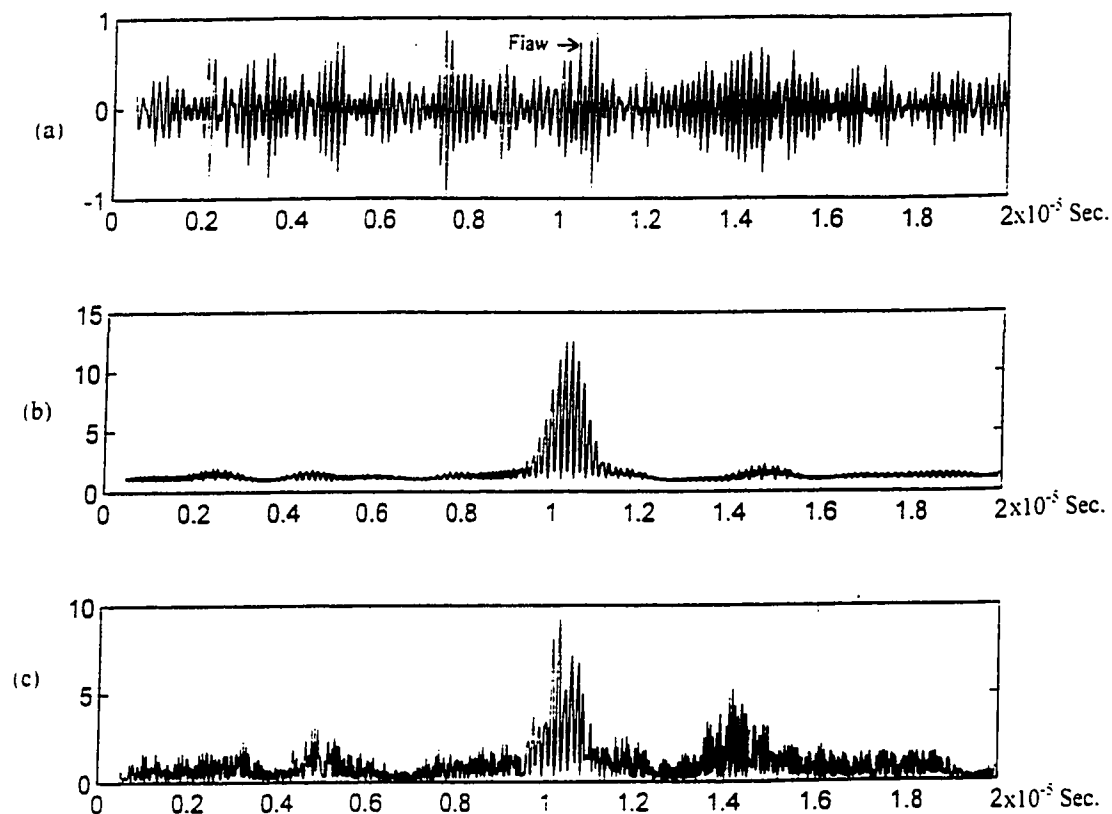


Figure 3.4 The Processed Results by using 4 SSP Channels (BW=1 MHz)
(a) The Simulated Ultrasonic Signal,
(b) The Processed Result by using Bayes Classifier,
(c) The Processed Result by using MAP Classifier.

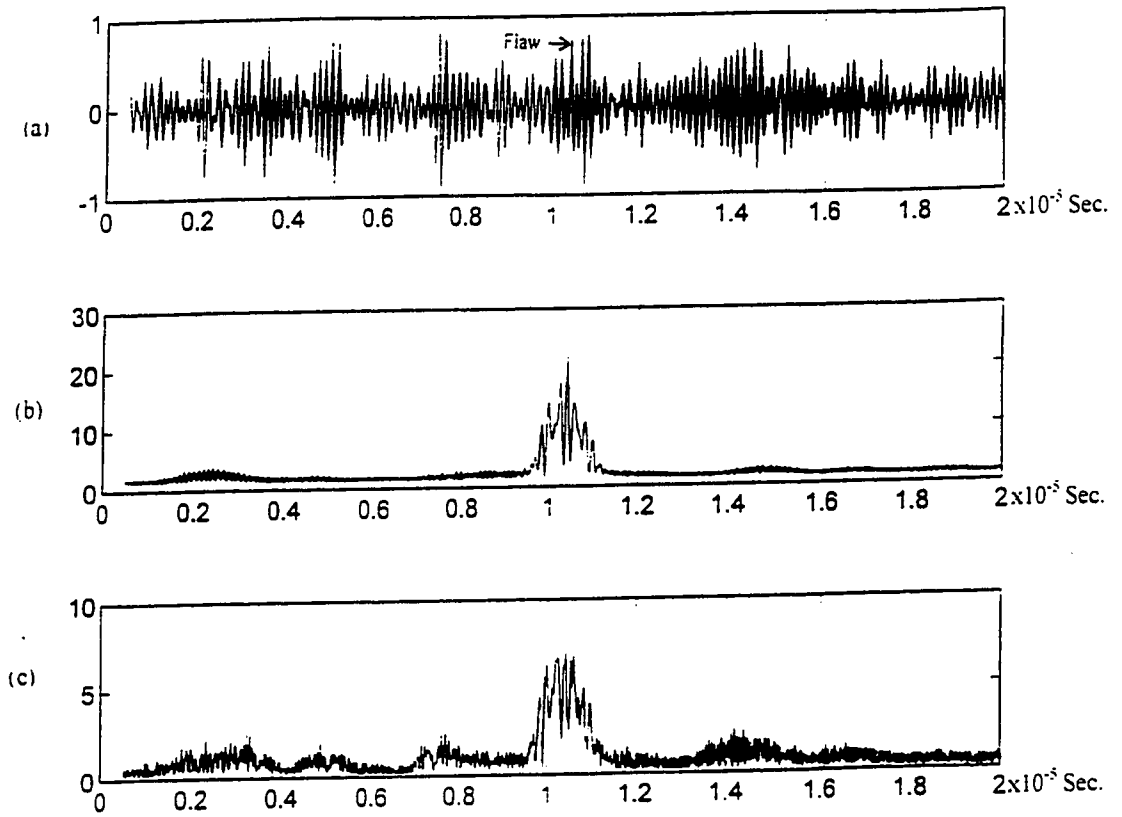


Figure 3.5 The Processed Results by using 8 SSP Channels (BW=1 MHz)

- (a) The Simulated Ultrasonic Signal,
- (b) The Processed Result by using Bayes Classifier,
- (c) The Processed Result by using MAP Classifier.

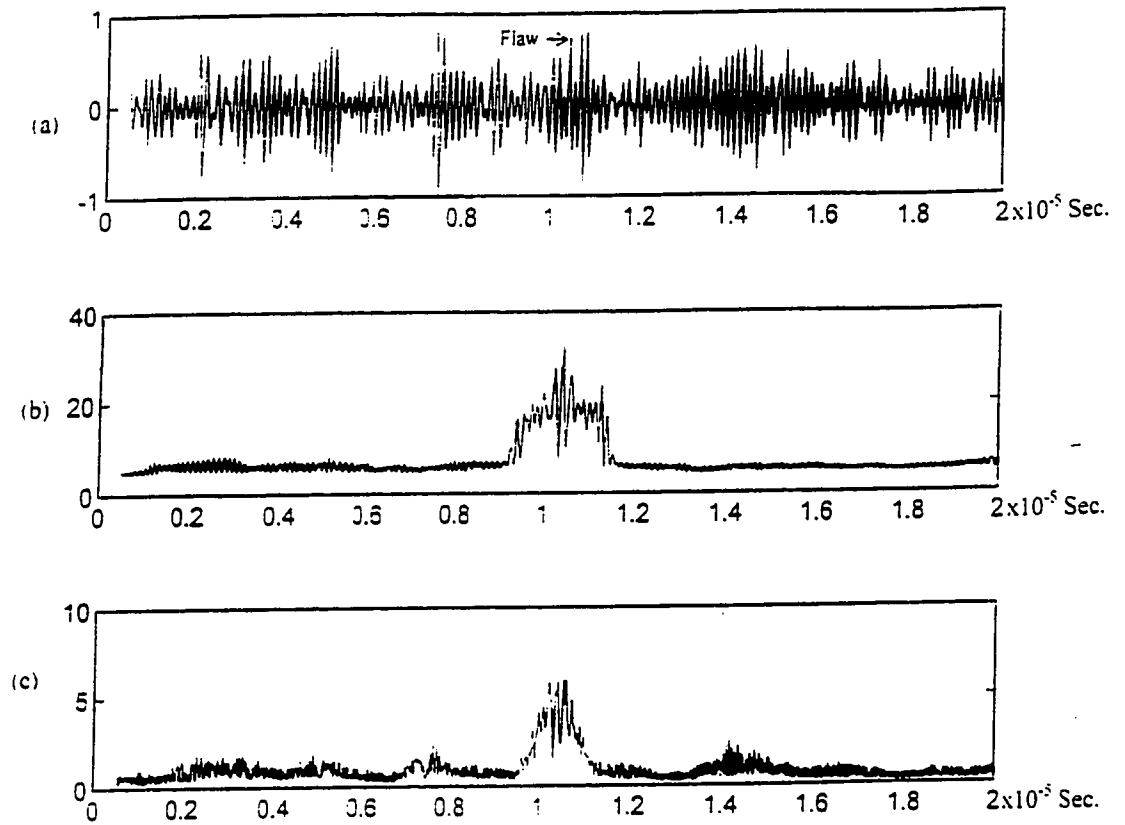


Figure 3.6 The Processed Results by using 16 SSP Channels (BW=1 MHz, Signal 1)

- (a) The Simulated Ultrasonic Signal,
- (b) The Processed Result by using Bayes Classifier,
- (c) The Processed Result by using MAP Classifier.

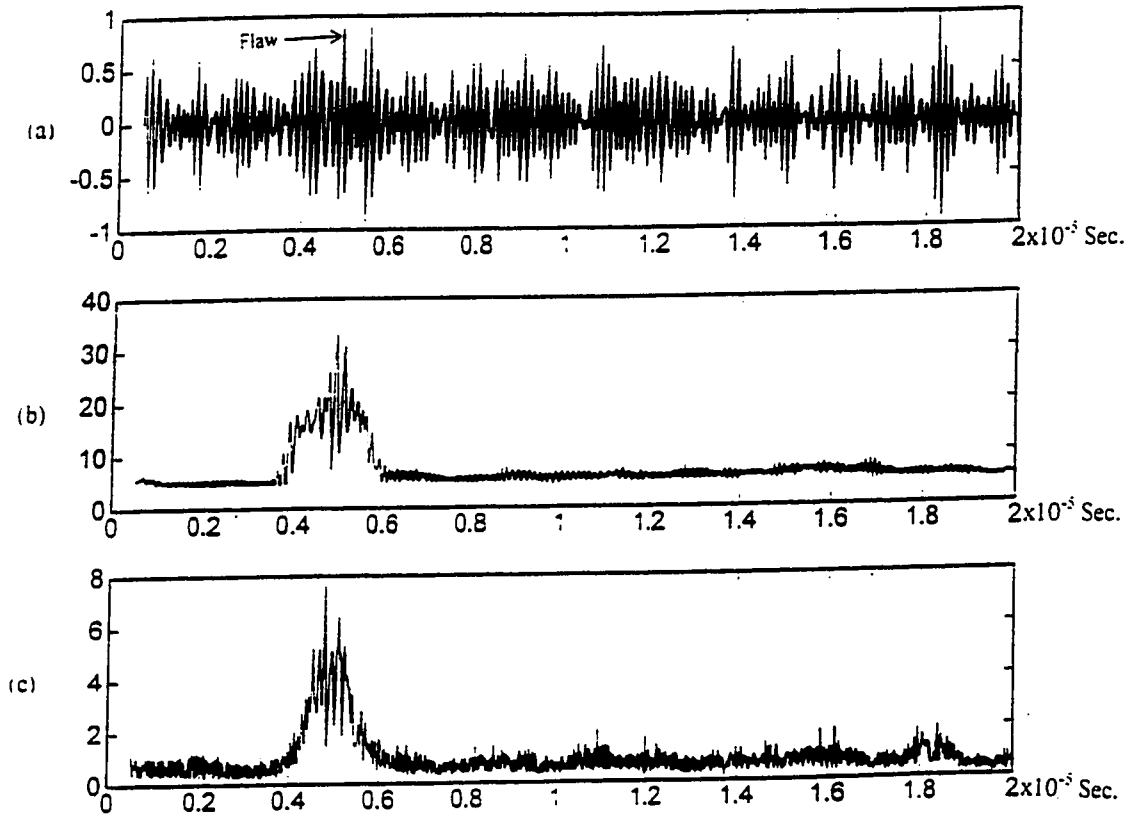


Figure 3.7 The Processed Results by using 16 SSP Channels (BW=1 MHz, Signal 2)

- (a) The Simulated Ultrasonic Signal,
- (b) The Processed Result by using Bayes Classifier,
- (c) The Processed Result by using MAP Classifier.

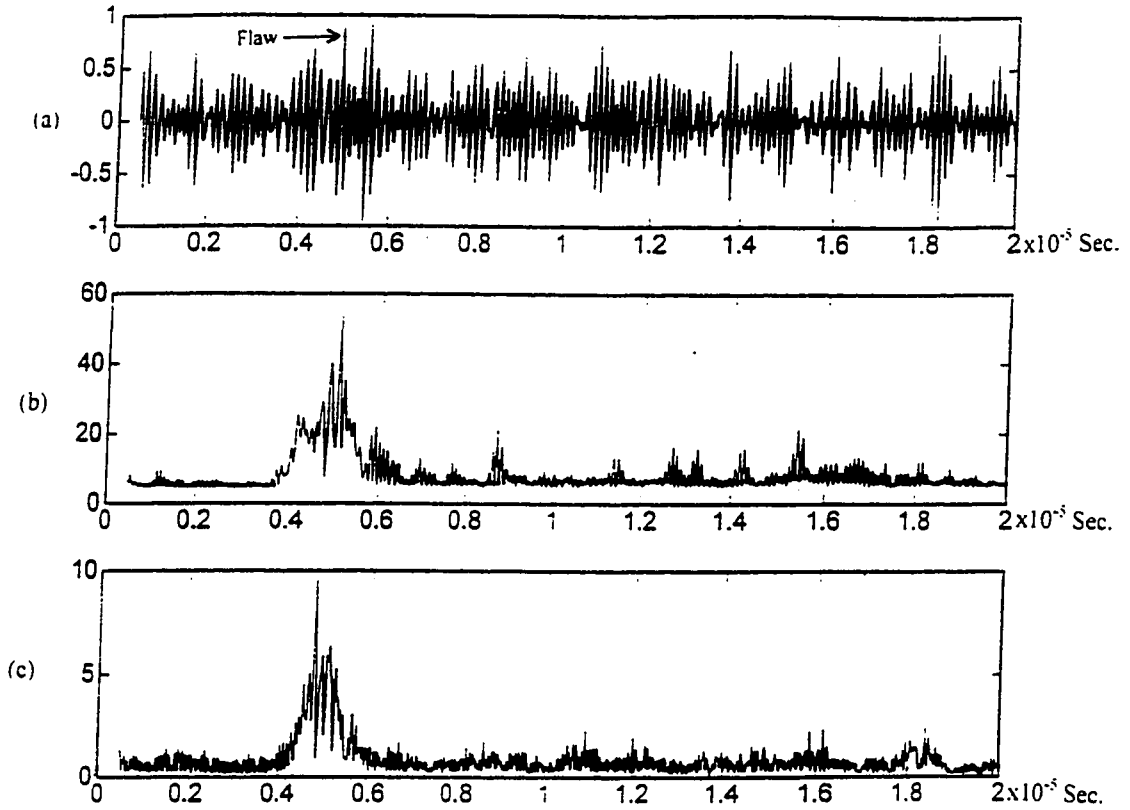


Figure 3.8 The Processed Results by using 16 SSP Channels (BW=1.5 MHz)

- (a) The Simulated Ultrasonic Signal,
- (b) The Processed Result by using Bayes Classifier,
- (c) The Processed Result by using MAP Classifier.

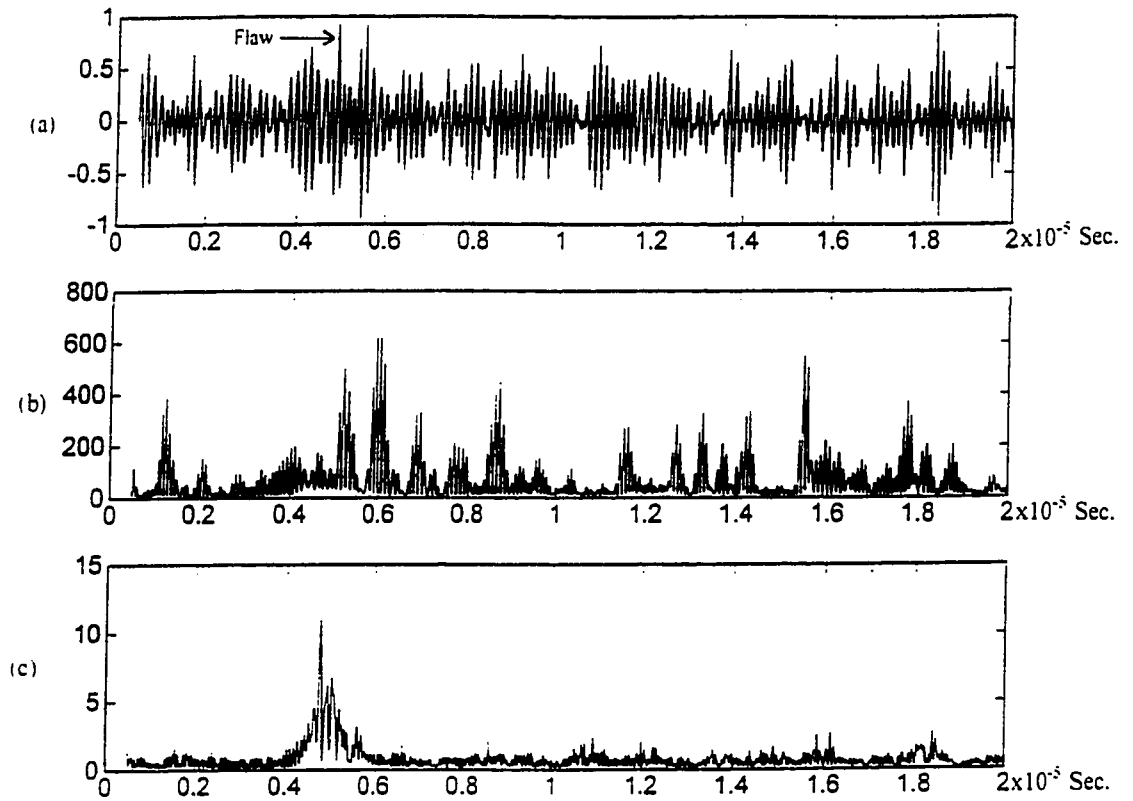


Figure 3.9 The Processed Results by using 16 SSP Channels (BW=2 MHz)

- (a) The Simulated Ultrasonic Signal,
- (b) The Processed Result by using Bayes Classifier,
- (c) The Processed Result by using MAP Classifier.

To compare the performance of Bayes classifier and MAP classifier, we use the computer simulated signals with different cutter patterns and flaw locations to test both the Bayes and the MAP classifiers. To achieve a reliable performance, 20 independently simulated signals were used. In the test, a total of 8 SSP channels with a 1.5 MHz 3-dB bandwidth ranging from 1.5 MHz to 13.5 MHz were used. The flaw-to-clutter (F/C) ratio for all simulated signals was kept about 0 dB. Then, the processed flaw-to-clutter ratio is examined and summarized in Table 3.1. As shown in this table, the average F/C ratio enhancement for Bayes classifier is about 5.95 and the standard deviation is 1.41. The average F/C ratio enhancement for the MAP classifier is 3.19 with a standard deviation of 0.77. This provides evidence that the performance of the Bayes classifier is better than that of the MAP classifier. The result is expected because the Bayes classifier utilizes not only the statistical properties of clutter signal but also the statistical properties of flaw echoes. However, the MAP utilizes the information of the clutter signal only and results in a poor performance.

3.5 Experimental Results

To illustrate the effectiveness of the SSP algorithm coupled with the Bayes classifier or the MAP classifier in the application of ultrasonic flaw detection, an experimental ultrasonic signal was measured as discussed in Chapter I. The experiment was conducted by using a steel specimen with an average grain size about 50 μ m. The experimental data was measured using a Panametrics broadband transducer with a 7 MHz center frequency. The measurement was made using the contact technique and the data was acquired using

Table 3.1 Flaw/Clutter Ratio Enhancement of Bayes Classifier and MAP Classifier using Simulated Signals

Trial No.	Before Enhancement	Bayes Classifier	MAP Classifier
1	0.98	5.33	1.79
2	0.95	4.52	2.72
3	0.99	4.50	3.52
4	0.85	5.66	3.00
5	0.99	3.42	1.82
6	1.01	8.80	4.66
7	0.94	6.60	4.01
8	1.01	5.33	2.20
9	1.00	5.87	4.16
10	0.89	6.60	3.14
11	0.93	7.15	3.86
12	1.04	7.01	3.50
13	0.92	5.57	3.25
14	1.00	7.20	3.57
15	0.98	7.19	3.50
16	0.99	3.71	2.10
17	1.00	4.03	3.10
18	0.82	7.21	3.02
19	0.99	6.53	3.34
20	0.85	6.80	3.68
Mean	0.95	5.95	3.19
STD	0.06	1.416	0.77

a 100 MHz sampling rate. The flaw was formed by drilling a hole with 1mm into the specimen. The measured signal, as shown in Figure 3.10 (a), has peak amplitude flaw-to-clutter (F/C) ratio slightly less than 0 dB. The SSP algorithm uses 8 channel Gaussian filters. These Gaussian channels have a 1.5 MHz bandwidth and 1 MHz frequency steps between adjacent channels starting at 1.5 MHz. The processed result is presented in Figure 3.10 (b) and (c). The F/C ratio for Bayes classifier is about 2.875 and the F/C ratio is 1.45 for the MAP classifier.

To obtain a consistent result we use the backscattered echo from the back surface of the test material to simulate the flaw echo and superimpose it in the experimental grain signal. The F/C ratio is about or small than 0dB. The results are shown in Table 3-2. In this table, for Bayes classifier, the average enhancement of F/C ratio is about 2.93 with a standard deviation of 0.67 and the F/C ratio is 1.527 for the MAP classifier with 0.257 standard deviation.

3.6 Conclusion

In this chapter, we developed two flaw detection algorithms, the Bayes and the MAP classifiers. Both algorithms were applied to the simulated and experimental data, and the results are consistent. Overall, the performance of the Bayes classifier is dependent on the statistical estimation of clutter and flaw echoes, and the performance of the MAP classifier is dependent on the statistical parameters of clutter. According to the results, the Bayes classifier presents better performance than the MAP classifier in the ability of suppressing clutter.

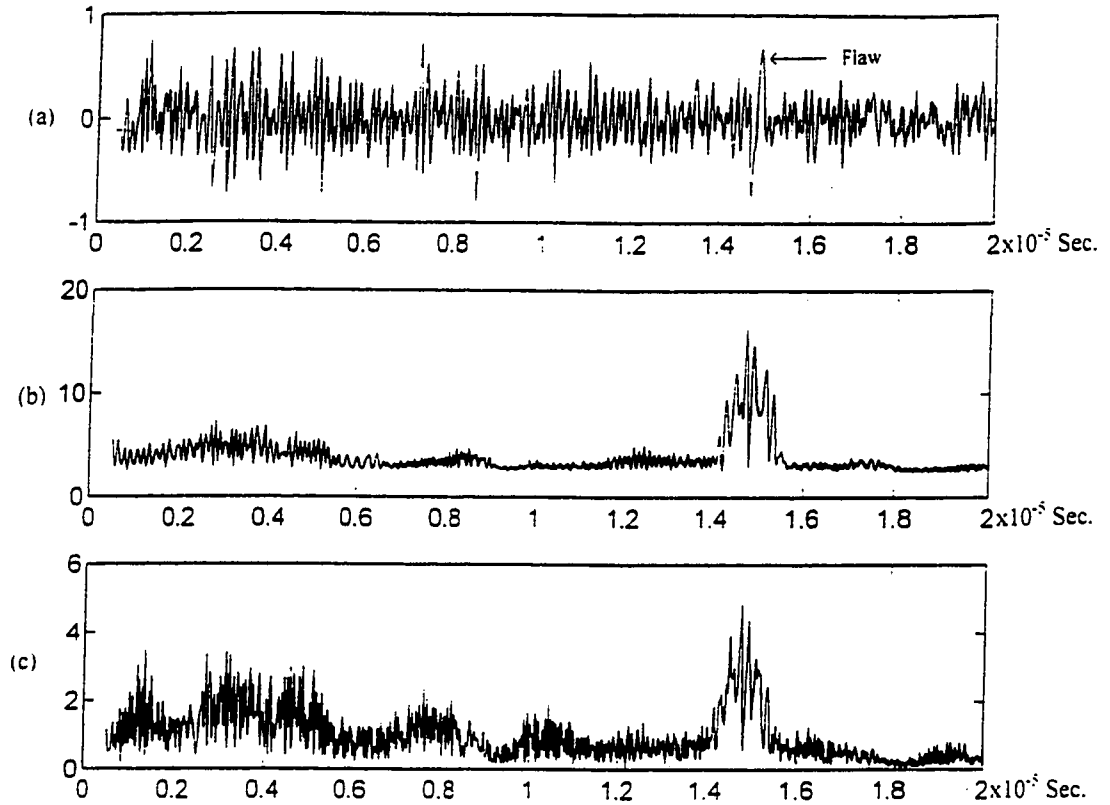


Figure 3.10 The Typical Processed Results by using Experimental Data

- (a) The Experimental Ultrasonic Signal (F/C= 0 dB),
- (b) The Processed Result by using Bayes Classifier (F/C= 2.875),
- (c) The Processed Result by using MAP Classifier (F/C=1.45).
(8 SSP Channels, BW=1.5 MHz).

Table 3.2 Flaw/Clutter Ratio Enhancement of Bayes Classifier and MAP Classifier using Experimental Signals

Trial No.	Before Enhancement	Bayes Classifier	MAP Classifier
1	0.85	2.75	1.51
2	0.90	2.23	1.22
3	0.95	2.62	1.25
4	1.01	3.20	1.41
5	1.00	3.33	1.57
6	0.98	2.38	1.44
7	0.99	2.60	1.25
8	0.98	4.5	1.85
9	0.99	2.43	1.67
10	1	3.28	2.01
Mean	0.96	2.93	1.527
STD	0.06	0.67	0.257

CHAPTER IV

FUZZY DISCRIMINANT FUNCTIONS

In the previous chapter, we presented the SSP algorithm combined with the Bayes and the MAP classifiers in the application of NDE. In this chapter, we develop a fuzzy classifier. The fuzzy classifier is obtained by modifying a fuzzy entropy to measure the existing possibility of flaw echoes in noisy environments. The difference between the fuzzy classifier and the Bayes or MAP classifiers is that instead of estimating the existing “probability” we measure the existing “possibility” of flaw echoes. The existing possibility, defined in the fuzzy space [42], is acquired by measuring the entropy of target signals. In this chapter, we introduce the fuzzy sets, the fuzzy entropy, and their usage in the application of NDE.

4.1 Introduction

Since 1965, when Zadeh introduced fuzzy sets, the researchers on the theory of fuzzy sets have been solving many problems such as artificial intelligence, control, pattern classification, [43]-[45], etc. Fuzzy sets are characterized by a class of membership functions which assign a grade (range between zero and one) to each member element, and these grades are worked as a pointer to indicate the existing possibility of signals. It should be noted that the characteristics of the fuzzy sets are established by the statistical properties of the membership functions. In addition, we need a discriminant function which can utilize the grades (i.e., feature vector) obtained

from the membership functions in order to separate the desired signal from background noise. The system diagram is shown on Figure 4.1. In this system, the backscattered ultrasonic signal is preprocessed by the SSP algorithm to obtain the feature vector $[z_1, z_2, \dots, z_n]$. Then the feature vector is applied to the membership functions to yield the fuzzy set $[\mu_1, \mu_2, \dots, \mu_n]$. Finally, a fuzzy discriminant function is able to use the fuzzy set to indicate the existing possibility of flaw echoes. In this study, the membership functions are obtained by investigating the statistical properties of both flaw and grain echoes. The fuzzy discriminant function is obtained by utilizing a fuzzy entropy. As the entropy in information theory, the fuzzy entropy can represent a quantitative measurement of signals in a fuzzy system. Then based on the information of the fuzzy entropy, the fuzzy discriminant function can make detection.

In the next section, the definition of the fuzzy sets is reviewed. Then a new definition of a fuzzy discriminant function used for the ultrasonic flaw detection is developed. In addition, the derivation of the membership functions is also present. In Section 4.4 both the simulated and experimental data are used to test the fuzzy classifier.

4.2 Fuzzy Sets and Membership Functions for Ultrasonic Signals

L.A. Zadeh [42] introduced the definition of fuzzy sets :

“ Let X be a space of points (objects), denoted by x (i.e., $X=\{x\}$). A fuzzy set (class) A in X is characterized by its membership functions $f_A(x)$ in the interval $[0,1]$ with the value of $f_A(x)$ at x representing the grade of membership of x in A ”. For most of the applications,

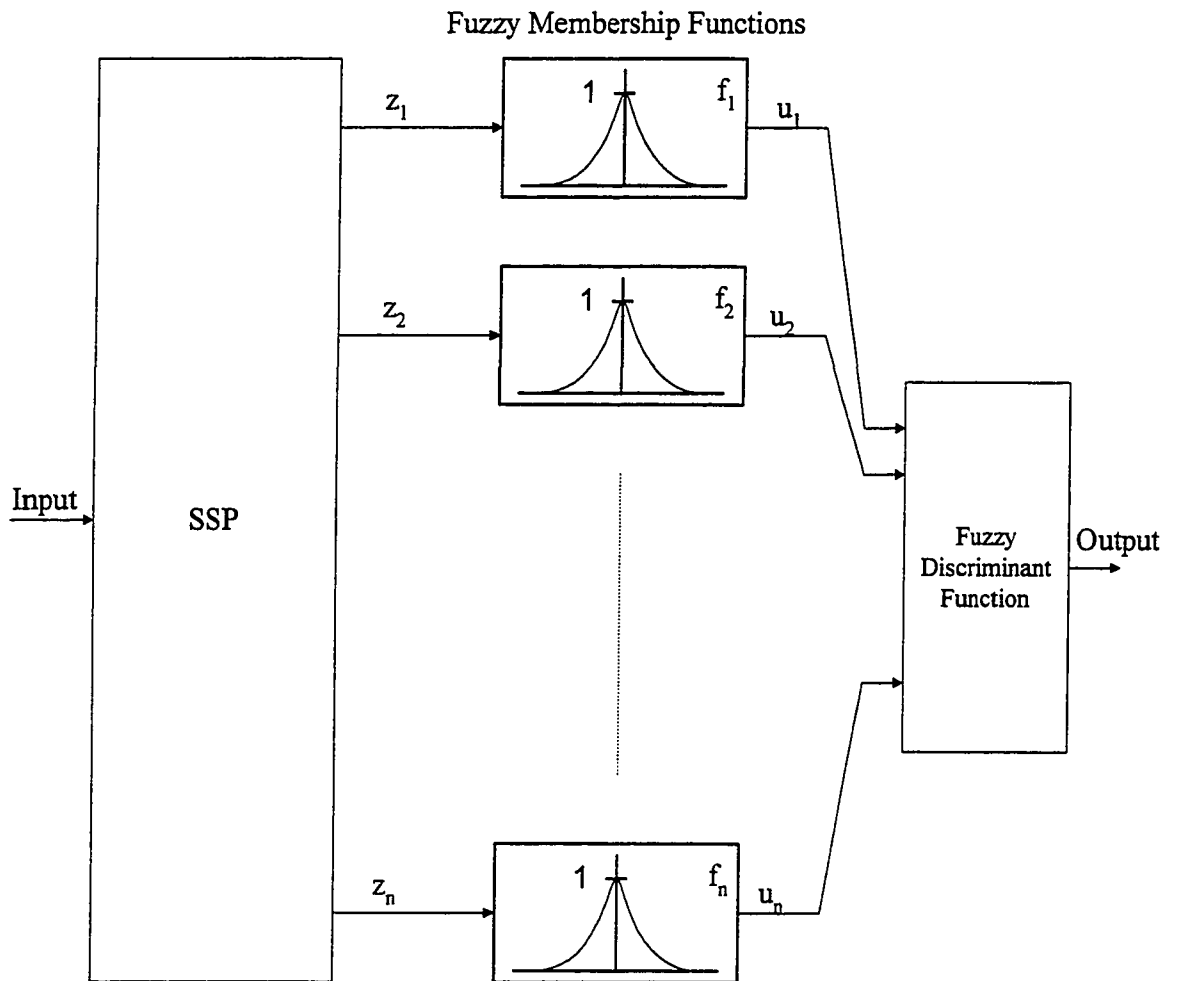


Figure 4.1 Fuzzy Discriminant System

large values denote higher degrees of set membership, and small values denote lower degree of set membership.

In mathematics, a fuzzy set A can be written in the form

$$f_A = (u_1 = f_1(z_1), u_2 = f_2(z_2), \dots, u_n = f_n(z_n)) \quad 0 \leq \mu_i \leq 1 \quad (4.1)$$

where u_i $i = 1 \dots n$ is the grade of the membership function f_i , and z_i is the input.

From the above definition, we are aware that the usefulness of the mathematical model of fuzzy sets depends on the capability to construct the appropriate membership functions. For stochastic signals, the membership function should be designed by their statistical properties. In this section, designing the membership function for each filter channel (SSP channels) has become the major task. In order to design the membership functions, we decomposed the scattered ultrasonic signal and examined the histogram at the output of the SSP channels which are found to be Gaussian in shape. Hence, this led us to assume that the distribution of the output from the SSP filters is a Gaussian distribution (as studied in Chapter II). To estimate the statistical parameters for the fuzzy membership functions, we use the sample mean and the sample variance

$$m_i = \frac{1}{N} \sum_{i=1}^N z_i \quad (4.2)$$

$$\text{and } \sigma_i^2 = \frac{1}{N-1} \sum_{i=1}^N (z_i - m_i)^2 \quad (4.3)$$

where z_i is the sampled data. It is important to point out that since the power spectrum amplitude of the ultrasonic signals is not equal on each channel, we need to modify the

amplitude probability density function such that it can be used as the membership function and still maintain the signal statistical property. This requirement can be achieved by using the following equation as the membership function

$$f_i(z) = e^{-\frac{(z-m_i)^2}{2\sigma_i^2}} \quad (4.4)$$

In this equation, the membership function has a Gaussian shape, but its amplitude has been normalized to have a maximum value of 1. This equalizes the amplitude on each channel, and this modification provides the membership grades between 0 and 1. This is desirable for implementation of the fuzzy membership function. Since the ultrasonic flaw signal is more concentrated on some frequency bands than clutter signal is, the variance of the membership function of flaw echo is in general bigger than the variance of the clutter signal. In other words, if given a signal, z , the output of the target membership function is μ_T , and the output of the clutter membership function is μ_C , then the value of μ_T is always greater than or equal to the value of μ_C as shown in Figure 4.2. Therefore, by using Equation 4.4, the membership function for both clutter and flaw echoes can be obtained, and the output of the membership function could be treated as a fuzzy set representing the signal features. In the next section, a fuzzy discriminant classifier will be defined, which utilizes the fuzzy set to classify the flaw and clutter signals.

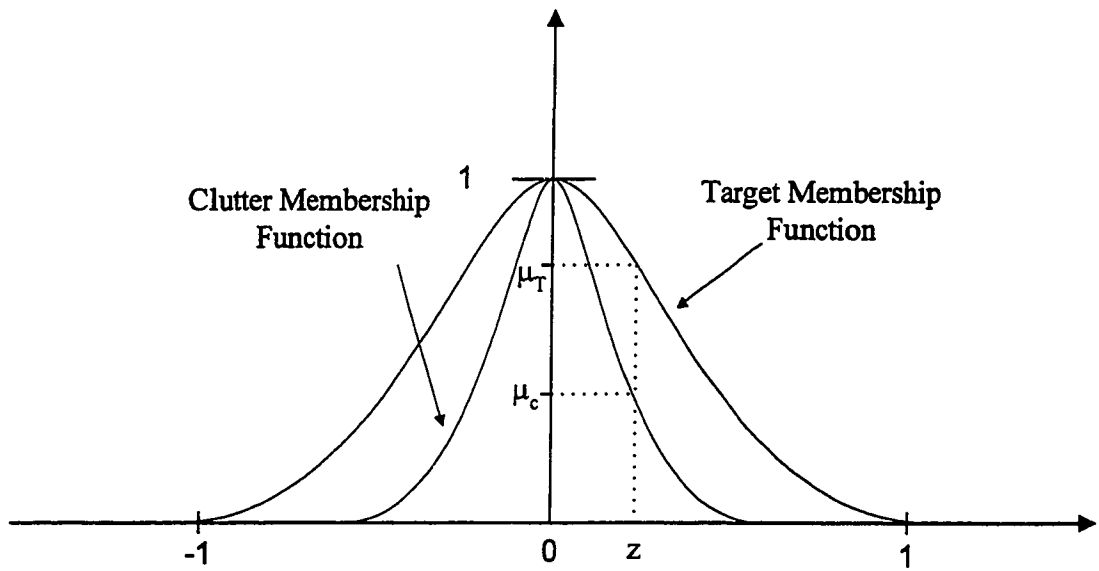


Figure 4.2 The Normalized Membership Functions of Clutter and Target Signals

4.3 Fuzzy Entropy

Fuzzy sets only extract the signal's characteristics by using the properly predefined membership functions. It still cannot decide whether the signal is a target or clutter. In order to make a decision, the discriminant function must be developed which allows making a decision from the information provided by the fuzzy sets. In information theory, entropy has been used as a measurement to represent the quantity of information. Therefore, entropy is suitable to serve as the discriminant function. In this chapter, we have been developing a modified fuzzy entropy to discriminate the signal from clutter. The first fuzzy entropy [46] was defined by Zadeh as the following:

$$H = -\sum_{i=1}^n u_i p_i \log(p_i) \quad (4.5)$$

where $u_i = f_i(x_j)$ is the grade and p_i is the probability of occurrence of x_j . This fuzzy entropy highly depends on the probability of occurrence, but in ultrasonic detection application, the probability of each channel is assumed to be equal. Therefore, Equation (4.5) is not suitable to the ultrasonic detection problems. S.K. Pal [46] modified the Equation (4.5) to a higher order fuzzy entropy as :

$$H^r = \left(\frac{1}{\binom{n}{r}} \right) \sum_{i=1}^{\binom{n}{r}} \{ [u_i^r \exp(1-u_i^r)] + [1-u_i^r] \exp(u_i^r) \} \quad (4.6)$$

where n is the number of elements in the fuzzy set and r is the order. This fuzzy entropy gives an average measurement. Considering two cases, when $u_i^r = 0.9$ and $u_i^r = 0.1$, the

equation inside the braces of Equation (4.6) will be equal. This example therefore reveals that this fuzzy entropy is not suitable for the ultrasonic detection problems. In ultrasonic detection problems, two objects possibly exist in the fuzzy space. Either an echo or a grain signal will be recognized at one location; therefore, the entropy should be modified to suit for this situation. In this section, we present a revised fuzzy discriminant entropy which can improve the performance of pattern recognition in ultrasonic nondestructed testing.

4.3.1 Fuzzy Discriminant Function. Let A be a fuzzy set $p=\{u_i/z_i, \dots\}$, and suppose that two patterns, p_0 and p_1 , exist in the fuzzy space. Therefore, for any object in fuzzy set A must be classified as either pattern p_0 (i.e., clutter) or pattern p_1 (i.e., flaw). To discriminate pattern p_0 and pattern p_1 , the fuzzy discriminant function is defined as :

$$H = \frac{H_T}{H_C} = \ln \left\{ \sum \frac{\mu_{T,i} \exp(1 - \mu_{T,i})}{\mu_{C,i} \exp(1 - \mu_{C,i})} \right\} \quad (4.7)$$

where i is the number of channels, H_T is the fuzzy entropy of flaw echoes, and H_C is the fuzzy entropy of clutter. These two values estimated by the *summation* of the ratio of each component in the fuzzy sets can reveal the signal information as shown in Figure 4.2 and Figure 4.3. Observing Figure 4.2, if given a clutter signal, both of the values of μ_T and μ_C are all close to the value of one. By using this reasoning, in Figure 4.3, the range for H_T and H_C is located in the upper right corner approaching one; therefore, the ratio H should close to one. If given a flaw echo, the values of μ_T and μ_C will be located far away from one as shown in Figure 4.2. Then in Figure 4.3, H_C will be located in the lower left

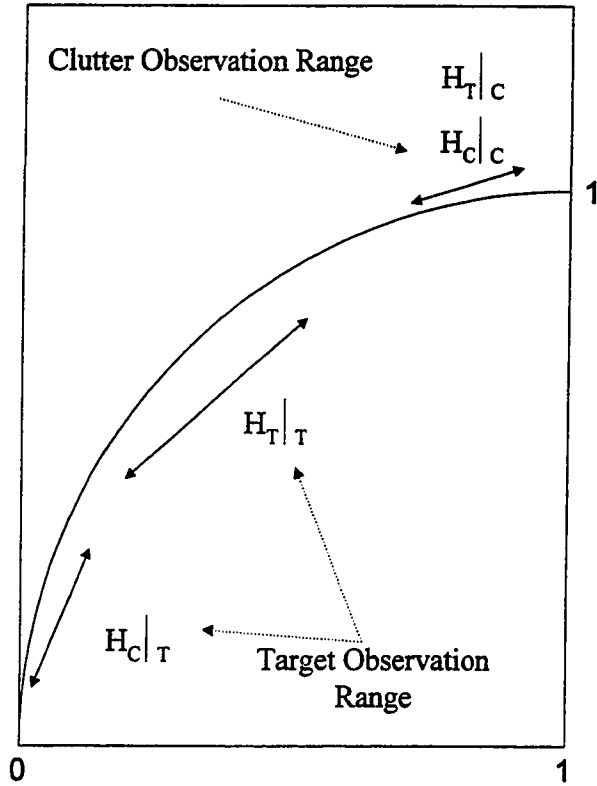


Figure 4.3 Graphic Display of The Function $\mu \cdot \exp(1-\mu)$ in Discrimination of Target and Clutter

corner approaching to 0 and H_T will be located in the middle of the curve resulting in the ratio, H , greater than 1. By using this property, the flaw echo is capable of being detected. In addition, the log term in Equation (4.7) is used to converge the output to a suitable range. In the next section, we apply both the simulated and experimental data used in Chapter II to test the fuzzy discriminant function and its performance will be compared with statistical discriminant functions.

4.4 Simulated and Experimental Results

In order to compare the performance of the fuzzy discriminant function with the statistical classifiers, we use the same simulated and experimental data in Chapter III to test the fuzzy classifier. In the SSP algorithm, the same 8 Gaussian channels are used. The frequency range start from 1.5 to 13.5 MHz, and the bandwidth of the filters is 1.5 MHz. A typical result of using simulated data is shown in Figure 4.4, which is able to detect the flaw location. The membership functions obtained by using the simulated data are shown in Figure 4.5. Observing Figure 4.5, we found that the variance of the membership functions of clutter signals has similar magnitudes on all channels. However, for flaw echoes, their membership functions present a higher variance on the low frequency bands. Therefore, we can conclude that most of the flaw energy is concentrated on the low frequency band. Specifically, on channel 6, 7, and 8, the membership functions for both flaw and clutter echoes are almost overlapped, which means that channel 6,7, and 8 are unable to provide the information to separate the flaw

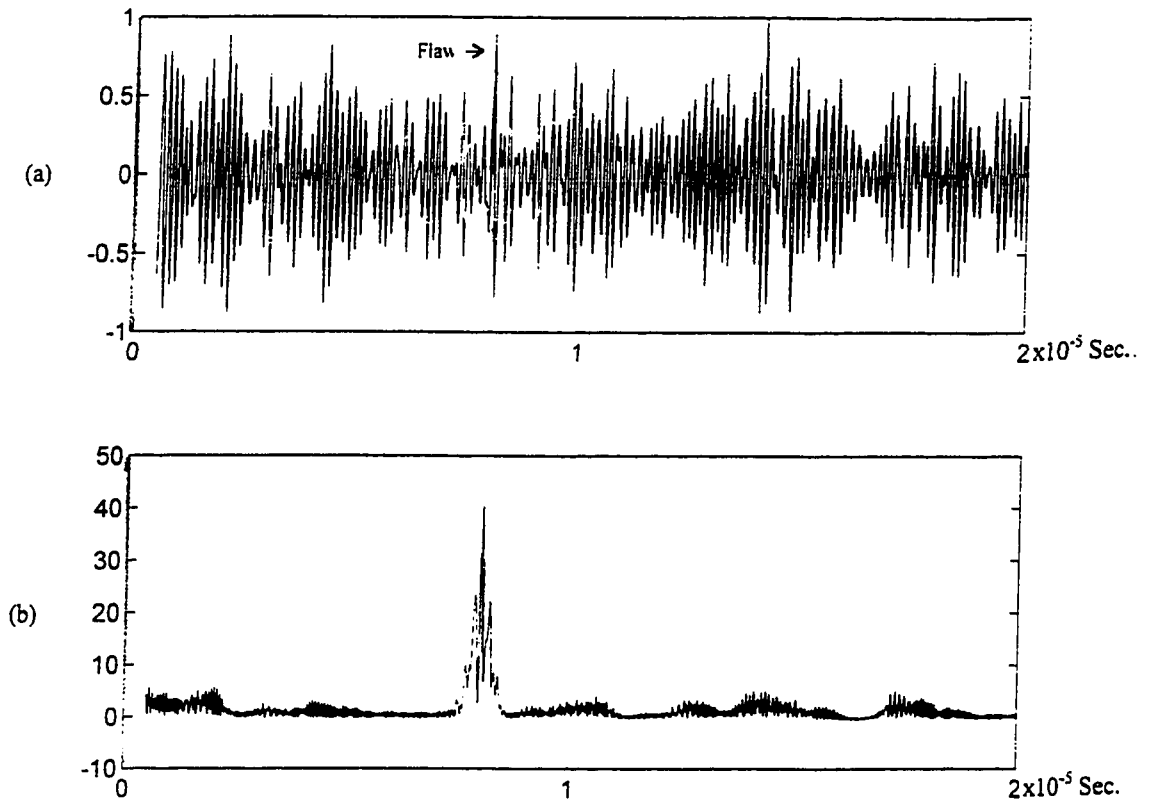


Figure 4.4 The Typical Processed Result by using Simulated Signal

- (a) The Simulated Ultrasonic Signal,
- (b) The Processed Result by using Fuzzy Classifier.

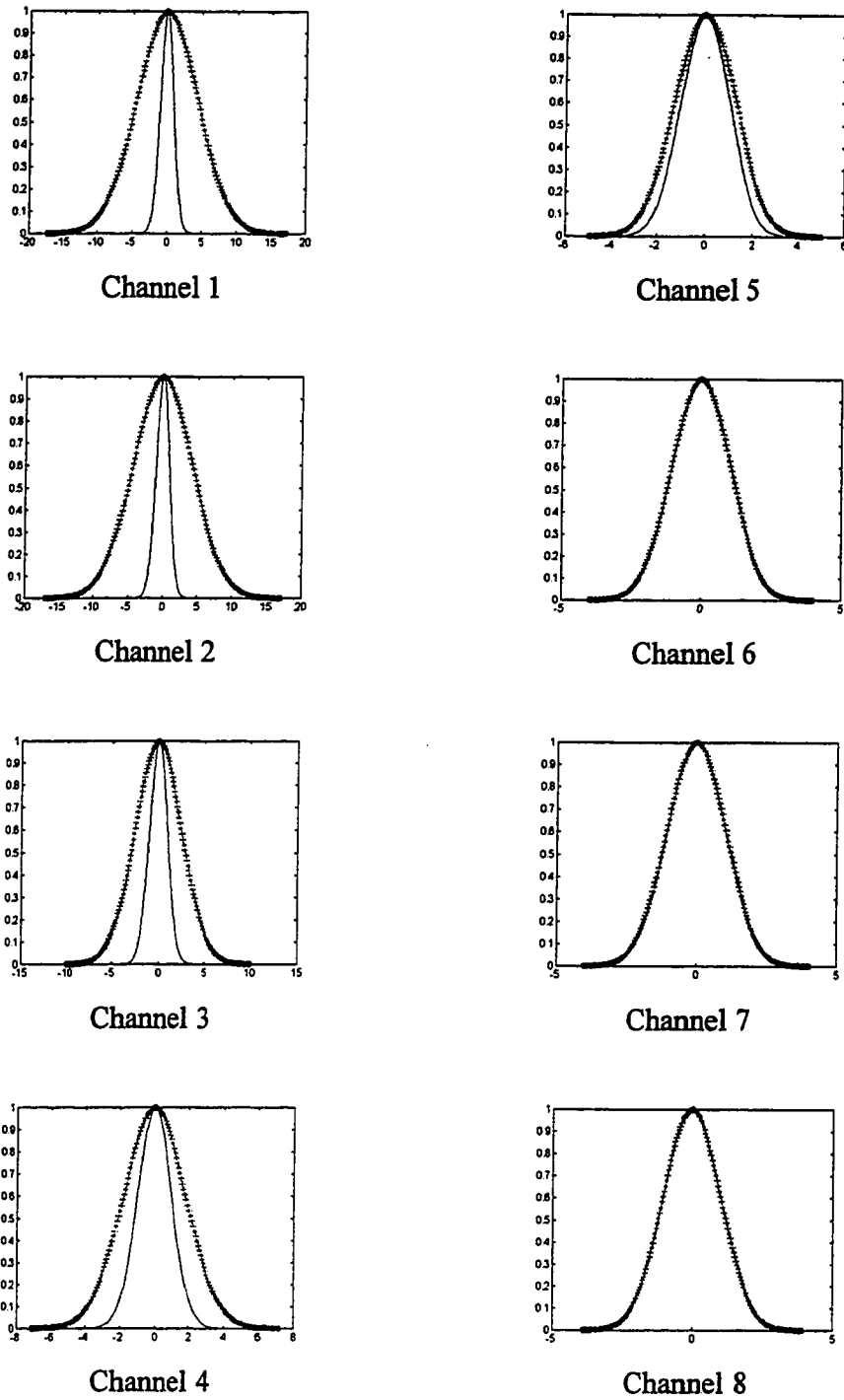


Figure 4.5 The Membership Functions Obtained by using Simulated Data

———— The Membership Function for Flaw Signal

———— The Membership Function for Clutter Signal

and clutter echoes. It is necessary to point out that whether we remove channel 6, 7, and 8 from discriminant function the result will not be affected because the ratio obtained on channel 6, 7, and 8 are all close to one. The overall performance is listed on Table 4.1. The average of the F/C enhancement is 5.93 with a standard deviation of 1.63.

A typical experimental data is shown in Figure 4.6, and the membership functions are shown in Figure 4.7 which present a similar result of the simulated result. The overall performance is listed on Table 4.2, and its F/C ratio enhancement is about 4.53 with a standard deviation of 2.32. Comparing Table 3.3 and 3.4. we found that the performance of fuzzy discriminant is similar to the Bayes classifier but is better than that of the MAP classifier. This is due to the fact that like the Bayes classifier, the fuzzy discriminant function uses membership functions to estimate the statistical property of clutter echoes as well as flaw echoes. These estimations contribute a similar effect to both the Bayes and fuzzy classifiers. In addition, due to the non-linear property of the fuzzy classifier, the fuzzy classifier presents a higher standard deviation in F/C enhancement than that of the fuzzy and Bayes classifiers.

In the next chapter, we will present feedforward neural networks. The purpose of this topic is to develop a neural network that can detect the ultrasonic flaw echoes without estimating any statistical parameters. Like the learning process in the human brain, the interested signal patterns are presented to the neural network again and again until it can recognize signal patterns. The advantage of using neural networks include: (1) Neural networks is a parallel computing machine, (2) System responses can be optimized, (3) The parallel structure of neural networks offers a training for recognizing a function

Table 4.1 Flaw/Clutter Ratio Enhancement of SSP Algorithm combined with Fuzzy Discriminant using Simulated Data

Trial No.	Before Enhancement	Fuzzy Classifier
1	0.98	3.6
2	0.95	7.21
3	0.99	4.81
4	0.85	6.32
5	0.99	3.1
6	1.01	8.34
7	0.94	7.80
8	1.01	4.42
9	1.00	7.71
10	0.89	5.06
11	0.93	6.9
12	1.04	6.3
13	0.92	6.55
14	1.00	6.57
15	0.98	8.3
16	0.99	3.81
17	1.00	3.7
18	0.82	5.7
19	0.99	7.15
20	0.85	5.41
Mean	0.95	5.93
STD	0.06	1.63

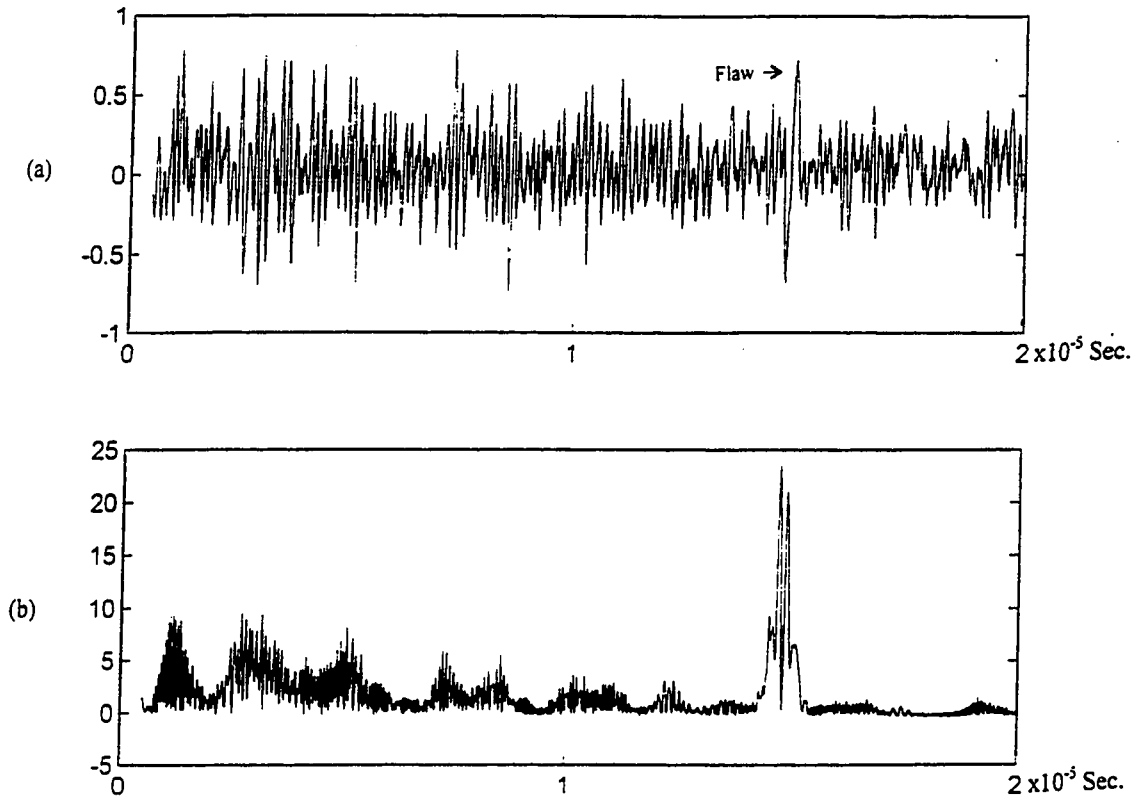


Figure 4.6 The Typical Processed Result by using Experimental Signal
(a) The Experimental Ultrasonic Signal,
(b) The Processed Result by using Fuzzy Classifier.

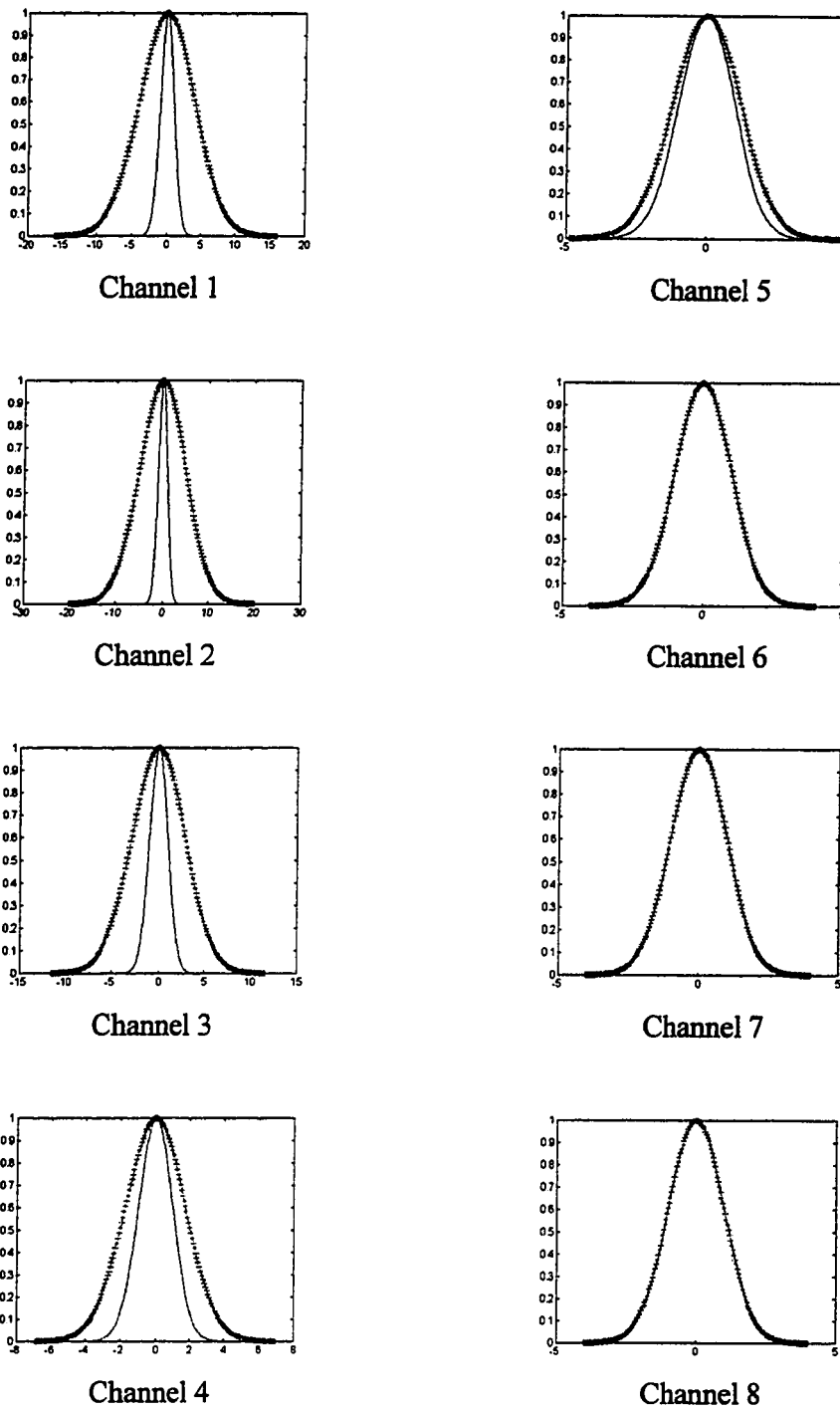


Figure 4.7 The Membership Functions Obtained by using Experimental Data

———— The Membership Function for Flaw Signal

..... The Membership Function for Clutter Signal

Table 4.2 Flaw/Clutter Ratio Enhancement of SSP Algorithm combined with Fuzzy Discriminant using Experimental Data

Trial No.	Before Enhancement	Fuzzy Classifier
1	0.85	8.8
2	0.90	5.92
3	0.95	3.8
4	1.01	1.46
5	1.00	2.3
6	0.98	1.88
7	0.99	7.05
8	0.98	4.5
9	0.99	4.6
10	1.00	5.01
Mean	0.96	4.53
STD	0.06	2.32

similar to the human brain, therefore any signal pattern could be learned. (4) No statistical estimation is necessary.

CHAPTER V

NEURAL NETWORKS

In this chapter, we develop an ultrasonic flaw detection system by utilizing the SSP algorithm combined with a three-layer neural network. Neural networks have been studied since mid 30's, and many exciting results and applications [47-49] support the fact that neural networks are powerful tools to solve problems in the signal processing field. The most critical advantage of using neural networks is their adaptive learning capability, which enables neural networks to be taught to interpret possible variations of target objects. More specifically, the following three reasons address the benefits of using neural networks. Firstly, neural networks are trained by examples, which means no mathematical model of signals is to be estimated. Secondly, neural networks provide a non-parametrical method to approximate unknown systems, which can deal with not only statistical models but also non-linear models. This non-linearity is a very important property, which enhances the network's classification or approximation capabilities without estimating any statistical parameter. Thirdly, their hierarchical and parallel structure also provides a speedy performance, which allows neural networks to be used in real time applications. In this chapter, we apply the SSP algorithm combined with a three-layer feedforward neural network to the application of ultrasonic flaw detection.

5.1 Introduction

Neural networks are made up by a number of simple highly interconnected signal processing units. These signal processing units are nonlinear mapping networks that allows training and adaptivity for a particular application. Classified by their interconnection architecture, neural networks can be classified in two types: feedforward neural networks and recurrent neural networks. The feedforward neural network is arranged in a feedforward manner in which neural nodes receive an input from external environment or other neural nodes, and pass the information to adjacent neural nodes without any feedback. Once feedforward neural networks have been trained, the networks compute an output in response to the input pattern. On the other hand, recurrent neural networks can be distinguished from the feedforward networks in that they have a feedback loop. In this chapter, a three layer neural network will be studied and combined with an SSP algorithm to make an ultrasonic flaw detection system.

The basic mathematical description of a three-layer neural network was found in 1987. Huang and Lippmann [50] demonstrated by simulations that a three-layer neural network could form several complex functions. More recently, several investigators [51-52] have demonstrated that a three-layer neural network can approximate continuous functions defined on compact sets. Particularly, in 1989, Cybenko [52] used the functional analysis method successfully proving that theory. In this chapter, we utilize the non-linear mapping property of a three-layer feedforward neural network and the SSP algorithm to develop a methodology that is capable of classifying the ultrasonic flaw echoes from clutter signals.

The next section presents the mathematical model of neural nodes and in particular, the backpropagation training method will be introduced to find the parameters of the three-layer neural network. Then both the simulated and experimental data will be applied to test the neural network.

5.2 Elementary Model of Neural Networks

A general three-layer feedforward neural network is shown in Figure 5.1. The neural nodes in the first layer do not perform any computation but feed signals to the second layer. The neural nodes in the second layer receive the weighted inputs from the first layer and then perform a large mapping calculation by using the activation function to yield the output of the second layer. Then the output neural nodes in the third layer sum up the output of the second layer to produce the net output. The basic neural node model consisting connection and activation is shown in Figure 5.2. The input connection weight w_{ji} indicates the effect of the i th input on the j th node. The cell body is represented by an activation function. The node sums the weighted inputs and passes the result through an activation function, $\varphi(\cdot)$, which is also called the threshold function and could be a sigmoid function, a ramping function, hyperbolic tangent function, or a hard-limiter function as shown in Figure 5.3. The mathematical equation for the neural nodes can be written as

$$u_j = \sum_{i=1}^n w_{ji} x_i + \theta_j \quad (5.1)$$

$$y_j = \varphi(u_j) \quad (5.2)$$

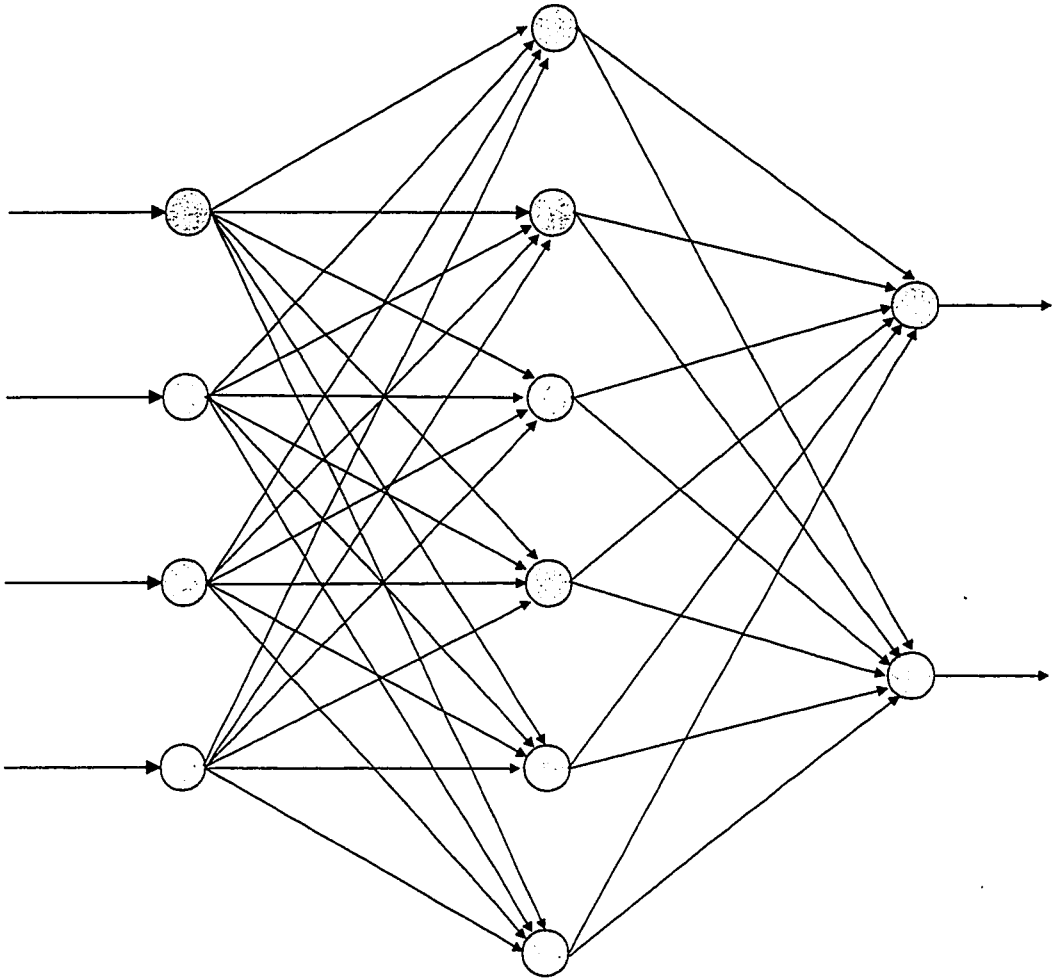


Figure 5.1 A General Three-Layer Feedforward Neural Network

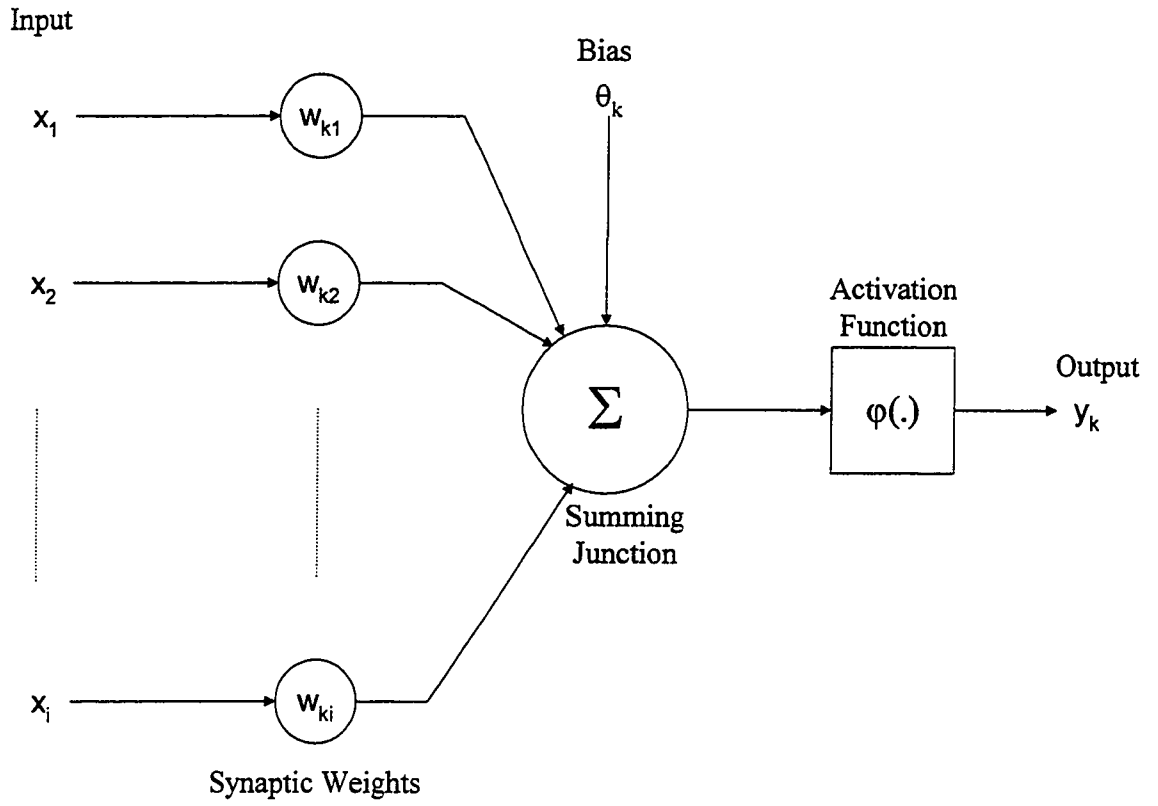


Figure 5.2 Nonlinear Model of a Neural Node

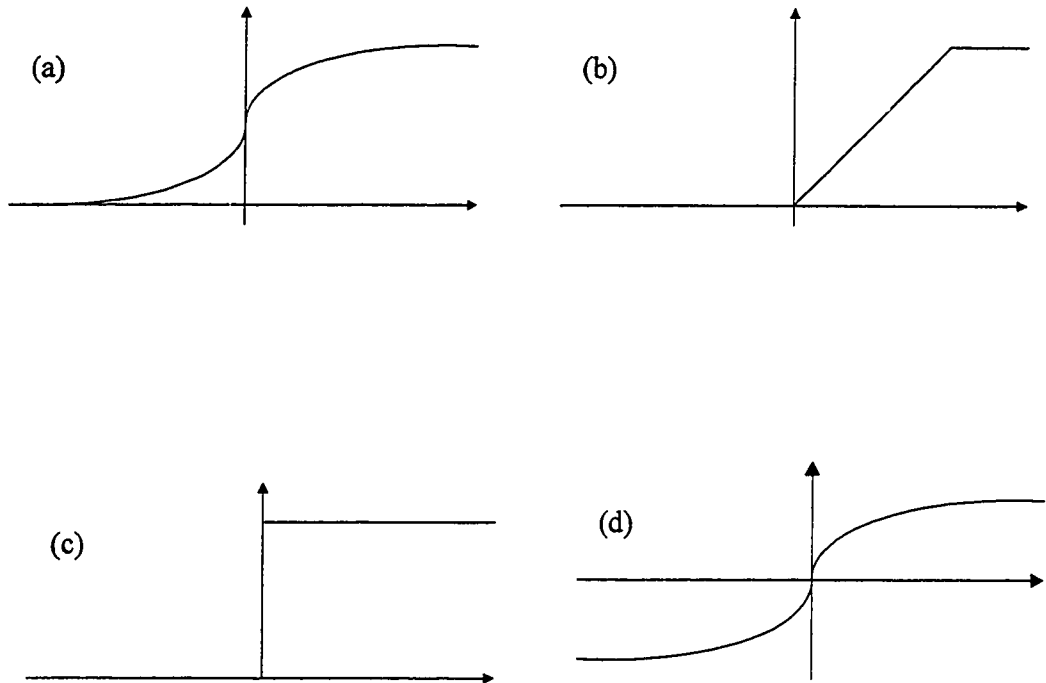


Figure 5.3 Four Different Neural Activation Functions

- (a) Sigmoid Function,
- (b) Ramping Function,
- (c) Hard-limiter Function,
- (d) Hyperbolic Tangent Function.

where θ_j is the external threshold of j th node also called the bias, w_{ji} is the input connection weight from i th input to j th node, x_i is the i th input, and y_j represents the j th output. In this model, these quantities will be represented as real numbers, and the network response will be completely controlled by, w , θ and the activation function $\varphi(\cdot)$.

5.3 Neural Network Detector

It has been proved by many researches [51-54] that a three-layer feedforward neural network can perform a highly non-linear mapping process, which is very suitable for the application of signal classifications. In this study, we combine SSP algorithm with a three-layer feedforward neural network to detect the ultrasonic flaw echoes. The representation of a three-layer feedforward neural network can be written as

$$f(\bar{x}) = \sum_{j=1}^N w_j \varphi(\bar{\alpha}_j^T \bar{x} + \beta_j) \quad (5.3)$$

where α_j , β_j and w_j are fixed parameters, and $\varphi(\cdot)$ is the nonlinear activation function. In this study, we use the hyperbolic tangent function as the activation function, and it can be written as:

$$\varphi(t) = \tanh(t) \quad (5.4)$$

In the implementation, the parameter α_j is the input connection weights, β_j is the biases, and w_j can be thought as the output connection weights.

Therefore, if we can find parameter w_j , α_j and β_j to perform a particular mapping function, we can then establish a neural network which can map target signals and noise

to different places in the signal space. In the following section, we present the backpropagation learning process, which is the most popular training method and is used in the training of our ultrasonic applications.

5.4 The Backpropagation Learning Process

The most significant capability of neural networks is their learning property. The learning process gives neural networks the ability to learn their environment and improve their performance. This learning process takes place through an iterative process of adjusting its connect weights. To be specific, we adopt the backpropagation algorithm[47] to train the neural network for the application of ultrasonic flaw detection. The backpropagation learning process is accomplished by successively adjusting synaptic weights based on a set of input patterns and the corresponding set of desired output.

To develop the backpropagation learning algorithm, the net input to the j th neural node could be written as

$$net_j = \sum_i w_{ji}x_i + \theta_j \quad (5.5)$$

where w_{ji} is the connect weight from the i th neural node to the j th neural node. θ_j is the bias. Then the output of j th neural node is

$$y_j = f_j(net_j) \quad (5.6)$$

where $f_j(\cdot)$ is the activation function of the j th neural node. The synaptic weights are adapted by minimizing the error function defined as

$$J = \frac{1}{2} E[(d - y)^2] = \frac{1}{2} E[e^2] \quad (5.7)$$

where e represents the error term, d is the desired response, and y is the actual output of the neural network. To minimize the error function, we differentiate the function J with respect to the synaptic weights

$$\nabla_{w_k} J = \frac{\partial J}{\partial w_k} \quad k = 1, 2, \dots, m \quad (5.8)$$

It is intuitive that the adjustment of synaptic weights is the direction of steepest descent of the error surface that is the direction of opposite to the gradient vector. Therefore the adjustment can be represented as

$$\frac{dw_k}{dt} = -\eta \frac{\partial J}{\partial w_k} \quad k = 1, 2, \dots, m \quad (5.9)$$

where η is the learning rate. Then the update equation can be written as

$$w_k(n+1) = w_k(n) + \eta \Delta w_k(n) = w_k(n) - \eta \nabla_{w_k} J(n) \quad k = 1, 2, \dots, m \quad (5.10)$$

In 1983, Rumelhart [55] added a momentum term to the update equation

$$w_k(n+1) = w_k(n) + \eta \Delta w_k(n) + \alpha \Delta w_k(n-1) \quad (5.11)$$

where α is the momentum parameter. The purpose of the momentum term is to damp out oscillations and to keep the weight correction going in one direction, and thereby speed up the convergence in the network. It is important to point out that the weights of the neural network are all initially randomly assigned. Therefore the training results could be limited by a local minimum on the error surface. If a local minimum is reached and the error at the output is still unacceptable, then an increase in the number of neural nodes or a change in the initial parameters will help fix the problem. It should be noted that

after the training, all the connection weights are fixed and their values, like the memory in human brain, determine the network's behavior.

To improve the network mapping results, we carefully examined the activation function (i.e., hyperbolic tangent function) of the hidden neural nodes, and found that the biases of these nodes play an important role in the mapping process. As shown in Figure 5.3, due to the nonlinear property of the sigmoid function, the output of the sigmoid function approaches one or zero when the input goes to a positive or negative infinity respectively. In other words, the output will become a constant value (i.e., either one or zero), when the magnitude of the input is a large value. This situation is undesirable because the nonlinear mapping will have failed. Therefore in order to sufficiently utilize the nonlinear property of the sigmoid function, we only allow the input existing between the rang of -3 to 3 . To reach this criterion, we normalize the input data such that the value of input data is between 1 and -1 . In addition, the selection of biases should also be initially assigned in the range of -3 to 3 such that the nonlinear curve of the sigmoid function can sufficiently be used.

In the next section we present the structure of a three-layer neural network and show how to train the neural network in order to apply it to the application of ultrasonic flaw detection.

5.5 The Design of the Neural Networks

The system diagram of the neural network used in the ultrasonic application is drawn in Figure5.4. There are two processes, pre-process and post-process, involved in

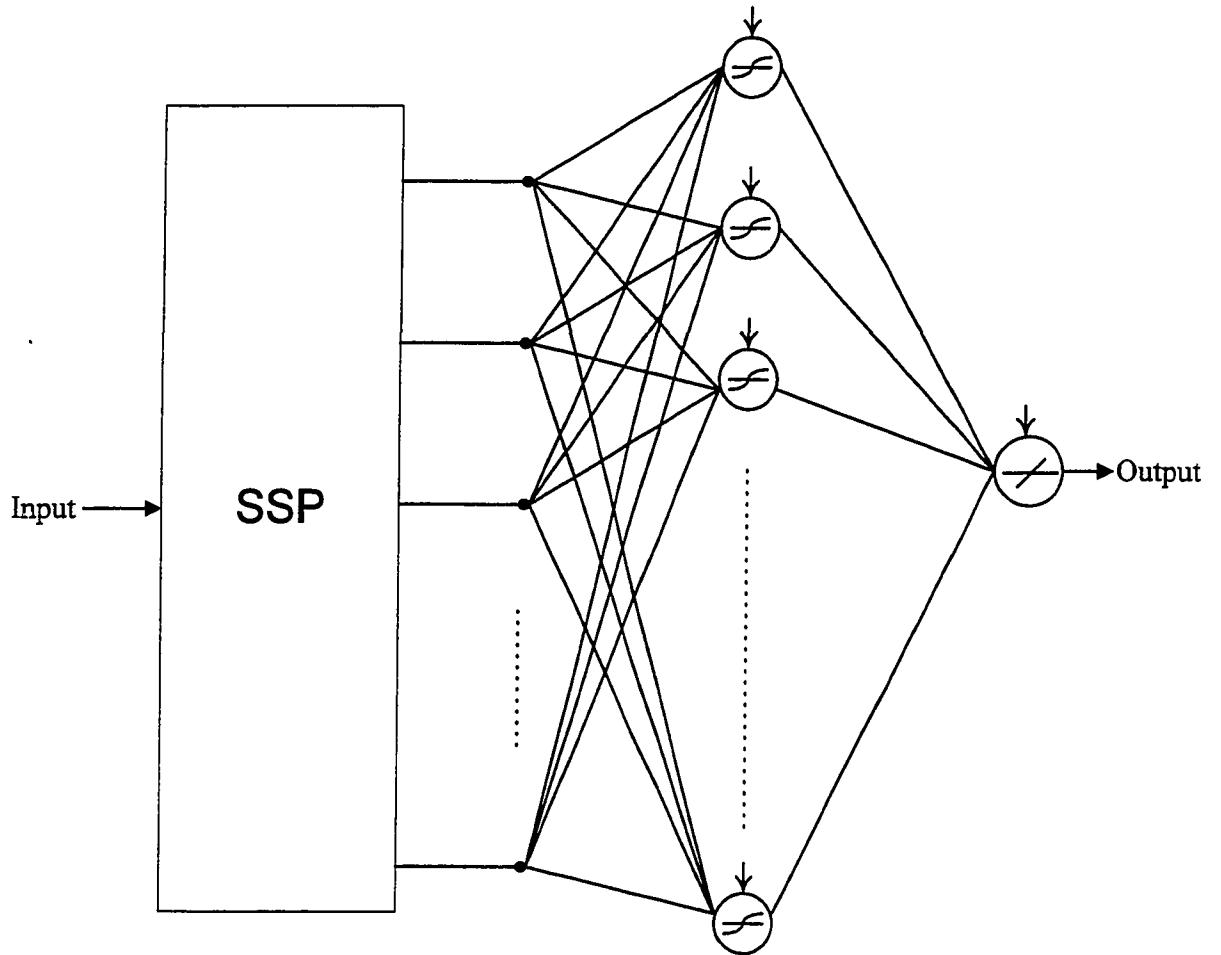


Figure 5.4 The Block Diagram of SSP Combined with a Three-Layer Neural Network.

our design. The pre-process is implemented by using the SSP algorithm, and its purpose is to extract signal features according to the frequency diversity of ultrasonic signals as discussed in Chapter II. In the post-process, a three-layer feedforward neural network will separate flaw and clutter signals according to their feature vectors obtained by using the SSP algorithm. Due to the non-linearity of sigmoid function, the neural network performs a highly complex nonlinear mapping, and this mapping operation is learned by repeatedly teaching the neural network both clutter and flaw echo patterns.

To teach the neural network the patterns of flaw and clutter signal, we have simulated an ultrasonic signal in which a flaw echo was embedded as shown in Figure 5.5(a). This signal was explored to the neural network and the neural network was taught that the desirable response is shown in Figure 5.5(b). In Figure 5.5(a), the flaw-to-clutter ratio is about the value of 2 such that the neural network can be impressed by the pattern of the flaw echo. The value of weights and biases of the neural network is randomly selected. The number of neural nodes in the first layer is equal to the number of the SSP channels (i.e., 8 in this study), and the number of neural nodes in the third layer is one (i.e., the output of the neural network). However nowadays there is still no specific way to decide the number of neural nodes in the hidden layers, but it can be done based on a trial-and-error method.

To complete the training processing, the sum-squared error (i.e., SSE, the sum of the squared differences between the network targets and actual outputs for a given set of vectors) or the mean-squared error is needed to reach a criterion. If the SSE criterion is met then the training is complete; otherwise, increasing the number of epochs (one complete presentation of the entire training set during the learning process is called an

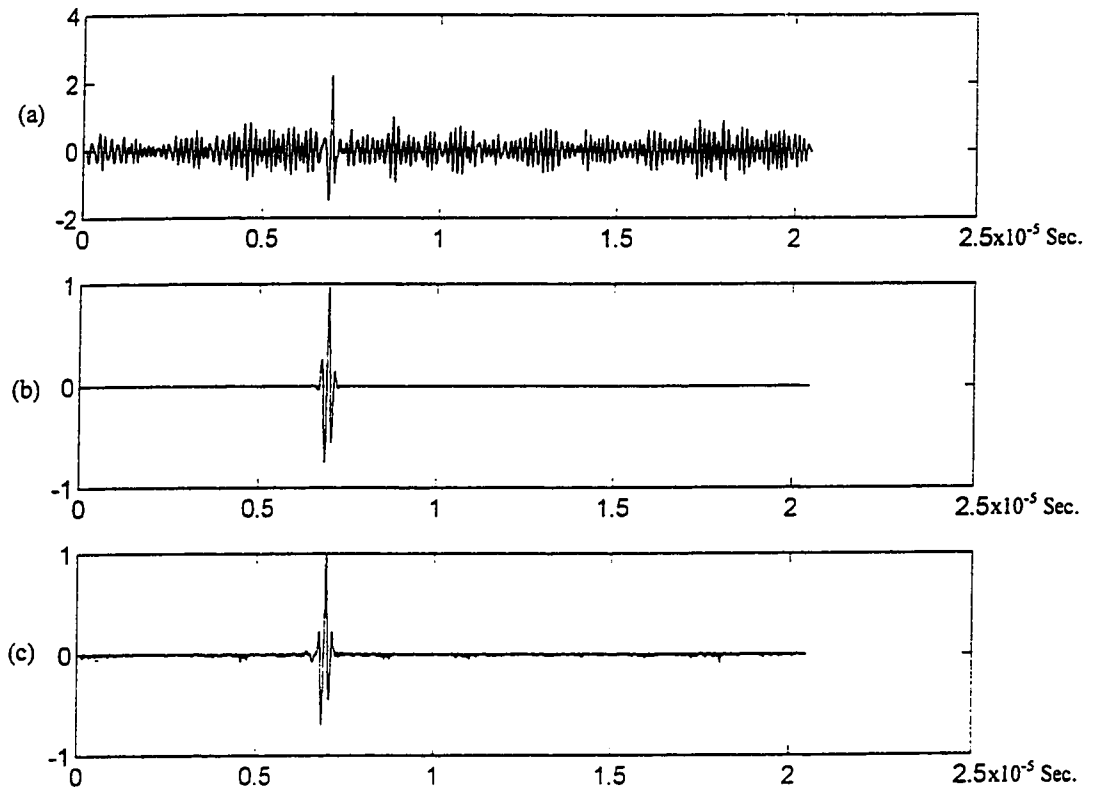


Figure 5.5 The Simulated Training Data and Desired Response (Hidden Neural Nodes = 20, MSE = 0.00026, and Epoch = 1500)

- (a) The Simulated Ultrasonic Training Signal,
- (b) The Desired Response,
- (c) The Output after Training Process.

epoch) becomes necessary. If increasing the number of the epoch still cannot reach the SSE criterion, then it is necessary to increase the neural nodes in the hidden layer. However, increasing the number of hidden neural nodes results in a longer training period. After the training, the neural network responds the training signal as shown in Figure 5.5(c). In this figure, the F/C ratio has been increased by around 10 –15, which proclaims that the training was very successful. After the training, the neural network is expected to respond to a flaw echo if the input is a flaw signal; and if the input is clutter, the neural network is expected to respond to nothing.

5.6 Simulated and Experimental Results

The objective of combining the SSP algorithm and the neural network is to detect the flaw location in the application of NDE. Begin with the simulated data, the simulated data has been used to test the Bayes, the MAP, as well as the fuzzy classifiers. In this section, the same data were used to test the neural network, and a typical processed result is shown in Figure 5.6.

According to the results of Figure 5.6, we can learn that a three-layer neural network combined with a SSP algorithm is capable of detecting the flaw signal. The neural network responds a pulse for a given flaw echo and small values or negative pulses for clutter echoes. This is because during the training process, a positive pulse was assigned to indicate a flaw echo and zero was assigned to indicate clutter signal. Therefore positive pulses with large amplitude on the output diagram can be classified as flaw echoes. In addition, in order to study the effect of the number of neural nodes in the

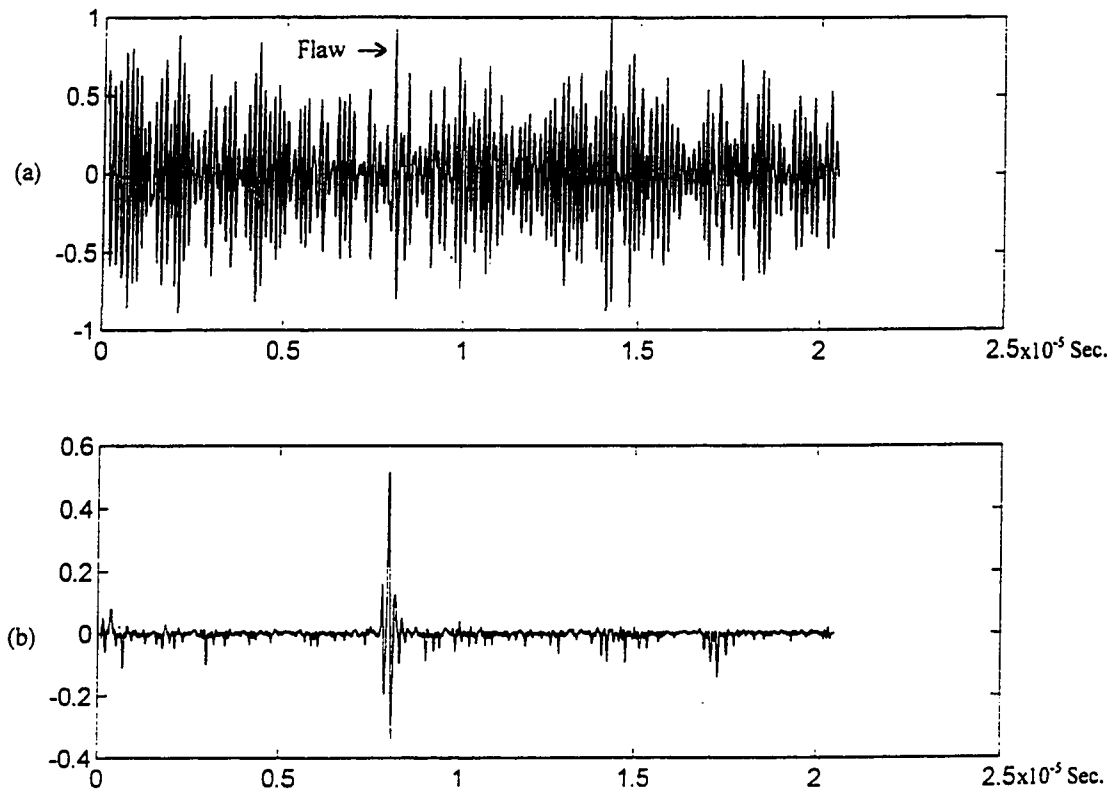


Figure 5.6 A Typical Processed Result by using Simulated Signal (Hidden Neural Nodes = 20, MSE = 0.00026, and Epoch = 1500)
(a) The Simulated Ultrasonic Signal,
(b) The Processed Result by using the Neural Network.

hidden layer to the system performance, we measured the F/C ratio by using different number of neural nodes in the hidden layer. An example is present in Figure 5.7. Figure 5.7(a) is the test signal, Figure 5.7(b) is the output produced by using two neural nodes in the hidden layer, and Figure 5.7(c) is the output of using 20 neural nodes in the hidden layer. As shown in these figures, the F/C ratio is increased from 2.5 to 12.5. In Figure 5.8 we measured the F/C ratio when the number of hidden neural nodes has been increased from 2 to 10. The result shows that increasing the number of neural nodes in the hidden layer we can improve the system performance by increasing the F/C ratio.

During the learning process, we also observed that the mean-squared error is decreased when the epoch is increased as shown in Figure 5.9. However, the error is converged when the epoch reached the number of 250. After the 250th epoch, a further increase of epochs cannot decrease the mean-squared error. Nevertheless, increasing the number of neural nodes in the hidden layer results in a further reduction of the mean-squared error as shown in Figure 5.10. In this figure, the mean-squared error was measured when increasing the number of neural nodes in the hidden layer. Therefore, the neural network can provide a better performance with more neural nodes in the hidden layer. The overall performance of using the simulated data is organized in Table 5.1. According to this table, the neural network can enhance the F/C ratio to an average of 12.12 with a standard deviation of 3.39.

To test the experimental data, we measured a grain signal and imposed a flaw echo (i.e., simulated by using the backscattered echo from the back surface of the specimen) in the middle as shown in Figure 5.11(a) to train the neural network. The desired response is presented in Figure 5.11(b), which is a single flaw echo. The network

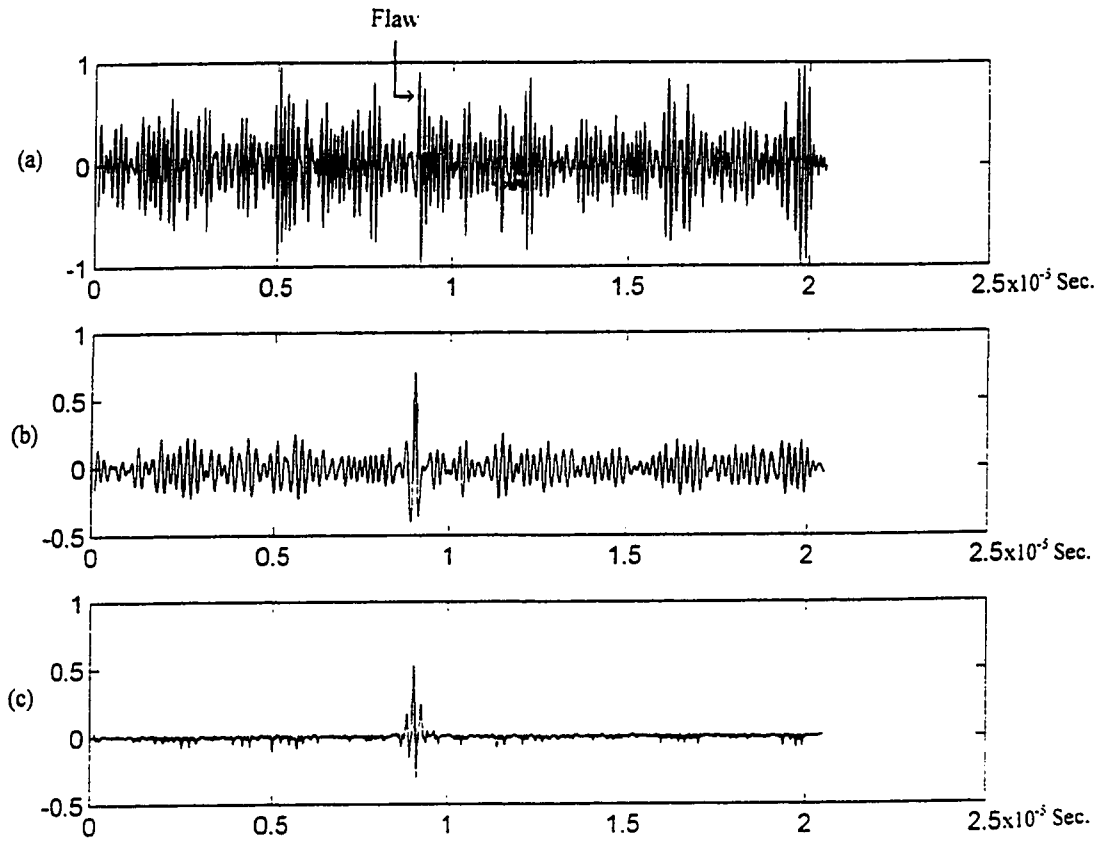


Figure 5.7 The Processed Results of using Different Numbers of Neural Nodes in the Hidden Layer

- (a) The Simulated Signal,
- (b) The Processed Result by using $n=2$ (MSE=0.002, Epoch=1500),
- (c) The Processed Result by using $n=20$ (MSE=0.0002, Epoch=1500).

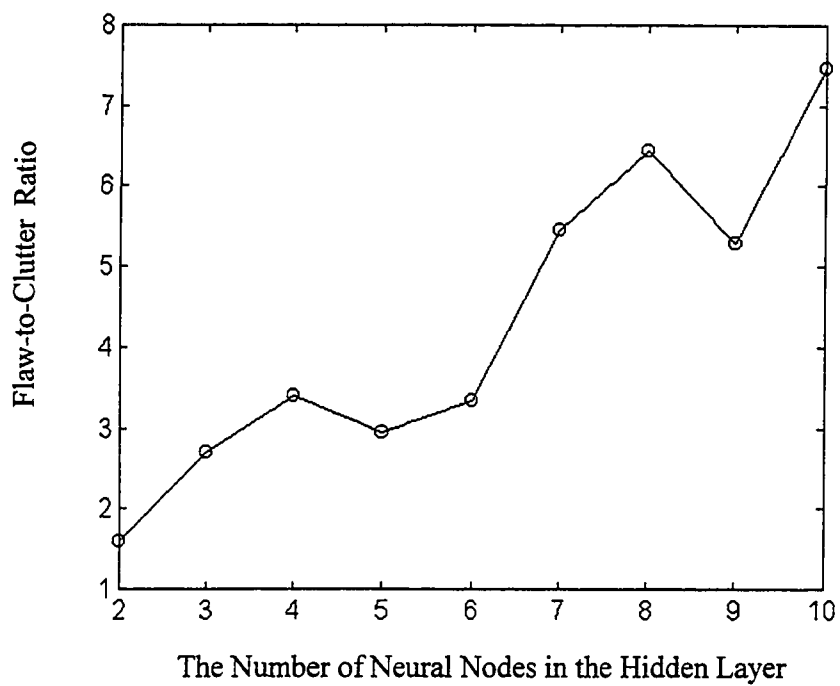


Figure 5.8 The Flaw-to-Clutter Ratio vs. the Number of Neural Nodes in the Hidden Layer.

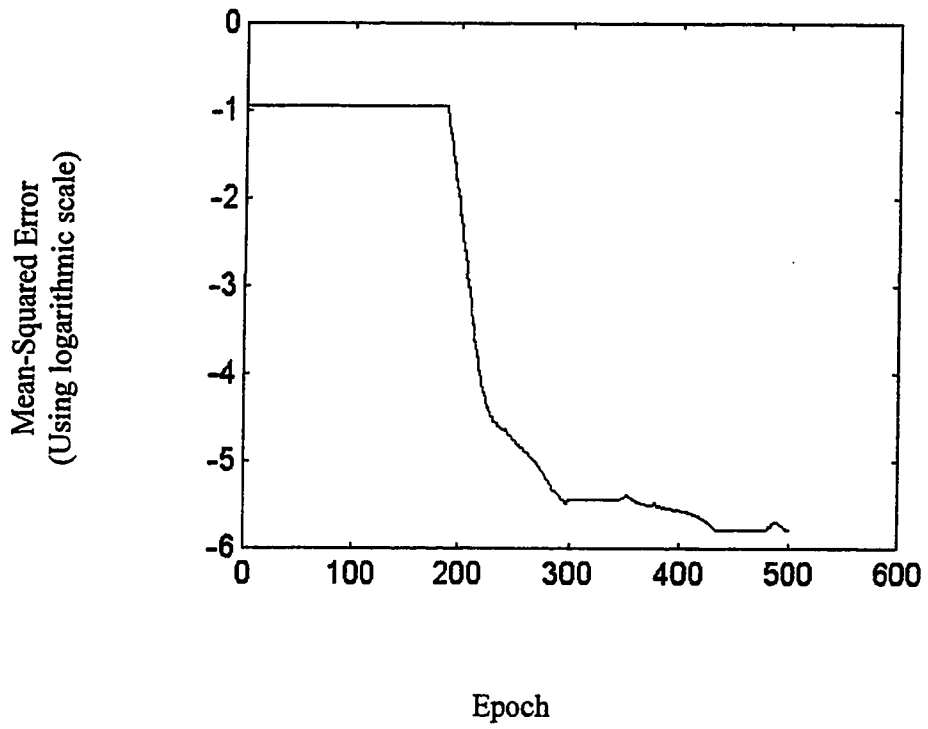


Figure 5.9 The Mean-Squared Error vs. Epoch (The Neural Nodes in the Hidden Layer $n=10$)

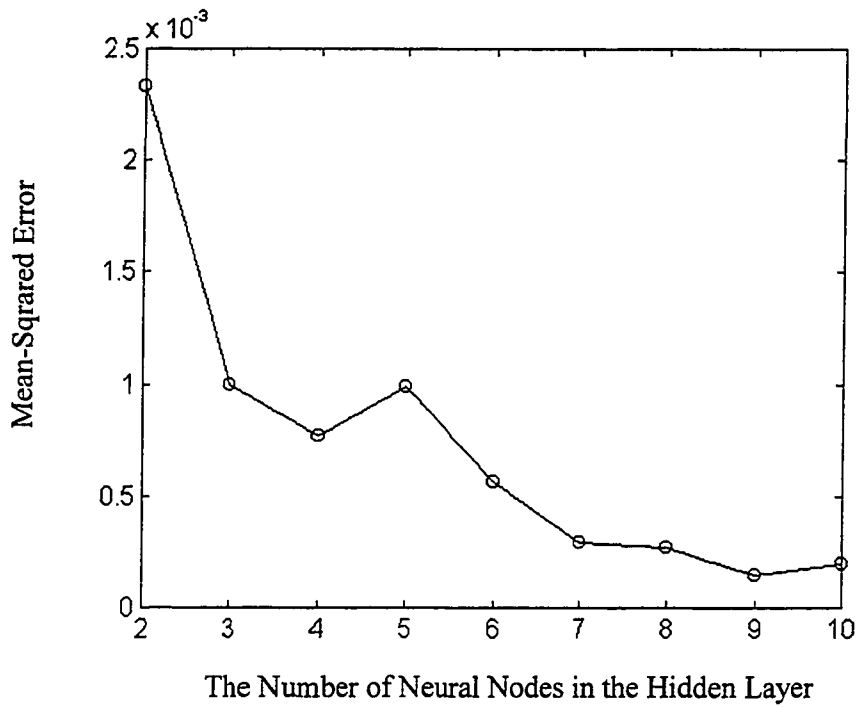


Figure 5.10 The Network Error vs. the Number of Neural Nodes in the Hidden Layer.

Table 5.1 Flaw/Clutter Ratio Enhancement of SSP Algorithm combined with Neural Networks using Simulated Signals

Trial No.	Before Enhancement	After Enhancement
1	0.98	11.23
2	0.95	6.89
3	0.99	9.28
4	0.85	10.91
5	0.99	8.49
6	1.01	15.99
7	0.94	16.568
8	1.01	11.97
9	1.00	12.39
10	0.89	8.57
11	0.93	12.39
12	1.04	17.50
13	0.92	15.92
14	1.00	14.20
15	0.98	12.99
16	0.99	11.55
17	1.00	5.95
18	0.82	16.81
19	0.99	13.81
20	0.85	9.07
Mean	0.95	12.12
STD	0.06	3.39

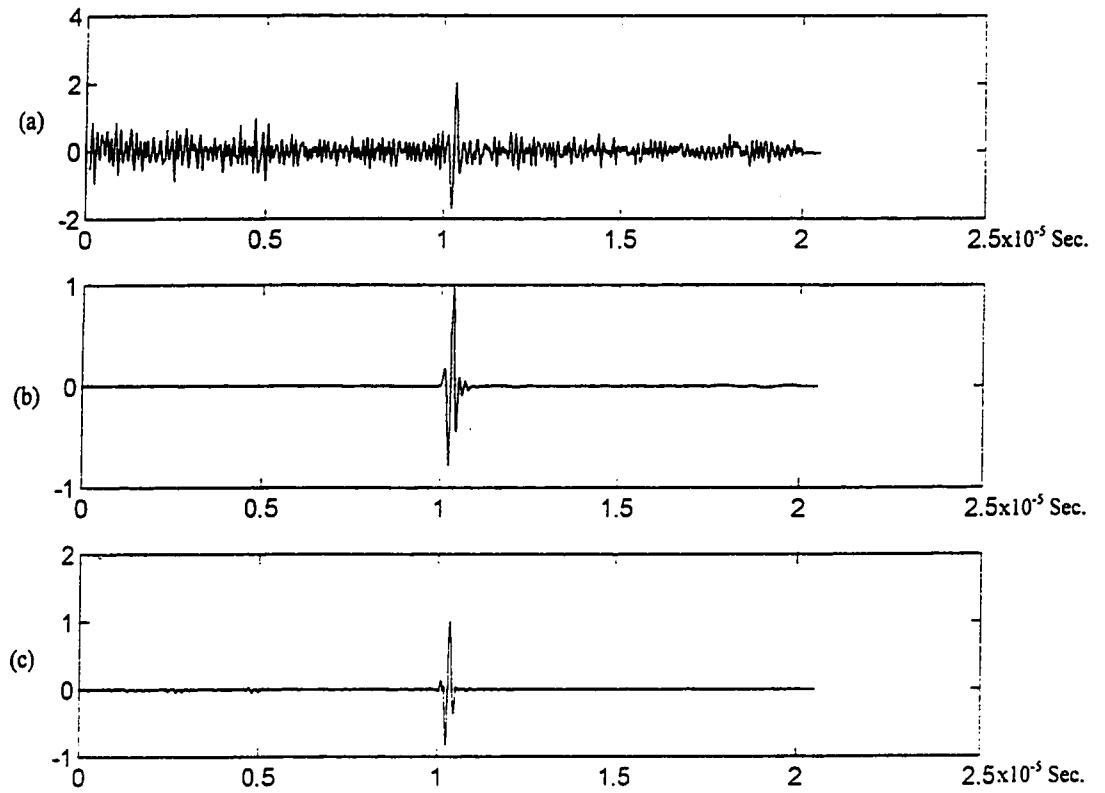


Figure 5.11 The Experimental Training Data and Desired Response (Hidden Neural Nodes = 20, MSE = 0.00028, and Epoch = 1500)

- (a) The Simulated Ultrasonic Training Signal,
- (b) The Desired Response,
- (c) The Output after Training Process.

response, after the training, is shown in Figure 5.11(c), in which the F/C ratio is around 15. A typical processed result of the experimental data is shown in Figure 5.12. To acquire the average performance, 10 experimental data are used, and the results are shown in Table 5.2. From this table, the F/C ratio is in an average of 12.02 with a standard deviation of 6.08.

5.7 Comparison of Neural Network with Bayes, MAP, and Fuzzy Classifier

The F/C ratio enhancement of the Bayes, MAP, fuzzy classifier, and neural network classifiers is summarized in Table 5.3. Comparing the Bayes, MAP, and the fuzzy classifiers, the neural network offers the highest F/C enhancement. Besides, it also precisely locates the position of flaw echoes and keeps them in a similar shape of their original echo.

Another critical issue in the application of ultrasonic flaw detection is to distinguish two adjacent flaws. In order to separate two adjacent flaw echoes, instead of responding to a flaw echo we teach the neural network to respond to a value of one if the input is a single flaw echo and respond to a value of zero if the input is clutter as shown in Figure 5.13. Therefore the interference between two adjacent flaw echoes can be eliminated. In Figure 5.13, (a) is the training data, and (b) is the desirable response in which only at the location of the flaw echo is assigned to be 1 and the other place is assigned to be zero. Figure 5.13 (c) is the output after the training, which clearly presents that the neural network is capable of recognizing the flaw echoes as we expected. However, in the training process, the response value for a flaw echo is around 0.31 which

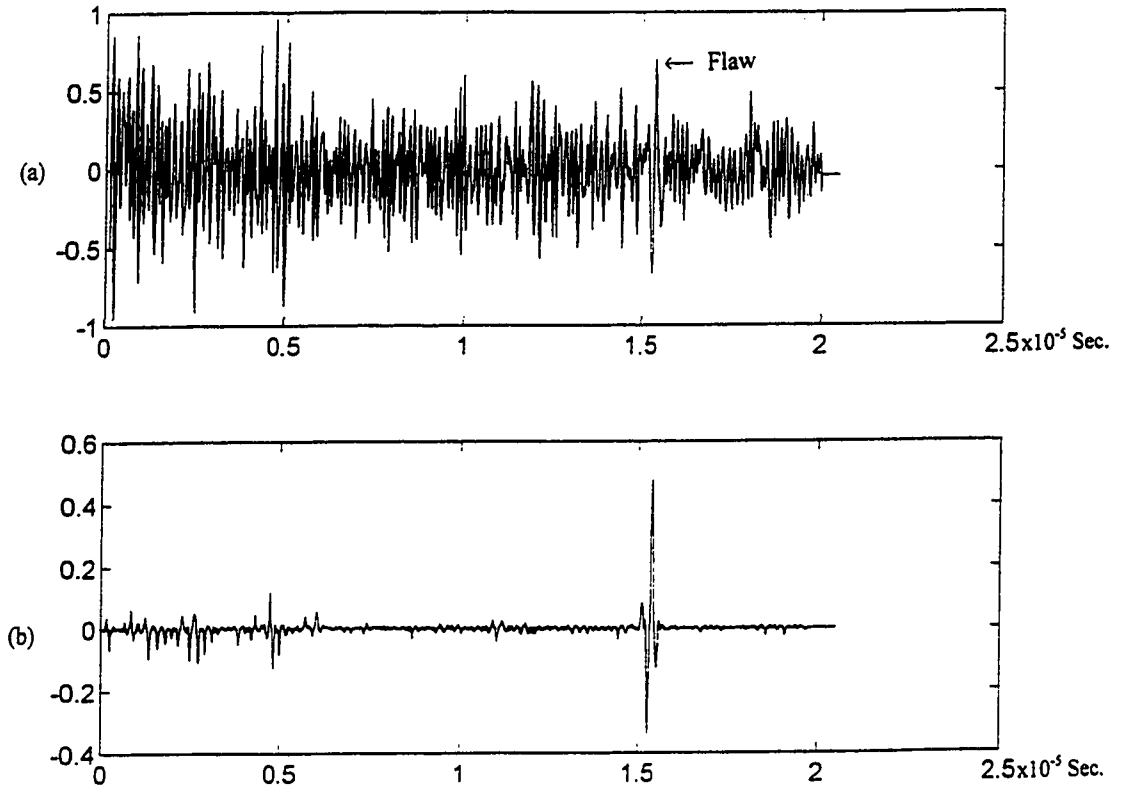


Figure 5.12 A Typical Processed Result by using Experimental Signal
(Hidden Neural Nodes = 20, MSE = 0.00028, and Epoch = 1500)
(a) The Experimental Ultrasonic Signal,
(b) The Processed Result by using the Neural Network.

Table 5.2 Flaw/Clutter Ratio Enhancement of SSP Algorithm combined with Neural Networks using Experimental Signals

Trial No.	Before Enhancement	After Enhancement
1	0.85	24.55
2	0.90	8.75
3	0.95	6.08
4	1.01	7.62
5	1.00	7.64
6	0.98	5.83
7	0.99	13.98
8	0.98	14.11
9	0.99	15.72
10	1.00	17.81
Mean	0.96	12.02
STD	0.06	6.08

Table 5.3 Flaw/Clutter Ratio Enhancement by using Bayes, MAP, Fuzzy and Neural Classifiers

	Bayes	MAP	Fuzzy	Neural Networks
Simulated Signal	5.95	3.19	5.93	12.12
Experimental Signal	2.93	1.53	4.53	12.02

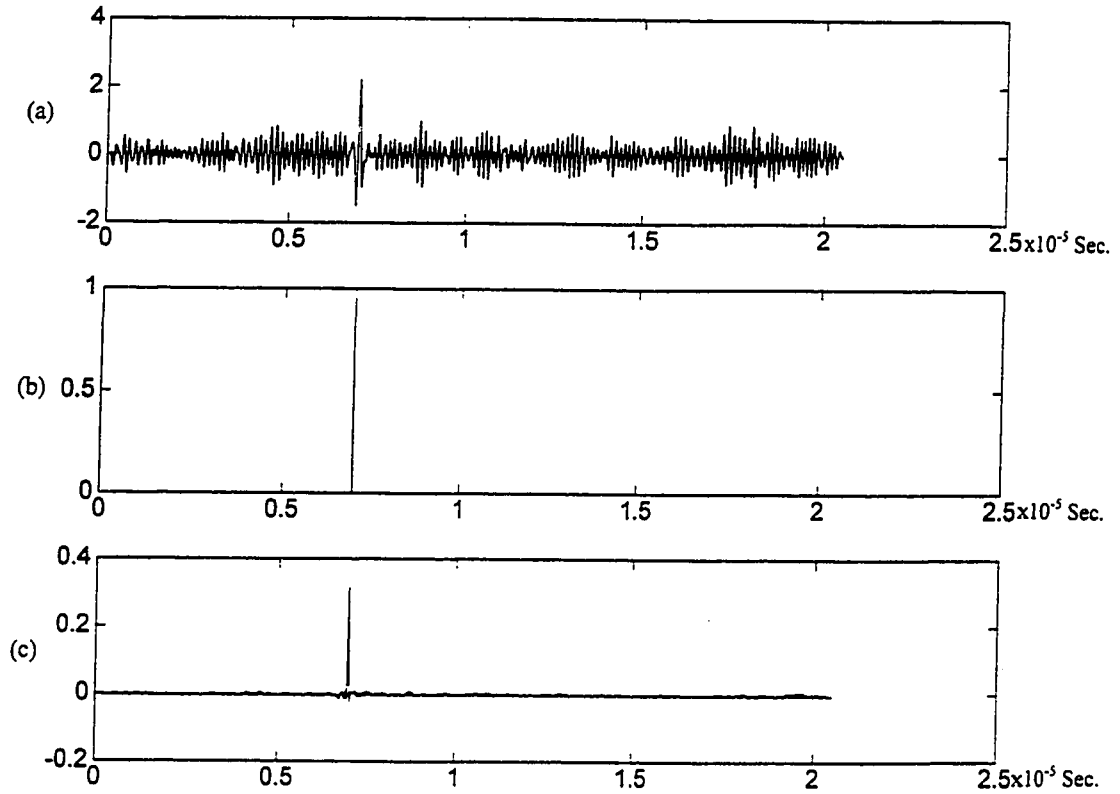


Figure 5.13 The Training Data for Separating Two Adjacent Flaw Echoes
(Hidden Neural Nodes = 20, MSE = 0.00054, and Epoch = 1500)

- (a) The Simulated Ultrasonic Training Signal,
- (b) The Desired Response,
- (c) The Output after Training Process.

doesn't reach the desirable value of 1. This situation suggests that the abruptness of the desirable response (i.e., Figure 5.13 (b)) might decrease the effective of the training results.

To test the ability of separating two adjacent echoes, we superimpose two flaw echoes in a clutter signal as shown in Figure 5.14(a). Then the Bayes classifier, the MAP classifier, the fuzzy classifier, and the neural network were all applied to this signal, and the results are presented in Figure 5.14(b)-(e). Figure 5.14(b) is the output using the Bayes classifier. This result shows that there is only one flaw echo and it is located between the locations of the two real flaw echoes. This phenomenon is the result of the additive effect of two adjacent flaw echoes which enhances and thereby creates a strong energy in the location between the flaw echoes. Figure 5.14 (c) and (d) are the output of MAP and the fuzzy classifiers respectively. Both of them present a similar result as the Bayes. However, the neural network is capable to distinguish two adjacent flaw echoes as shown in Figure 5.14 (e).

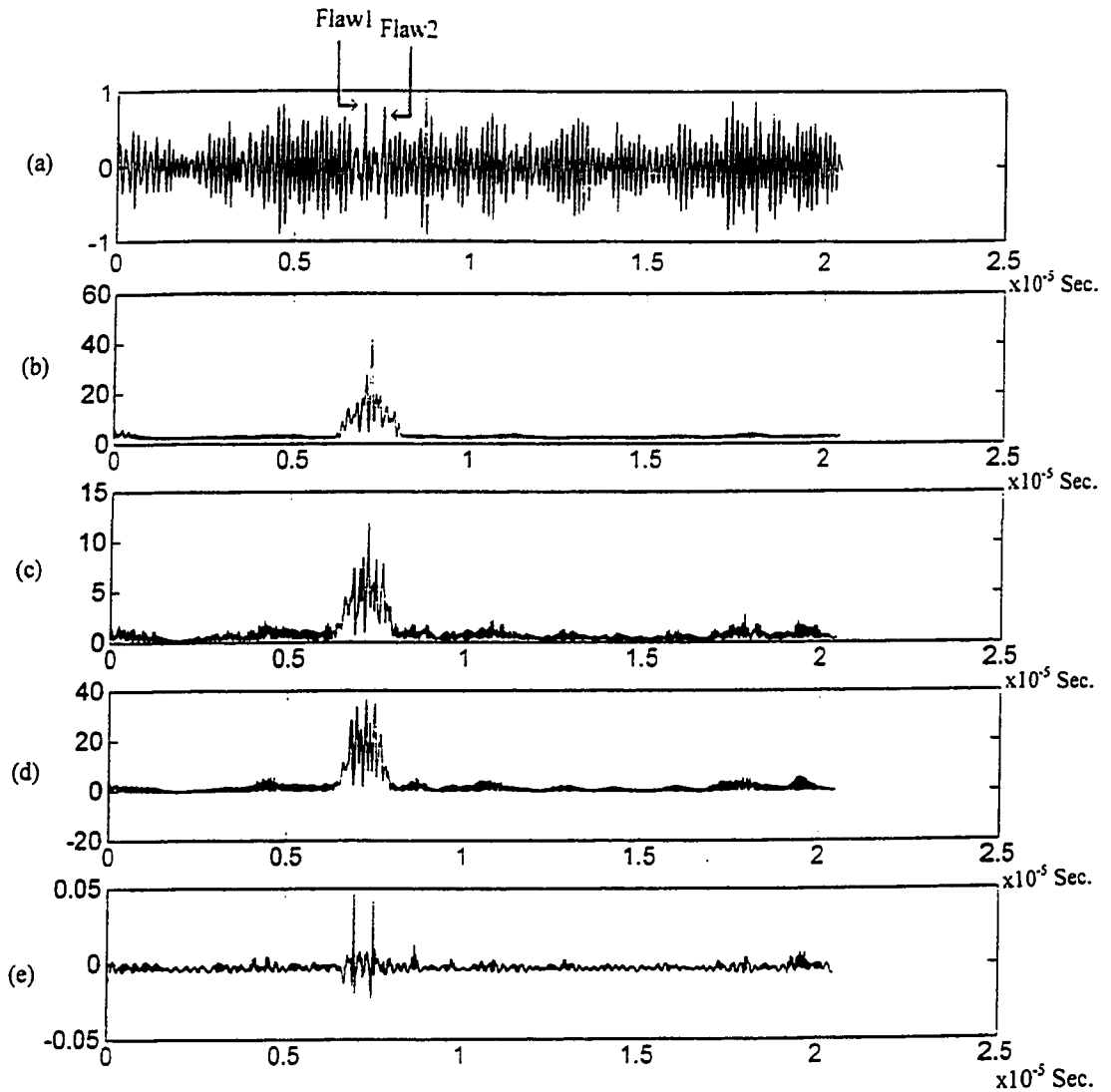


Figure 5.14 The Processed Results of Separating Two Adjacent Flaw Echoes
(Hidden Neural Nodes = 20, MSE = 0.00054, and Epoch = 1500)

- (a) The Simulated Ultrasonic Signal,
- (b) The Processed Output by using Bayes Classifier,
- (c) The Processed Output by using MAP Classifier,
- (d) The processed Output by using Fuzzy Classifier,
- (e) The Processed Output by using Neural Classifier.

CHAPTER VI

THE COMPARISON OF NEURAL NETWORKS WITH OTHER DETECTION TECHNIQUES

6.1 Introduction

In recent years, many frequency diverse flaw enhancement techniques[8],[26] have been used for ultrasonic flaw detection. These techniques include the maximum method, the median detector, the minimization method, the average method, and the polarity thresholding. The objective of this chapter is to introduce these techniques and compare their performances with the performances of the neural network and the statistical Bayes classifiers. In order to evaluate and compare the performance of all these techniques, it has been assumed that the flaw echoes cover the same frequency band as the background grain echoes. This assumption provides an opportunity that not only can challenge all the enhancement techniques but also best evaluate their performance, although in certain experimental situations, flaw echoes may show different frequency content. To completely cover the above two situations, both the simulated and experimental data are used to test all flaw detection algorithms. In the following sections, the mathematical models of the recently proposed enhancement techniques are introduced. Then the simulated and experimental data are applied to test their performances and their results are used to illustrate how these techniques work. The performance comparison with the neural network and the Bayes classifier is given in Section 6.3 as well.

6.2 Recently Proposed Techniques

In Chapter II, we explained that the split-spectrum processing can provide a set of observation feature vectors according to the signal frequency diversity. However, the patterns of signal features are affected by the interference of the microstructure of the testing materials on the transmitted ultrasonic echo, and, in general, are decided by the size and orientation of the reflectors (i.e., grain or flaw). Therefore, flaw echoes and grain echoes present various statistical properties on their feature vectors and these differences can be used to classify flaw echoes. When some of the observations deviate from the statistical pattern of an assumed grain hypothesis, we can measure the statistical parameters of the feature vectors to obtain the existing possibility of flaw echoes. Among all statistical parameters, the first order statistical parameter, the average, is useful to discriminate signals when target and clutter features have different DC values. Therefore, if the average values of the feature vectors of flaw and grain echoes are different, the average detector can be combined with the SSP to detect ultrasonic flaws. The mathematical expression of the average detector is given as the following:

$$\phi_{av}(n) = \frac{1}{k} \sum_{j=1}^k |z_j(n)| \quad (6.1)$$

where z_j is the SSP output on channel j , and k is the number of the SSP channels. In addition, in certain situations, inspecting only some elements of the feature vector can separate the feature vectors. Therefore, selecting the maximum value, the median value, or the minimum value of the feature vectors could be useful in these situations. The mathematical models of the above detectors can be written in the following form:

Maximum detector:

$$\phi_{\max}(n) = \text{Maximum}[|z_j(n)|, j = 1, 2, \dots, k] \quad (6.2)$$

Median detector:

$$\phi_{\text{med}}(n) = \text{median}[|z_j(n)|, j = 1, 2, \dots, k] \quad (6.3)$$

Minimum detector:

$$\phi_{\min}(n) = \text{minimum}[|z_j(n)|, j = 1, 2, \dots, k] \quad (6.4)$$

Another theory proposed by Bilgutay [26] is the polarity thresholding. This method sets the output to zero when the output of the SSP algorithm exhibiting a polarity reversal, otherwise keeps the input as the output. Basically, this method is effective when the flaw echoes could dominate the grain noise such that all the elements of feature vectors can have the same polarity. The expression of the polarity thresholding is modeled as following

$$\begin{aligned} \phi_{\text{pt}}(n) &= x(n), & \text{if } z_j(n) > 0 \text{ or } z_j(n) < 0 \text{ for all } j = 1, 2, \dots, k. \\ &= 0, & \text{otherwise} \end{aligned} \quad (6.5)$$

The previous detectors are developed for certain situations; therefore, they might be able to detect flaw echoes when certain situations are satisfied. In the following section, we apply the simulated and experimental data to the above methods, and the results are discussed to present their performances.

6.3 Simulation and Experimental Results

In this section, two types of ultrasonic signals are used to test above techniques as well as the neural network and the Bayes classifiers. The first type of ultrasonic signal

assumes that there is a small deviation on the frequency bands between flaw and grain echoes. Specifically, the center frequency of flaw echoes is smaller than the center frequency of grain echoes. This type of ultrasonic signals, in general, presents similar properties compared to the experimental data; therefore, the experimental data is directly used as the first type ultrasonic signal. Another type of ultrasonic signal which assumes both flaw and grain echoes exhibit the same frequency components resulting in a difficult situation for detection. The simulated clutter signals of the second type ultrasonic signal are simulated using 1024 superimposed echoes. These echoes have a 7 MHz center frequency and a 2.5 MHz 3-dB bandwidth. The flaw echo is simulated using a single echo. This flaw echo is then superimposed in the pseudo-clutter signal with a desirable amplitude such that the ratio of the flaw echo to the largest possible clutter ratio is about 0 dB. In the SSP algorithm we adopt 8 Gaussian bandpass filters. These bandpass filters have a 1.5 MHz 3-dB bandwidth and their center frequencies are uniformly distributed in the range of 1.5 MHz to 13.5 MHz. The output of the bandpass filters is then normalized by its standard deviation (STD). To inspect the affects of the SSP algorithm on the simulated signals, we graphically display a decomposed signal before and after the normalization on the joint time-frequency plane, in which the patterns of flaw and grain features can be observed. Figure 6.1 shows the decomposed signal of the first type ultrasonic signal on the joint time-frequency plane. Figure 6.1 (a) is the output of the Gaussian bandpass, and Figure 6.1 (b) is the signal features after the normalization. The flaw echo is embedded in the location around 500. As shown in the figure, in the lower frequency bands, we can observe a small variation at the location around 500, which is the result of the decomposition of a flaw echo on the joint time-frequency plane. Figure

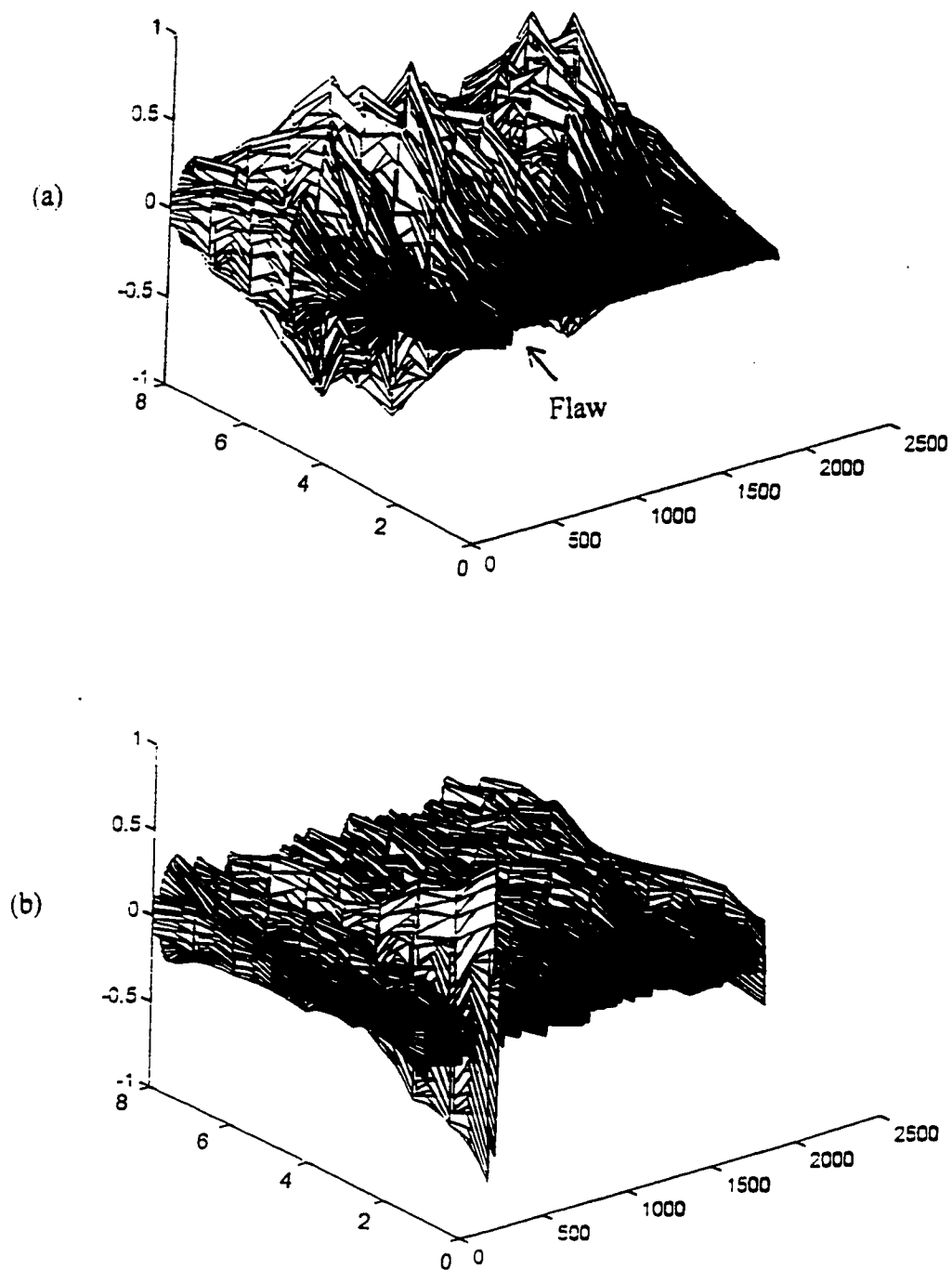


Figure 6.1 The Decomposed Signal on Time-Frequency Plane (The flaw and grain echoes have different frequency components)

- (a) Before Normalization,
- (b) After Normalization.

6.1 (b) shows the result of the normalization, and it is observable that the pattern of the flaw echo has been emphasized over the pattern of grain echoes. This is due to the fact that the statistical property of flaw and grain echoes are different, so normalization using the STD can equalize the signal energy on all SSP channels resulting in the suppressing of grain echoes and the enhancement of flaw echoes. In Figure 6.1 (b) at the location around 500, we can observe the pattern of a flaw echo which is much varied from the pattern observed at other locations (i.e., the pattern of grain echoes). Obviously, the elements of the flaw feature on the lower frequency bands present big magnitudes compared to the elements of grain features. Therefore, we can expect that if the flaw echo exhibits different frequency components, the recently proposed techniques including the maximum detector and the average detector are suitable for detecting the first type flaw echoes. However, the performances of the minimum detector and the polarity thresholding might be poor. An example of the processed signal using the techniques discussed in the previous section is given in Figure 6.2. Figure 6.2 (a) is the input signal and a flaw echo is embedded at the location about 1750. Figure 6.2 (b) is the processed output using a three-layer feedforward neural network, and the result shows that the neural network is able to detect the flaw echo and eliminate the grain echoes. Figure 6.2 (c) is the processed output using the polarity thresholding, and its performance is unacceptable. Figure 6.2 (d) is the processed output using Bayes classifier, and this result shows that Bayes classifier can locate the flaw position too. Figure 6.2 (e) to (h) are the processed output using the average, the minimum, the median, and the maximum detectors respectively. From these results, we can determine the flaw position by observing the output of the average and the maximum detectors. However the

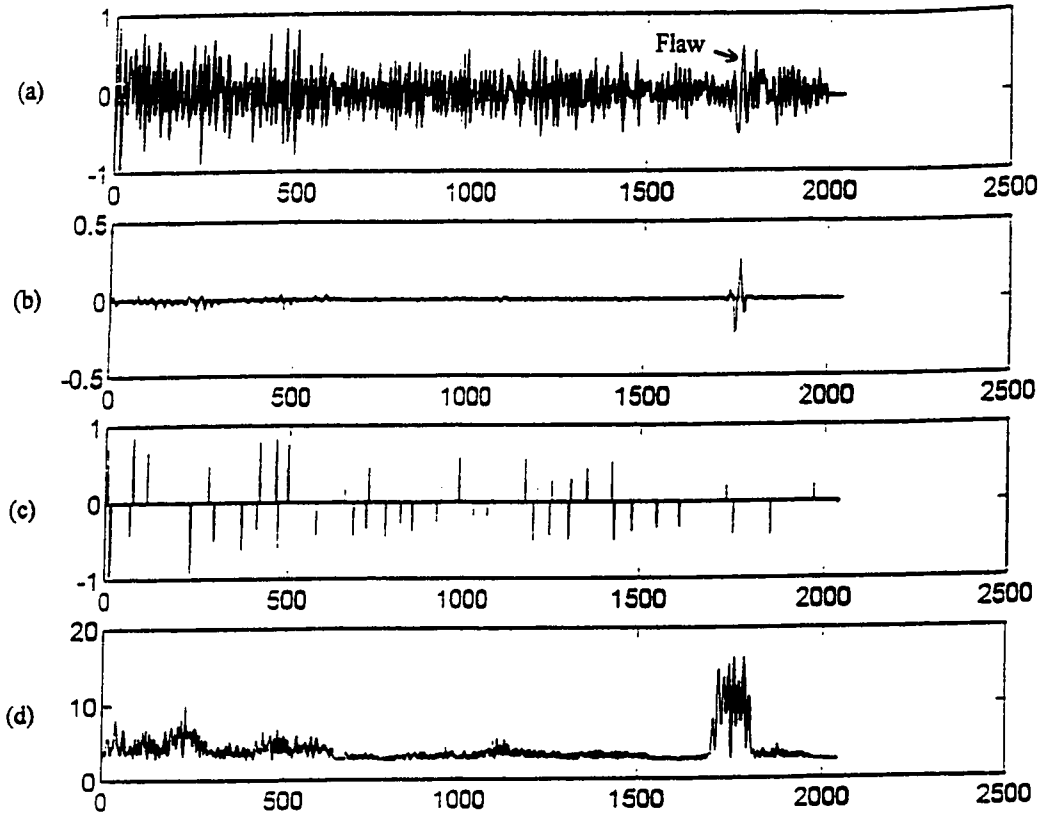


Figure 6.2 The Processed Output by using Experimental Data (The flaw and grain echoes have different frequency components) (Page 1 of 2)

- (a) The Original Signal,
- (b) The Processed output using Neural Network,
- (c) The processed output using Polarity Thresholding,
- (d) The Processed output using Bayes Classifier.

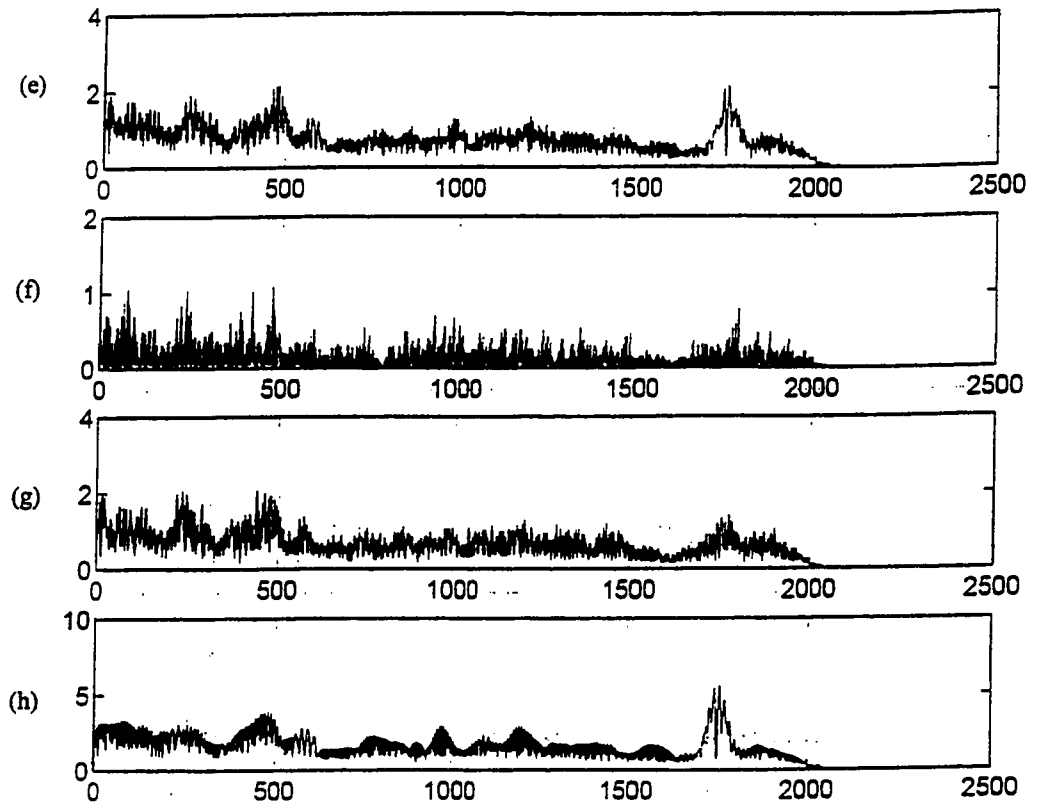


Figure 6.2 Continued (Page 2 of 2)

- (e) The Processed output using the Average Detector,
- (f) The Processed output using the Minimum Detector,
- (g) The processed output using the Median Detector,
- (h) The Processed output using the Maximum Detectors.

performances of the minimum and the median detectors are poor. In order to obtain an average performance, all flaw detection algorithms are examined by 10 experimental data with different flaw locations to measure the enhancement of flaw-to-clutter ratio, and the results are presented in Table 6.1. From this table, we learn that the neural network can enhance the flaw-to-grain ratio to a factor of 12.02, which is superior when compared to other flaw detection algorithms. The enhancement of the Bayes classifier is about 2.93, which is the second best among all these techniques. This table gives the evidences that the performance of the neural network is the best and is much higher than other techniques to a factor of 12.

Another type of the ultrasonic signals is obtained using the same frequency components for both flaw and grain echoes. An average result is presented in Table 6.2. In this table, the flaw-to-clutter enhancement results from 10 independent simulations where the flaw echoes were embedded at different locations. The result show that compared to other flaw detection algorithms, the neural network is outstanding, and the flaw-to-clutter enhancement can reach to the factor of 3.35.

A typical decomposed signal of the second type signal is displayed in Figure 6.3. Figure 6.3 (a) is the decomposed signal on the time-frequency plane before normalization in which the flaw echo is embedded in the location about 500 and is invisible due to the masking of grain echoes. Figure 6.3 (b) is the signal after the normalization, and it is very difficult to directly discriminate the flaw and grain echoes. A typical test result is given in Figure 6.4. Figure 6.4 (a) is the input signal, and Figure (b) to (h) is the processed results of using the neural network, the polarity thresholding, the Bayes, the average, the minimum, the median, and the maximum detectors respectively. As shown in this figure,

Table 6.1 Flaw/Clutter Ratio Enhancement of Various Processing Techniques using Experimental Signals

Trial No.	Neural Network	Polarity Detector	Bayes Detector	Average Detector	Minimum Detector	Median Detector	Maximum Detector
1	24.55	0.76	2.75	2.41	1.18	1.71	2.66
2	8.75	1.01	2.23	1.74	0.85	1.69	1.80
3	6.08	0	2.62	1.46	0.83	1.35	1.33
4	7.62	0.89	3.20	1.42	1.21	1.43	1.34
5	7.64	0.74	3.33	1.43	0.50	1.50	1.46
6	5.83	1.22	2.38	1.43	1.44	1.43	1.21
7	13.98	0.72	2.60	1.17	1.13	0.78	1.45
8	14.11	0.58	4.50	1.38	1.10	0.72	1.54
9	15.72	0.3	2.43	1.58	1.10	1.09	1.90
10	17.81	0.92	3.28	1.30	1.28	0.82	1.61
Mean	12.02	0.72	2.93	1.53	1.06	1.25	1.63
STD	6.08	0.35	0.67	0.34	0.27	0.37	0.42

Table 6.2 Flaw/Clutter Ratio Enhancement of Various Processing Techniques using Simulated Signals (Flaw and grain echoes have same frequency components)

Trial No.	Neural Network	Polarity Detector	Bayes Detector	Average Detector	Minimum Detector	Median Detector	Maximum Detector
1	3.63	1.07	1.22	1.13	1.15	1.14	1.15
2	3.56	1.21	0.92	1.19	1.72	1.10	1.08
3	3.98	1.42	1.07	1.41	1.57	1.34	1.09
4	4.01	1.18	1.11	1.34	1.80	1.20	0.98
5	3.02	1.02	1.08	1.46	1.66	1.54	1.06
6	1.82	1.24	0.87	1.19	1.52	1.23	0.98
7	3.75	1.17	0.92	1.24	1.45	1.10	0.96
8	4.36	1.36	0.96	1.12	1.57	1.10	1.03
9	2.50	0.94	1.10	1.06	1.27	1.14	1.04
10	2.85	1.21	0.94	1.27	1.68	1.21	1.03
Mean	3.35	1.18	1.02	1.24	1.54	1.21	1.04
STD	0.79	0.15	0.12	0.13	0.20	0.14	0.05

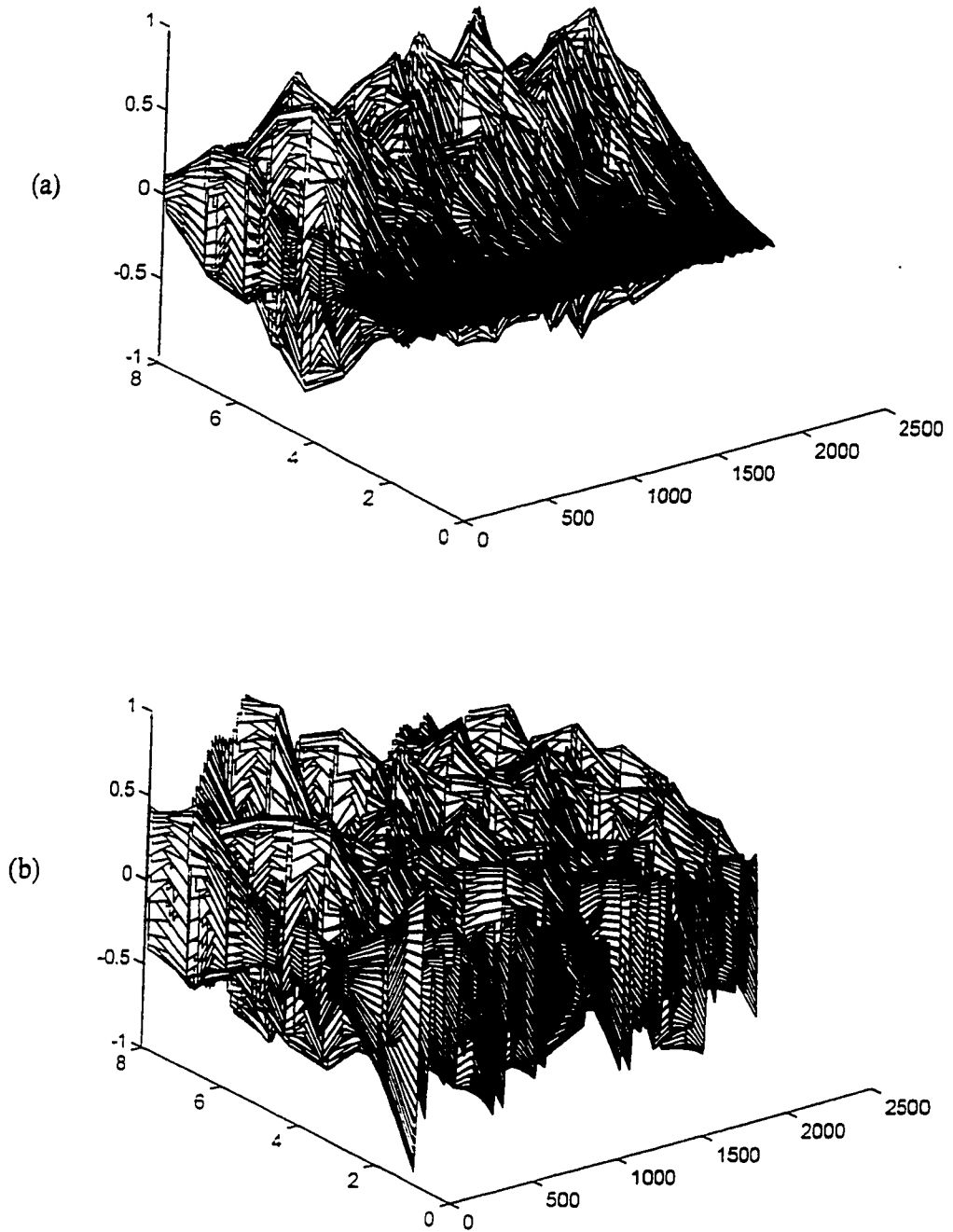


Figure 6.3 The Decomposed Signal on Time-Frequency Plane (The flaw and grain echoes have same frequency components)
(a) Before Normalization,
(b) After Normalization.

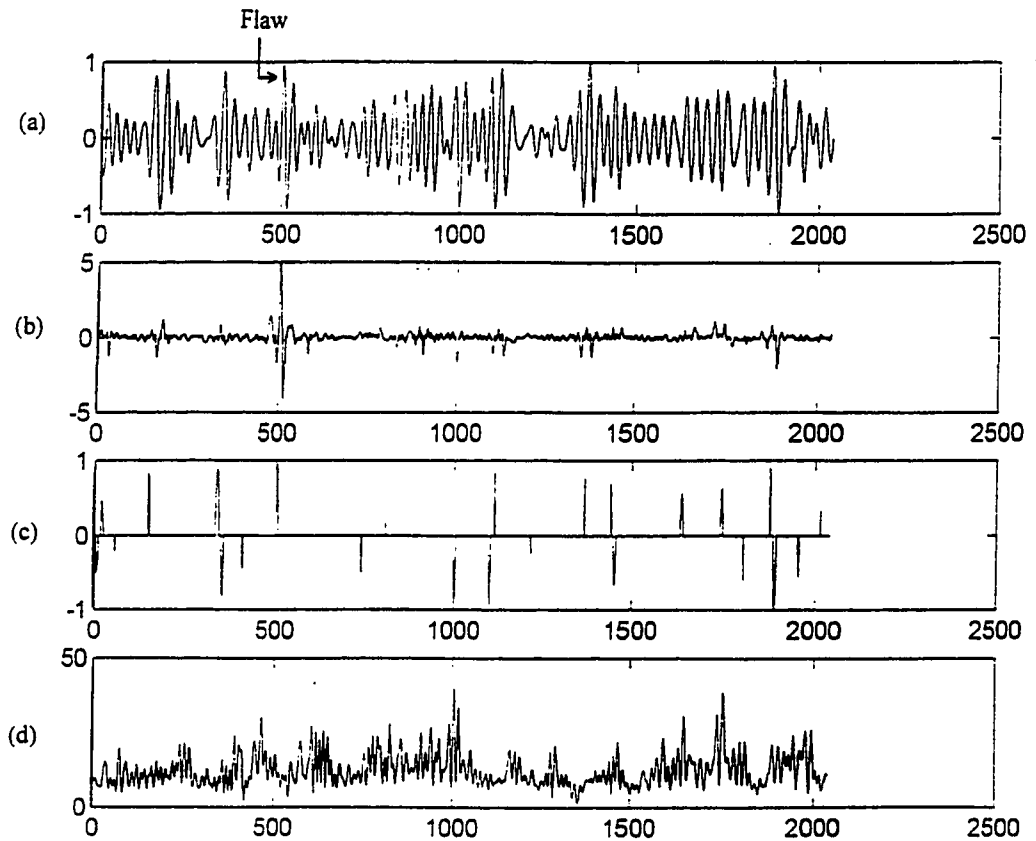


Figure 6.4 The Processed Output by using Simulated Data (The flaw and grain echoes have same frequency components) (Page 1 of 2)

- (a) The Original Signal,
- (b) The Processed output using Neural Network,
- (c) The processed output using Polarity Thresholding,
- (d) The Processed output using Bayes Classifier.

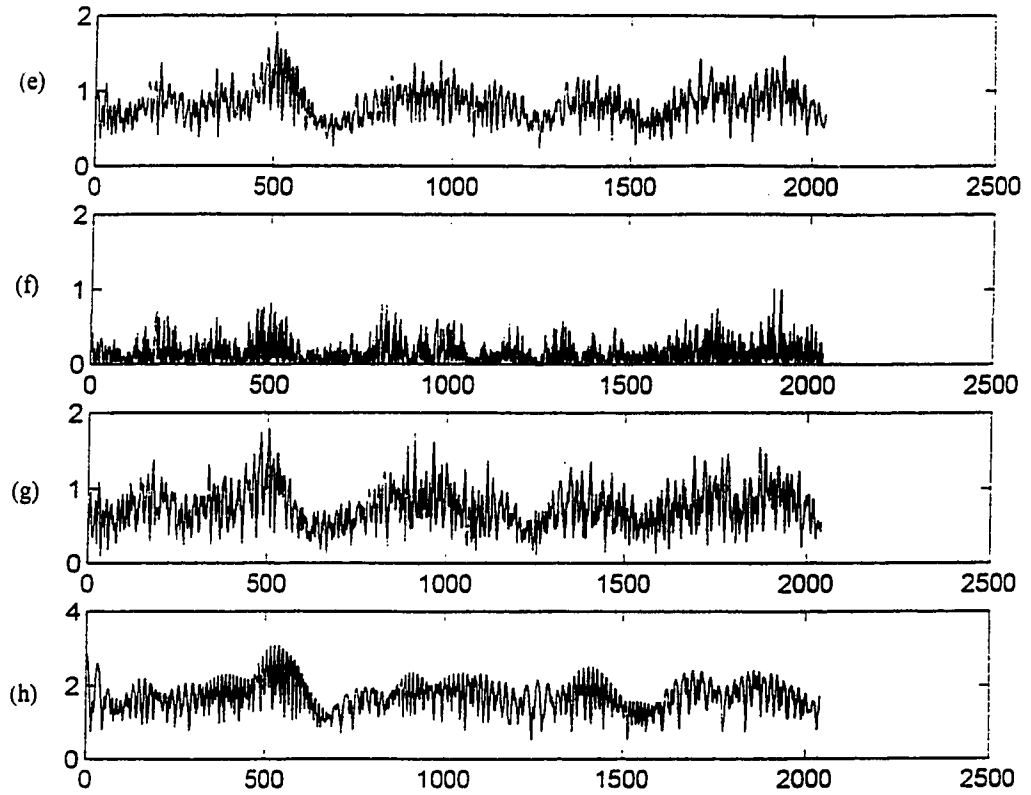


Figure 6.4 Continued (Page 2 of 2)

- (e) The Processed output using the Average Detector,
- (f) The Processed output using the Minimum Detector,
- (g) The processed output using the Median Detector,
- (h) The Processed output using the Maximum Detectors.

the neural network clearly locates the position of the flaw echo; however, other techniques failed to detect the flaw echo. Inspecting the signal in Figure 6.3 (b), we find that since the flaw echo has the same frequency bands as grain echoes, the enhancement of using the SSP algorithm is limited. Therefore the statistical parameters are unable to separate the flaw and grain echoes resulting in the failure of the Bayes classifier.

This result suggests that the Bayes classifier can properly work when the flaw and the clutter echoes have a good statistical separation situation [1]. This happens in the first type ultrasonic signal; however, in the second type signal situation, the estimations of the probability density functions of flaw and grain are highly dependent on the selection of filters' parameters and the signal's frequency components. If these parameters were unable to build a statistical separation situation, then the Bayes algorithm would be unable to detect the flaw echoes. The statistical situation also affects the performance of the maximum, the median, the minimum, and the average detectors [8]. In the first type signal, the flaw echo presents a strong statistical deviation on lower frequency bands that help the maximum and the average detectors to gain a better performance. However, The conditions in the first type ultrasonic signal are no longer existed in the second type signal, therefore both the maximum and the average methods failed. To improve their performances in the second type signal situation we need to properly select the SSP channels such that we can have a statistical separation situation. However this is hard to acquire in the experimental situation. The polarity thresholding can properly work only when the flaw echo can dominate the grain echoes [26], and this does not happen in the above two cases, so in both types of ultrasonic signals, the results are very poor.

6.4 Conclusion

This chapter presents a comparison result of the SSP combined with several classified techniques including the neural network, the Bayes classifier, the polarity thresholding, the average, the minimum, the median, and the maximum detectors in the application of ultrasonic flaw detection problems. The result shows that the neural network is the best detector compared to other techniques by testing both the simulated and experimental data. In the comparison, the neural network demonstrates the ability to recognize flaw and grain echoes no matter what their frequency components were. However, other techniques could detect flaw echoes only when certain conditions are satisfied. This result gives the fact that the neural network is able to learn and recognize objectives in a highly noisy environment, and its performances are better than that of the statistical methods. The experimental result shows the flaw-to-clutter ratio enhancement can reach the factors of 12 and 3 for using the neural network and the Bayes classifier respectively, and other techniques can only reach the factors smaller than 2 when the flaw-to-clutter ratio of the input is about 0dB.

CHAPTER VII

SUMMARY AND CONCLUSION

In this thesis, we have applied the SSP algorithm combined with nonlinear classifiers including the Bayes classifier, the MAP classifier, the fuzzy discriminant classifier, and the neural network for the ultrasonic flaw detection application. The SSP algorithm utilizes the inherent property of ultrasonic signals on the frequency domain to enhance the SNR of flaw echoes. This algorithm also provides the signal features on the joint time-frequency plane, which are used by the nonlinear classifiers for detection purpose. In the implementation of the SSP filters, the affecting factors include the number, the bandwidth, and the center frequencies of the SSP channels. In addition, the overlap among the SSP channels decides the correlation of the SSP channels. These parameters are very sensitive to affect the result of the SSP algorithm. In our design, the number and the bandwidth of the SSP channels are selected to cover the entire frequency bands of the transmitted broadband ultrasonic echoes. The signal correlation on the SSP channels is obtained by carefully adjusting the filters' parameters as well as inspecting the frequency property of the grain and flaw echoes, and filters are selected to optimize the system performance. The signal properties and the signal models processed by the SSP algorithm have been studied and presented in Chapter II.

In Chapter III, we developed two statistical classifiers, the Bayes and the MAP classifiers. Basically, the Bayes classifier estimates the PDF of both grain and flaw echoes, and then utilizes the maximum likelihood ratio as the discriminant function to detect the flaw echoes. Therefore, our main concern is to estimate the signal's PDF. If

the estimation is able to create a statistically separable environment, then the Bayes classifier is able to classify the flaw echoes from grain echoes. The experimental results show that using Bayes classifier the flaw-to-clutter ratio can be enhanced to a factor of 2.9. The MAP classifier works like the Bayes classifier, but instead of estimating the PDF for both grain and flaw echoes MAP classifier only estimates the PDF of grain echoes. Then the maximum of the posteriori conditional density is used to enhance the signal's features, which basically modifies the feature vectors according to the estimated PDF. Since the signal features have been modified by the maximizing operation, the variance of the feature vector is used as an indicator to detect the flaw echoes. The experimental results show that the flaw-to-clutter enhancement of the MAP classifier can reach a factor of 1.527. Comparing the performances of the Bayes and the MAP classifiers, we conclude that the Bayes classifier is better than the MAP classifier. This result is due to the fact that the MAP classifier only utilizes the grain information; however, the Bayes classifier estimates not only the grain information but also the flaw information.

In Chapter IV, a novel fuzzy classifier is introduced. According to the fuzzy theory, we build a class of membership functions to assign the degree (i.e., grade) of set membership to the signal features (i.e., fuzzy set). These membership functions are established by investigating the signal statistical properties. Therefore, the fuzzy set could be used to indicate the existing "possibility" of target signals (i.e., flaw echoes). The fuzzy set is then processed by the fuzzy classifier, which is obtained by modifying the fuzzy entropy to measure the quantity of information. According to the grades of the fuzzy set the fuzzy classifier is able to decide whether the input signal is a grain or a flaw echo. The experimental results show that the fuzzy classifier can enhance the flaw-to-

clutter ratio to a factor of 4.53 that is a better performance compared to that of the statistical classifiers.

In the implementation of the previous techniques a prior knowledge of grain and flaw echoes need to be estimated. However, this estimation depends on the assumption of signals' PDF. Therefore, the estimation results might be biased, which is undesirable. In Chapter V, a three-layer feedforward neural network is used to perform the classification task. Without estimating any mathematical model of the ultrasonic signals the neural network can learn the patterns of flaw and grain echoes. This recognition ability is learned through a backpropagation learning process. In addition, the results show that the neural network performance can be improved by using more neural nodes in the hidden layer. However, this may increase the time of training. The experimental results show that using the neural network the flaw-to-clutter ratio enhancement can reach a factor of 12.02. From all experimental results, we conclude that the three-layer neural network is better classifier among all discussed techniques. In Chapter VI, a performance comparison of the Bayes classifier, the neural network, and the recently proposed techniques including the order statistical filter and the polarity thresholding is presented. According to the results, the performance of the neural network is superior, and it can detect the flaw echo embedded in the grain echoes that occupied the same frequency bands as flaw echoes.

In this thesis, we have applied various nonlinear classifiers to the ultrasonic flaw detection problems, and found that the three-layer neural network is a better classifier to detect the flaw echo in a highly noisy environment. We recommend the following future research work based on the finding of this study:

- Utilize other time-frequency representations to display signal features for improved target detection.
- Train the neural network to recognize the size and orientation of flaw echoes.
- Train the neural network to recognize 2-D objects in ultrasonic images.
- Improve the training strategy such that the training period can be reduced.
- Implement the neural network by using modern VLSI technology.
- Evaluate time-frequency neural network techniques for both industrial and medical applications.

BIBLIOGRAPHY

- [1] J. Saniie, Tao Wang and X. Jin, "Performance Evaluation of Frequency Diverse Bayesian Ultrasonic Flaw Detection," *J. Acoust. Soc. of Amer.*, Vol. 91, No. 4, pp. 2034-2041, April 1992.
- [2] J. Saniie and Motaz A. Mohamed, "Ultrasonic Flaw Detection Based on Mathematical Morphology," *IEEE Transactions on Ultrasonics, Ferroelectrics and Frequency Control*, Vol. 41, No. 1, pp. 150-159, January 1994.
- [3] J. Saniie, M. Unluturk and T. Chu, "Frequency Discrimination Using Neural Networks with Applications in Ultrasonics Microstructure Characterization," *IEEE Ultrasonic Symposium Proceedings*, pp. 1195-1199, 1992.
- [4] J. Saniie and N. M. Bilgutay, "Quantitative Grain Size Evaluation Using Ultrasonic Backscattered Echoes," *J. Acoust. Soc. of Amer.*, Vol. 80, pp. 1816-1824, Dec. 1986.
- [5] W. Sachse, I Grabec and Sribar, "Intelligent Proceeding of Ultrasonic Signals for Quantative Material Testing," *IEEE Ultrasonic Symposium Proceedings*, pp. 767-776, 1991.
- [6] T. Wang, J. Saniie and X. Jin, "Analysis of Low-Order Autogressive Models for Ultrasonic Grain Signal Characterization," *IEEE Transactions on Ultrasonics, Ferroelectrics and Frequency Control*, Vol. 38, pp. 116-124, March 1991.
- [7] J. Saniie and Daniel T. Nagle, "Analysis of Order-Statistic CFAR Threshold Estimators for Improved Ultrasonic Flaw Detection," *IEEE Transactions on Ultrasonics, Ferroelectrics and Frequency Control*, Vol. 39, No. 5, pp. 618-630, September 1992.
- [8] J. Saniie, Daniel T. and Kevin D. Donohue, "Analysis of Order Statistic Filters Applied to Ultrasonic Flaw Detection Using Split-Spectrum Processing," *IEEE Transactions on Ultrasonics, Ferroelectrics and Frequency Control*, Vol. 38, No. 2, pp. 133-140, March 1991.
- [9] Sam-kit Sin and Chi1-Hau Chen, "A Comparison of Deconvolution Techniques for The Ultrasonic Nondestructive Evaluation of Materials," *IEEE Transactions on Image Processing*, Vol. 1, No. 1, pp. 3-10, January 1992.
- [10] Cohen, "Time-Frequency Distribution - A Review," *Proceedings of the IEEE*, Vol. 77, No. 7, pp. 941-981, July 1989.

- [11] C.H. Chen and G.G. Lee, "Neural Networks for Ultrasonic NDE Signal Classification Using Time-Frequency Analysis," *IEEE International Conference on Acoustics, Speech, and Signal processing* Vol. 1, pp493-496, 1993.
- [12] K.K. Chin, X. Jin and J. Saniie, "Spectral Analysis of Ultrasonic Flaw Echoes Using Wigner Distribution," *IEEE Ultrasonic Symposium Proceedings*, 1990.
- [13] H. I. Choi and W. J. Williams, "Improved Time-Frequency Representation of Multicomponent Signals Using Exponential Kernels," *IEEE Transaction on Acoustics Speech and Signal Processing*, Vol. 37, No. 6, pp. 862-871, June 1989.
- [14] D. S. K. Chan, "A Non-Aliased Discrete-Time Wigner Distribution for Time-Frequency Signal Analysis," *Proc. Int. Conf. Acoust., Speech, Signal Processing*, pp. 1333-1336, 1982.
- [15] Charles K. Chui, *An Introduction to Wavelets*, New York : Academic, 1992
- [16] X. Jin , *Spectral Analysis for Ultrasonic Non-Destructive Evaluation*, Ph. D. Dissertation, Illinois Institute of Technology, Chicago, IL 1994.
- [17] M.A. Malik, *Unified Time-Frequency Analysis of Ultrasonic Signals*, Ph. D. Dissertation, Illinois Institute of Technology, Chicago, IL 1995.
- [18] Y. Zhao, L.E. Atlas and R.J. Marks II, "The Use of Cone-Shaped Kernels for Generalized Time-Frequency Representation of Nonstationary Signals," *IEEE Transaction on Acoustics, Speech, and Signal Processing*, Vol. 38, No. 7, pp. 1084-1091, July, 1990.
- [19] F. Hlawatsch and W. Krattenthaler, "A New Approach to Time-Frequency Signal Decomposition", *IEEE ISCAS*, pp. 1248-1251, 1989.
- [20] P. Flandrin, "Some Features of Time-Frequency Representation of Multicomponent Signals", *IEEE ICASSP Proceedings*, pp. 41B41-41B44, San Diego, 1984.
- [21] R. O. Duda, and P. E. Hart, *Pattern Classification and Scene Analysis*, John Wiley & Sons, Inc., 1973.
- [22] V.L. Newhouse, N.M. Bilgutay, J. Saniie, and E.S. Furgason, "Flaw-to-Grain Echo Enhancement by Split-Spectrum Processing," *Ultrasonics*, pp. 59-68, March, 1982.

- [23] N.M. Bilgutay, and J. Saniie, "The Effect of Grain Size on Flaw Visibility Enhancement Using Split-Spectrum Processing," *Materials Evaluation*, 42, pp. 808-814, May, 1984.
- [24] P.M. Shankar, U. Bencharit, N.M. Bilgutay, and J. Saniie, "Grain Noise Suppression through Bandpass Filtering," *Materials Evaluation*, 46, pp. 1100-1105, July, 1988.
- [25] N.M. Bilgutay, X. Li, and J. Saniie, "Spectral Analysis of Randomly Distributed Scatterers for Ultrasonic Grain Size Estimation," *Ultrasonics*, Vol. 27, pp. 19-25, January, 1989.
- [26] Nihat, M. Bilgutay, U. Bencharit, and J. Saniie, "Enhanced Ultrasonic Imaging with Split-Spectrum Processing and Polarity Thresholding," *IEEE Transactions on Acoustics, Speech, and Signal Processing*, Vol. 37, No. 10, pp. 1590-1592, October, 1989.
- [27] J. Saniie, T. Wang, and X. Jin, "Performance Evaluation of Frequency Diverse Bayesian Ultrasonic Flaw Detection," *J. Acoust. Soc. of Amer.*, 91 (4), pp. 2034-2041, April, 1992.
- [28] M.G. Gustafsson, and T. Stepinski, "Split Spectrum Algorithms Rely on Instantaneous Phase Information-A Geometrical Approach," *IEEE Transactions on Ultrasonics, Ferroelectrics, and Frequency Control*, Vol. 40, No. 6, pp. 659-665, November, 1993.
- [29] M.G. Gustafsson, "Nonlinear Clutter Suppression Using Split Spectrum Processing and Optimal Detection," *IEEE Transactions on Ultrasonics, Ferroelectrics, and Frequency Control*, Vol. 43, No.1, pp. 109-124, January 1996.
- [30] J. Saniie, and M.A. Mohamed, "Ultrasonic Flaw Detection Based on Mathematical Morphology," *IEEE Transactions on Ultrasonics, Ferroelectrics, and Frequency Control*, Vol. 41, No. 1, pp. 150-159, January, 1994.
- [31] M. Schwartz, *Information Transmission, Modulation, and Noise*, McGraw-Hill Book Company, New York, 1990.
- [32] P. Beckmann, and A. Spizzichino, *The Scattering of Electromagnetic Waves from Rough Surfaces*, The Macmillan Company, New York, 1963.
- [33] J. Saniie, T. Wang, and N.M. Bilgutay, "Optimal Ultrasonic Flaw Detection Using a Frequency Diversity Technique," in *Review of Progress in Quantitative Nondestructive Evaluation*, edited by D.O. Thompson and D.E. Chimenti, Vol. 8A, pp. 751-758, Plenum, New York, 1989.

- [34] K. W. Fertig, J. M. Richardson, and R.K. Elsley, "Statistical Flaw Detection in a Scanning Mode," in *Review of Progress in Quantitative Non-destructive Evaluation*, edited by D.O. Thompson and D.E. Chimenti, Vol. 4A, pp. 27-35, Plenum, New York, 1989.
- [35] R. K. Elsley, K.W. Fertig, J.M. Richardson, and F. Cohen, "Statistical Approach to the Automation of Flaw Detection," in *Review of Progress in Quantitative Nondestructive Evaluation*, edited by D.O. Thompson and D.E. Chimenti, Vol. 4A, pp. 19-26, Plenum, New York, 1989.
- [36] K. W. Fertig, J. M. Richardson, and R.K. Elsley, "Statistical Flaw Detection: Theory," in *Review of Progress in Quantitative Non-destructive Evaluation*, edited by D.O. Thompson and D.E. Chimenti, Vol. 3A, pp. 65-79, Plenum, New York, 1989.
- [37] R. K. Elsley, K.W. Fertig, J.M. Richardson, and R. S. Linebarger, "Statistical Flaw Detection: Application to Flaws below Curved Surfaces," in *Review of Progress in Quantitative Nondestructive Evaluation*, edited by D.O. Thompson and D.E. Chimenti, Vol. 3A, pp. 81-93, Plenum, New York, 1989.
- [38] S. Finette, A. Bleier, and W. Swindell, "Breast Tissue Classification using Diagnostic Ultrasound and Pattern Recognition Techniques, I. Method of Pattern Recognition," *Ultrason. Imag.* 5, pp. 87-93, 1983.
- [39] S. Finette, A. Bleier, W. Swindell, and K. Habei, "Breast Tissue Classification using Diagnostic Ultrasound and Pattern Recognition Techniques, II. Experimental Results," *Ultrason. Imag.* 5, pp. 87-93, 1983.
- [40] R. O. Duda, and P. E. Hart, *Pattern Classification and Scene Analysis*, John Wiley & Sons, Inc., 1973.
- [41] A. Papoulis, *Probability, Random Variables, and Stochastic Processes*, McGraw-Hill, Inc., 1991.
- [42] L. A. Zedah, "Fuzzy sets," *Inform. Control*, Vol. 8, pp. 338-353, 1965.
- [43] L. A. Zadeh, "Outline of a New Approach to the Analysis of Complex Systems and Decision Process," *IEEE Transactions on Man. Cybern.*, Vol. SMC-3, No. 1, pp.28-44, January, 1973.
- [44] Yaling Cai and Kon Koung Kwan, "A Fuzzy Neural Classifier for Pattern Classification," *IEEE International Symposium on Circuits and Systems* Vol 4., pp. 2369-2370, 1993.

- [45] Takeshi Yamakawa, "A Fuzzy Inference Engine in Nonlinear Analog Mode and Its Application to a Fuzzy Logic Control," *IEEE Transactions on Neural Networks*, Vol. 4., No 3, May 1993.
- [46] N. R. Pal and S. K. Pal, "Higher Order Fuzzy Entropy and Hybrid Entropy of a Set," *Information Sciences* 61, pp.211-231, 1992.
- [47] Simon Haykin, *Neural Networks*, IEEE Press 1994.
- [48] Andreas Tirakis, "Efficient Image Classification Using Neural Networks and Multiresolution Analysis," ICASSP-93, *IEEE International Conference on Acoustics, Speech and Signal Processing*, Vol. 4, pp. 641-644, 1993.
- [49] C. H. Chen "On the Relationships between Statistical Pattern Recognition and Artificial Neural Networks," *IEEE International Conference on Systems, Man and Cybernetics Conference Proceedings*, pp.182-183, 1990.
- [50] W. Y. Huang and R. P. Lippmann, *Comparisons Between Neural Net and Conventional classifiers*, Technical Report, Lincoln Laboratory, MIT, 1987.
- [51] G. Cybenko, "Approximate by Superpositins of A Sigmoidal Function," *Mathematics of Control, Signals and Systems*, pp. 303-324, (1989)2.
- [52] David A. Sprecher, "A Representation Theorem for Continuous Functions of Several Variables," *Proc. Amer. Math. S-C*, pp.200-203, 16(1965).
- [53] A. N. Kolmogorov, "On the Representation of Continuous Functions of Several Variables by Superpositions of Continuous Functions of a Smaller Number of Variables," *Dokl. Akad. Nauk SSSR*, pp.179-182 , 108(1956).
- [54] G. G. Lorentz, "The 13-th problem of Hilbert," *American Mathematical Society*, Vol 28, pp.419-430, 1976.
- [55] D. E. Rumelhart, J. L. McClelland and the PDP Research Group, *Parallel Distributed Processing*, MIT Press, Vol. 1, pp.318-362, 1986.